2-1-2012

Studying signatures of water on Mars at two macro and micro scales : orbital analyses of hillslope geomorphology and ChemCam calibration for surficial rock chemistry

Nina Lanza

Nina Lanza
Candidate

Earth and Planetary Sciences Department
Department

This dissertation is approved, and it is acceptable in quality and form for publication:

Approved by the Dissertation Committee:

Dr. Carl Agee, Chairperson

Dr. Horton Newsom, Chairperson

Dr. Grant Meyer

Dr. Roger Wiens

Dr. Darby Dyar

STUDYING SIGNATURES OF WATER ON MARS AT THE MACRO AND MICRO SCALES: ORBITAL ANALYSES OF HILLSLOPE GEOMORPHOLOGY AND CHEMCAM CALIBRATION FOR SURFICIAL ROCK CHEMISTRY

by

NINA LANZA

A.B, Astronomy, Smith College, 2001
M.A., Earth and Environmental Sciences, 2006

DISSERTATION

Submitted in Partial Fulfillment of the
Requirements for the Degree of

Doctor of Philosophy
Earth and Planetary Sciences

The University of New Mexico
Albuquerque, New Mexico

December 2011

DEDICATION

For Mouser, who knew that I could do this before I did.

ACKNOWLEDGEMENTS

Funding for this dissertation work was provided by a NASA Graduate Student Researcher Fellowship, the Zonta International Amelia Earhart Fellowship, the New Mexico Space Grant Graduate Fellowship, and an EPS departmental scholarship.

I am grateful for the support and guidance of my advisor, Horton Newsom, who has generously allowed me to explore a range of scientific projects during my time at UNM. I am also indebted to the members of my committee for their encouragement and excellent advice: Carl Agee, Grant Meyer, Roger Wiens, and Darby Dyar. I also thank Shannon Clark, Lee Ann Lloyd, and Cindy Jaramillo for their excellent support, which has made my time at UNM infinitely easier.

I could never have learned so much or lasted this long without the help of my peers. I am deeply grateful for the support of my fellow graduate students, both past and present, and in particular Ann Ollila, who has been on this journey with me since almost the beginning. Many thanks are also due to the graduate student writing group Agraphia, who kept me on schedule with positive encouragement and the occasional disapproving look. I also owe a great debt to the Winning Coffee Company and Annapurna's World Vegetarian Café for providing me with my ideal office environment.

I am thankful for the continued guidance of my parents, Richard and Sylvia Lanza, and to my many wonderful friends who have kept me in their thoughts despite my physical distance and increasingly anti-social tendencies.

And finally, I am forever indebted to my best friend and future husband, Richard Williams, for his unwavering love and steadfast encouragement.

STUDYING SIGNATURES OF WATER ON MARS AT THE MACRO AND MICRO SCALES:
ORBITAL ANALYSES OF HILLSLOPE GEOMORPHOLOGY AND CHEMCAM CALIBRATION FOR SURFICIAL ROCK CHEMISTRY

by

Nina Lanza

A.B., Astronomy, Smith College, 2001
M.A., Earth and Environmental Science, Wesleyan University, 2006
Ph.D., Earth and Planetary Sciences, University of New Mexico, 2011

ABSTRACT

Questions about the presence, amount, and nature of liquid water on Mars remain major research topics in planetary science because of the implications they have for the geological history and potential habitability of the planet. Here, the signatures of liquid water on Mars are studied at two scales from two different disciplines: hillslope geomorphology and chemistry from laser-induced breakdown spectroscopy (LIBS). In the first set of studies on hillslopes, the expected differences in hillslope processes in extraterrestrial environments are explored. As on Earth, the major drivers of these processes are gravity and climate. Extraterrestrial hillslopes are unique environments that may be similar, but not identical, to hillslopes found on Earth, and care must be taken to understand how differences in hillslope parameters on these bodies may lead to changes in familiar processes and potentially form. Next, a study testing a debris flow initiation hypothesis for martian gullies was performed. Measurements of the contributing areas and slope gradients were made at the channel heads of martian gullies seen in three high resolution image stereo pairs. Our results show an area-slope relationship for these

martian gullies that is consistent with that observed for terrestrial gullies formed by debris flow, supporting the hypothesis that these gullies formed as the result of saturation of near-surface regolith by a liquid. In the second set of studies, carbonate minerals and rock coatings and rinds were measured by LIBS in a simulated martian environment to better understand the signature of these materials on Mars. This work is in preparation for the Mars Science Laboratory (MSL) rover mission, in which a LIBS instrument will be part of the ChemCam suite of instruments on the rover. In the carbonate study, both chemical composition and rock type are determined using multivariate analysis (MVA) techniques. Composition is confirmed using scanning electron microscopy (SEM). Our results show that ChemCam can recognize and differentiate between different types of carbonate materials on Mars. In the weathered rock study, depth profile data are analyzed using principal component analysis (PCA) and coatings and rinds are examined using SEM and electron probe microanalysis (EPMA). Our results show that LIBS is sensitive to minor compositional changes with depth and correctly identifies rock type even if the series of laser pulses does not penetrate to unweathered material.

TABLE OF CONTENTS

PREFACE

Some of the most enduring questions about the planet Mars involve water and its role throughout the planet's history. Orbital images of the surface reveal what appear to be water-related morphologies at many scales, while spectroscopic observations indicate the presence of minerals at the surface that are hydrated or that likely formed in water. The martian atmosphere contains water vapor, and the polar caps contain water ice. A wealth of both remote sensing and in situ data returned from the planet show conclusively that there is water on Mars. Yet many mysteries remain. Today, Mars is a cold, dry planet that has no observable liquid of any kind on its outermost surface. How did large, apparently fluvial outflow channels form in such an environment? Was Mars once warmer and wetter? Today martian surface conditions in many locations periodically reach the triple point of water, allowing all three phases to be stable. The current atmospheric pressure is ~6 mbar and temperatures often reach 0º C. Could liquid water still be active at the surface or near-surface today? On Earth, where there is liquid water, there is life; the presence of liquid water on Mars opens up the possibility of a habitable environment in which life may have existed—or may still exist.

The overarching goal of the work presented in this dissertation is to better understand how to recognize and interpret the signatures of liquid water on the martian surface from the past and the present, at different scales, and using different techniques. The first two chapters use macro-scale observations and measurements to characterize the martian hillslope environment using terrestrial geomorphological techniques and currently existing datasets. The second two chapters present work that will help enable ChemCam,

an instrument on the Mars Science Laboratory (MSL) rover, to analyze geological materials at micro-scales on the surface of Mars during the MSL mission. Each chapter is written as an independent manuscript that has been published or submitted separately. As a result, there is some repetition in the introductory and methodology sections. Each chapter represents a collaborative effort, but the majority of the analytical work, data interpretation, and writing were done by me and I am the lead author on all of the manuscripts.

Chapter 1, "Extraterrestrial hillslope processes," provides an introduction to hillslope processes and how they are expected to differ in a variety of extraterrestrial environments. Many types of processes act to create, modify, and attenuate slopes at every scale. Processes such as mass movement and overland flow can shed light on the presence and amount of liquid water in the region, a key component for determining an environment's habitability potential. Chapter 2, "Evidence for debris flow gully formation initiated by shallow subsurface water on Mars," is a study of three specific hillslopes on Mars where debris flow morphologies are observed. Debris flow is a mass movement process that is triggered by saturation-induced failure in regolith, which requires the presence of some amount of fluid to occur. Results from this chapter suggest that debris flows have been active on some martian hillslopes, and may also be occurring in the present day.

In contrast to the macro scale observations described in Chapters 1 and 2, Chapters 3 and 4 are concerned with detecting the signatures of water at the micro scale. They describe

work that has been undertaken to support future analyses on the surface of Mars by the ChemCam laser-induced breakdown spectroscopy (LIBS) instrument on the MSL rover. LIBS is a microbeam analysis technique that provides chemical information about samples of interest, and it requires calibration for specific atmospheric environments. Chapter 3, "Calibrating the ChemCam laser-induced breakdown spectroscopy instrument for carbonate minerals on Mars," presents measurements of carbonate minerals, which are water-formed minerals that are predicted to have formed on the martian surface but have yet to be observed in any great abundance. Because carbonates are difficult to detect through the CO_2 atmosphere, it is unclear whether carbonate minerals are absent or if they are simply invisible to remote sensing instruments currently in orbit around the planet. Chapter 4, "Examining natural rock varnish and weathering rinds with laser-induced breakdown spectroscopy for application to ChemCam on Mars," describes measurements of rock varnishes and rinds on naturally weathered terrestrial basalt samples. Many previous in situ and orbital observations suggest that martian rocks have weathered surfaces that have likely interacted with water. These surfaces both obscure the fresh rock composition and provide information about the aqueous alteration environment. It is anticipated that the studies presented in Chapters 3 and 4 will help to provide context for measurements of unknown materials returned by ChemCam on the martian surface.

Chapter 1

Extraterrestrial hillslope processes

Article citation: Lanza, N.L. and Newsom, H.E. (in press). Extraterrestrial Hillslope Processes. In: Stoffel, M. and Marston, R. (Eds.), *Treatise on Geomorphology*, v.7: Mountain and Hillslope Geomorphology. Elsevier, Amsterdam.

Abstract

Hillslope processes may differ either subtly or significantly in extraterrestrial environments. As on Earth, the major drivers of these processes are gravity and climate. In lower gravity fields, the angle of repose of unconsolidated materials remains the same for noncohesive materials. Where cohesion is present, as in fine-grained or moist materials, the angle of repose may be increased under lower gravity conditions. The shear strength of materials is also expected to vary as gravity is decreased, with the effects of cohesion and pore pressure and the strength of competent rock effectively greater than on Earth. These changes will, in turn, affect the actions of mass movements. Hillslope processes are also altered by climate, which includes the amount of insolation received by a planet; the type and amount of atmosphere; and the presence, distribution, and behavior of volatiles. Insolation amounts may vary significantly over the course of a single orbit and can change the phase and distribution of any volatiles that are present in hillslope materials. On Earth, the addition of fluids to slope materials is usually accomplished via precipitation; on planets with little or no atmosphere, no precipitation is possible. Thus, important hillslope processes – such as overland and subsurface flow and raindrop impact – may not be significant contributors in hillslope processes on low atmosphere planets.

For planets with precipitation, the composition of the precipitating fluid and surface bedrock will determine the types of erosion and subsequent landforms that will occur. Extraterrestrial hillslopes are unique environments that may be similar, but not identical, to hillslopes found on Earth, and care must be taken to understand how differences in hillslope parameters on these bodies may lead to changes in familiar processes and potential form.

Introduction

Hillslopes are one of the dominant landform features on Earth. Many types of processes act to create, modify, and attenuate slopes. The advent of space exploration has opened up new frontiers for the study of hillslope processes and indeed geomorphology in general (e.g., Baker, 1993). All terrestrial bodies in the solar system have hillslopes to some degree, including other planets, asteroids, moons, and even comets. Most observations of hillslopes on these bodies have come from orbital remote sensing, although to date there have been surface landers on Venus, the terrestrial Moon, Mars, Titan (a moon of Saturn), and the asteroids Eros and Itokawa. The bulk of this extraterrestrial research has focused on determining surface compositions and global-scale processes, although new high resolution imagery of planetary surfaces, notably on Mars, has allowed for the study of smaller scale landforms that can provide insight to processes on the hillslope scale.

Despite these new orbital data sets, the study of extraterrestrial hillslope processes is complicated in particular by a lack of observational data of the near subsurface of other

planetary bodies. In terrestrial studies, it is relatively straightforward to dig a trench to examine a soil profile or to drill down in several locations to determine how and where water flows through the subsurface. With few exceptions, extraterrestrial studies have only satellite images and perhaps some remote sensing spectroscopy data with which to explain the processes that formed the observed landforms. In the case of Venus, most surface data is in the form of radar imagery, which shows surface roughness. Few if any terrestrial geomorphologists have experience determining hillslope processes from such a data set! As Baker (1993) points out, it may be dangerous to make assumptions about the processes that have created a particular extraterrestrial landform. The idea of equifinality is thus of particular importance when assessing hillslopes on other planets, where processes that are unusual on Earth may be commonplace. Conversely, similar processes may be operating on these extraterrestrial hillslopes but in ways that are somewhat different than those same processes on Earth.

The goal of this chapter is to examine how changes in major hillslope system attributes may be expected to alter processes and, potentially, the resultant landforms. The major drivers of hillslope processes on Earth are gravity and climate, and so the discussion will focus on what is expected to occur on planets on which either gravity or climate (or both) differs from that of Earth. Climate here includes insolation, atmosphere, and the phase and behavior of volatiles. There are many potential hillslope processes that, while interesting and important, shall not be discussed here. Although the mineralogical composition of slope material has an effect on some hillslope processes, it shall not be discussed in any detail except in cases in which materials are unusual in some way (e.g.

the water ice bedrock of Titan). Similarly, chemical weathering of slope materials will not be examined, although such weathering has a significant effect on slope strength. Our understanding of compositions of the near surface environment of most planetary bodies is as of yet incomplete; only the Moon has had its subsurface environment studied in any meaningful way. Even so, it may be possible to broadly model subsurface processes on extraterrestrial bodies by modifying our assumptions about slope environments using the data we have obtained about surface conditions. Our purpose is to provide a baseline understanding of how changes in major hillslope system parameters may be expected to generally affect some important processes, including mass movement and overland flow. In light of the relative lack of information about most extraterrestrial subsurface environments, subsurface flow will be discussed in the context of observed surface morphologies.

Before examining how changes in gravity and climate may affect hillslopes, it is necessary to briefly discuss how extraterrestrial hillslopes may be formed and how slope materials may differ from those on terrestrial slopes. On Earth, surface topography is generally created by tectonics and volcanism, and is destroyed by erosion. To a certain extent, all three of these processes may act on extraterrestrial hillslopes, albeit in different ways and at different rates. Relief may be created by emplacing material (e.g., lava) on the surface or by faulting. Morphological evidence for volcanism is found on many solar system bodies, most notably on Venus, the Moon, Mars, and Io (a moon of Jupiter). The largest volcano in the solar system is Olympus Mons on Mars, although it is no longer active. Also on Mars is the great Valles Marineris rift valley, which is thought to have

been created as the result of uplift during the formation of the volcanic Tharsis bulge (Banerdt et al., 1992). Recently, new observations of young thrust faults on the Moon suggest that tectonics may be active there despite a lack of active volcanism (Watters et al., 2010).

In addition to these constructive processes, the topography of many extraterrestrial surfaces is also significantly altered by the process of impact cratering. On all solar system bodies, there is a constant influx of meteoric material from space, the vast majority of which is in the form of micrometeorites (~10-100 μm in diameter). Larger impactors are not common, but were more numerous in the early solar system. Impact cratering produces topography very quickly, with hillslopes that have distinct initial morphologies. The Earth and the Moon have had approximately the same rate of impacts over time, with a similar distribution of impactor sizes. However, the surface of the Moon retains a detailed history of these impact events, while few impact structures are observed on the Earth. This is because the Moon has few resurfacing mechanisms to rework crater materials. In contrast, the surface of the Earth is constantly reworked by erosion from the water cycle, as well as from the action of plate tectonics. As a result, relatively few impact crater structures remain on the Earth's surface today, and impact craters are not an important source of topography here. Figure 1.1 shows how the surface topography of Mars' moon Phoebus is dominated by a large impact structure; material appears to be shedding from the upper slope and collecting near the bottom.

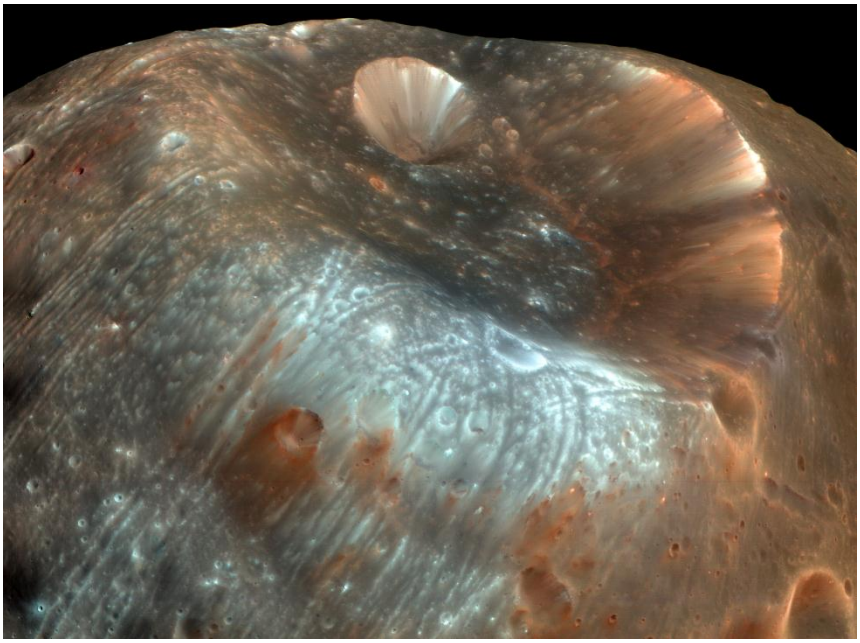

Fig. 1.1 Surface of Phobos, a moon of Mars ~ 22 km in diameter (north is to the left). The large 9-km diameter impact crater Stickney is a major topographic feature. Note the slope streaks on the interior walls of the crater and deposits of materials shed from the slopes at the base of the crater walls (center right). The gravity of Phobos is ~ 1/1000 that of Earth. Image credit: HiRISE PSP_007769_9015 (NASA/JPL/University of Arizona).

Notably, plate tectonics, a major mechanism for surface reworking, has not been observed to occur on any other planetary body, although some workers suggest that it may have occurred very early in Mars's history (Sleep, 1994; Connerney et al., 1999). Erosion from wind and the movement of liquids has been inferred on some planetary bodies, but the present day rates of erosion in those environments appear to be far lower than those on Earth (this will be discussed in more detail in the section on climate). As a result, impact structures will persist longer on these bodies and form a larger proportion of topographic features. Thus, many extraterrestrial hillslopes are found on the walls of impact craters. This has implications for both the structure and behavior of potential hydrological systems as well as slope profiles, and should be considered when examining specific hillslopes on other planets. On small bodies, the seismic shaking induced by

impacts can trigger mass movements on hillslopes (Moore et al., 1999a; Dombard et al., 2010) and may be a major factor in reworking surface materials (Miyamoto et al., 2007).

In addition to forming topography, impact cratering also creates the majority of unconsolidated materials on many extraterrestrial bodies. Each impact pulverizes some amount of surface material; while micrometeorites may only disturb the surface to a depth of a few millimeters, large impacts may fracture the crust as much as 20-30 km below the surface (de Pater and Lissauer, 2004). Over time, this fractured material will accumulate as more impacts occur. This material is called regolith, although oftentimes it will also be referred to as 'soil' in the planetary literature even though it has no organic component. Regolith that is mantled over a bedrock hillslope provides a source of sediment that may be transferred off of the slope via a number of processes. Even on airless bodies with no moisture, the presence of regolith allows for hillslope processes such as mass movements to occur. In the next section on gravity, we shall discuss how the behavior of regolith is expected to change under differing gravity fields.

The effects of gravity

Gravity affects almost every process that occurs on hillslopes, from mass movements to hydrology. It drives the detachment of materials from a slope and their subsequent behaviors, and is a major factor determining slope angle. Gravity also indirectly controls the chemical weathering rates of slope materials by controlling, in part, how quickly fluids percolate through the regolith. Each body within the solar system has its own unique gravitational acceleration at its surface due to its particular mass. In many cases,

this acceleration (g) is significantly different than Earth's, where g = 9.8 m s^{-2}. In contrast, on Mars g = 3.7 m s^{-2} and on the Moon g = 1.6 m s^{-2}.

On a terrestrial body, gravity works to move hillslope materials closer to the center of mass, i.e. down the slope. However, hillslope materials have a variety of properties that may allow them to resist this pull downslope, which are known collectively as the shear strength. The relationship between gravity and shear strength is dependent on many variables, but some systematic changes in response to lower gravity may be expected. In this section, we will examine how a change in gravity field may affect the behaviors of both unconsolidated and solid slope materials.

Angle of repose

The simplest model of a hillslope is a homogeneous pile of granular material. Piles of such unconsolidated material on a horizontal surface will form a cone whose internal angle between the surface of the cone and the horizontal surface is called the critical angle of repose. This angle describes how steep a slope made of unconsolidated materials may become; once this critical angle is exceeded, slope failure will occur. Although slopes are rarely made of simple piles, the angle of repose also dictates how steep a regolith mantle may become on a bedrock slope. Thus, understanding the angle of repose is important for predicting slope failure and understanding slope morphology.

The angle of repose may be thought of as the sum of the forces pulling a particle off of the slope and the forces keeping the particle in place. Gravity works to keep the particle

on the slope through friction and to pull it off the slope through the particle's mass. If we set aside for the present other factors that are not related to gravity (such as cohesion and pore pressure), then the forces acting on a grain on the slope of a sand pile at the angle of repose can be expressed as the sum of the resisting (frictional) and driving (gravitational) forces (Fig. 1.2). Friction is both a function of gravity and also the intrinsic properties of the slope material. This intrinsic component is expressed as the static coefficient of friction μ, which is an empirically derived, dimensionless quantity. The total force felt by a grain on the slope can be expressed as

$$F_t = mg \sin\theta - \mu mg \cos\theta \tag{1.1}$$

where m = mass of the grain; g = acceleration of gravity; θ = critical angle of the slope (angle of repose); and μ = coefficient of friction.

In the case where material is at the critical angle of repose, the forces on the grain are equal:

$$mg \sin\theta = \mu\, mg \cos\theta \tag{1.2}$$

Now the gravity term factors out, and the relationship can be rewritten as

$$\mu = \tan\theta \tag{1.3}$$

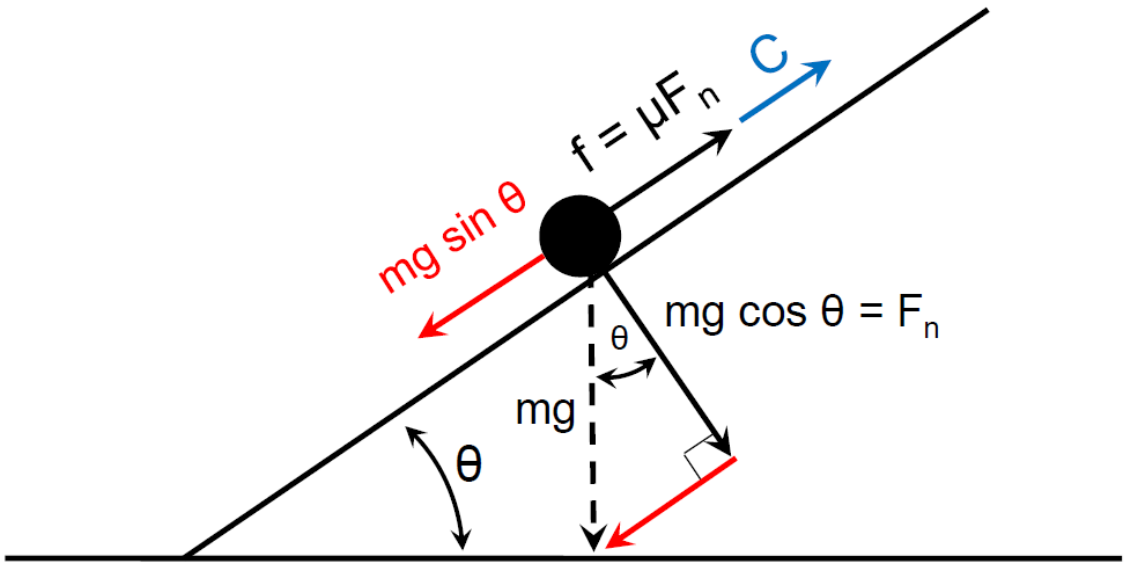

Fig.1.2. Inclined plane model of slope stability, where m = mass, g = gravity, θ = slope angle, f = friction, μ = coefficient of friction, F_n = normal force, and C = cohesion. The forces acting on a grain on the exterior slope of a pile of unconsolidated materials can be expressed as the sum of the forces pulling it down the slope (gravity) and the forces holding it on the slope (friction and cohesion). When the grain is motionless, the sum of these forces is 0.

From Eq. (1.3), we can see that the coefficient of friction is not dependent on gravity but rather on the angle of the material only. Thus, for a particular cohesionless granular material, the angle of repose will be the same regardless of gravity.

In slope materials with relatively large particles, the angle of repose generally increases with particle size. For example, the angle of repose of sand is generally smaller (~30-35°) than that of talus (~35-40°). However, there is a limit to this relationship; in very fine-grained materials, the angle of repose begins to increase again as particle sizes decrease (e.g. Zhou et al., 2002). This is the result of cohesion between grains produced by van der Waals forces. Halajian (1964) points out that even in the very dry environment found on the Moon, fine-grained lunar regolith is still expected to have cohesion. If cohesion (C) is added to the model shown in Fig. 1.2, Eq. (1.1) now becomes

$$mg \sin\theta = \mu\, mg \cos\theta + C \qquad (1.4a)$$

or

$$\sin\theta - \mu \cos\theta = \frac{C}{mg} \qquad (1.4b)$$

This demonstrates that when cohesion is taken into account, the gravity term remains; now the angle of repose may be increased in a cohesive material in a lower gravity environment. Thus, on a planet with lower gravity, fine-grained materials may have a higher angle of repose if enough moisture is available or if grain sizes are small enough (Fig. 1.3).

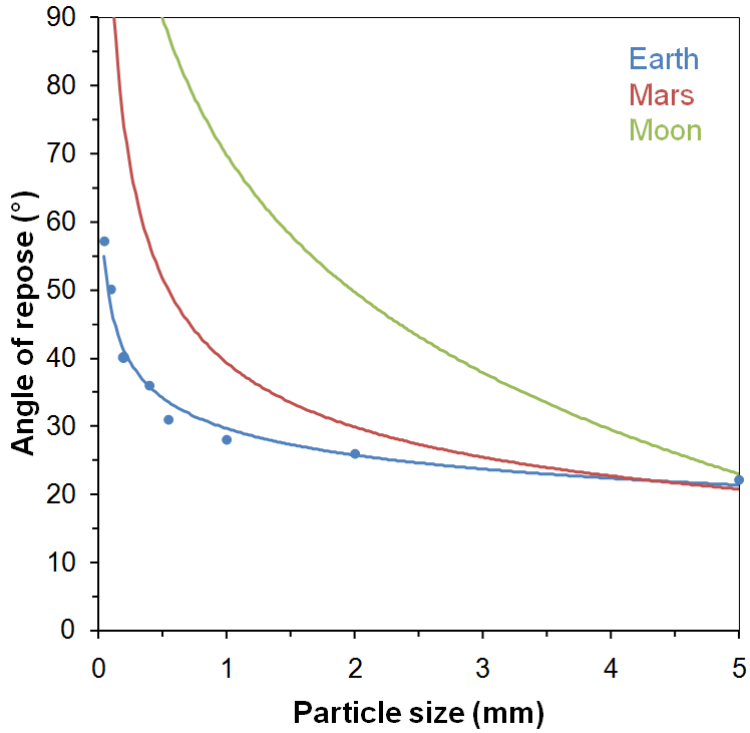

Fig. 1.3. Relationship between particle size and angle of repose in cohesive materials for Earth (blue), Mars (red), and the Moon (green). Curves for Mars and Moon derived from terrestrial experimental work by Carstensen and Chan (1976) and Zhou et al. (2002) (blue circles). In lower gravity fields, the angle of repose of dry unconsolidated materials may be significantly increased if grain sizes are small; this is due to the relative strength of intergrain attraction from van der Waals forces in relation to the weight of the particle.

Shear strength

Shear strength is the maximum strength of a material to resist deformation or yielding. In the above discussion of angle of repose, we see that both friction and cohesion provide shear strength to an unconsolidated material. Cohesion broadly refers factors that contribute to the shear strength of the material that are independent of friction, including root strength, van der Waals forces, and cementation. Because plant life has not yet been observed in extraterrestrial environments, this mechanism will not be addressed here.

The van der Waals forces are the weak attractive forces between molecules, and they are particularly important in producing cohesion in materials with small grain sizes. While this cohesion is often the result of thin films of water between grains, it may also occur in the absence of moisture in very fine-grained materials. The size at which van der Waals cohesion between grains becomes effective will differ in different gravity fields; at lower gravities, larger grains may still exhibit cohesion. This is due to the fact that as gravity is reduced, the apparent strength of the van der Waals forces increases in relation to the weight of a particle. Figure 1.4 shows how cohesion and weight change with increasing particle size. As cohesion decreases, the weight of the particle increases. However, for lower gravity fields such as the Moon, the weight of the particle is less than that of the same size grain on Earth. As a result, the total weight force felt by the grain is less on the Moon than on the Earth, and so cohesion is a relatively larger force in the system. Theoretical and experimental work by Halajian (1964) and Walton et al. (2007) showed that granular material on the Moon (where g = $1/6$ Earth g) may exhibit cohesion at grain sizes >1 mm, in contrast to the largest cohesive grains on Earth that are typically no

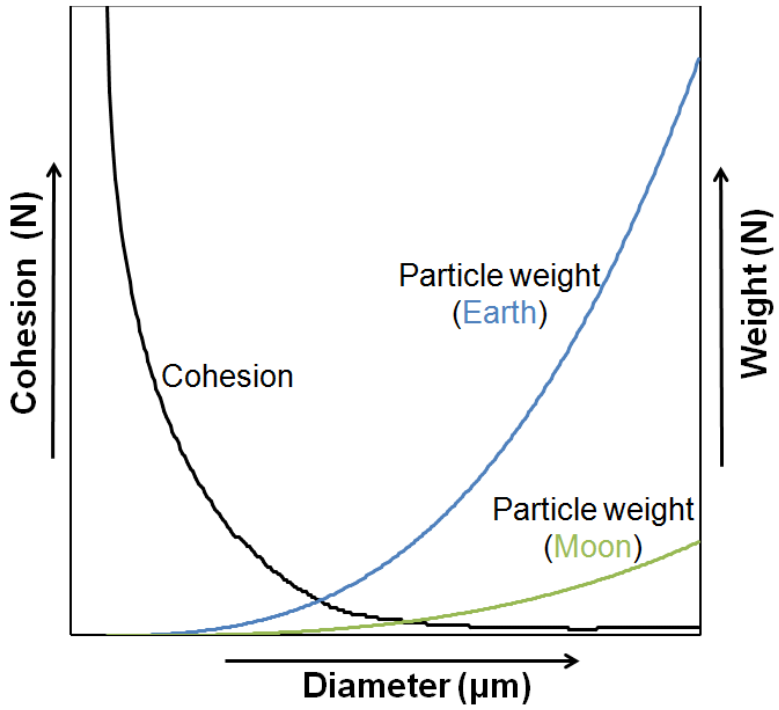

Fig. 1.4. Relative relationships between cohesion (N), weight (N), and grain diameter (μm) (note not to scale). On Earth (blue), the weight of the grain surpasses intergranular cohesion at a smaller grain size than on the Moon (green), leading to lowered angles of repose (see Fig. 1.3). Cohesion curve data from experimental work by Batel (1959).

larger than ~0.3 mm. Observations of slopes on the asteroid Eros suggest that electrostatic cohesion may be playing a role in slope steepening. Slopes on this body are relatively steep, with ~4% of the total surface area covered by slopes exceeding 30^{o} (Zuber et al., 2000).

In addition to van der Waals forces, cementation of grains also provides cohesive shear strength to slope materials. Grains may be bonded together either during their formation (such as occurs in rock) or by a secondary cement that forms between grains of unconsolidated materials. Such cohesion is chemical in nature and independent of gravity.

The shear strength (τ) of a slope material is the summation of resisting forces (friction and cohesion) and driving forces, and can be described with the Mohr-Coulomb model:

$$\tau = \sigma_n \tan \phi + C \tag{1.5}$$

where σ_n = effective normal stress (normal force); ϕ = angle of internal friction; and C = cohesion.

This is quite similar to Eq. (1.4a), which describes the total force acting on a grain at rest on a slope. As in that case, the angle of internal friction (ϕ) here is equivalent to the angle of repose when cohesion $C = 0$.

As previously discussed, the addition of water between grains can enhance cohesion. However, this effect is limited to small amounts of water. Once enough water is present between grains, van der Waals and hydrogen bonding are no longer effective, and the water now acts to push grains apart. This pore pressure acts against the normal force, which holds materials together. Equation (1.5) can be modified to

$$\tau = (\sigma_n - \mu_p) \tan \phi + C \tag{1.6}$$

where μ_p is pore pressure.

Because gravity is a component in the normal force, shear strength decreases with a decrease in gravity. However, recall from Eq. (1.4a) that when a particle is at rest on a slope, the resisting forces are equal to the driving forces. If Eqs. (1.4a) and (1.6) are combined, we can see that

$$mg\ \sin\phi = \left(\sigma_n - \mu_p\right)\ \tan\phi + C \tag{1.7}$$

Gravity is a term on both sides of the equation and will cancel out; and so even as shear strength decreases, the pull of gravity will be proportionally smaller. Since pore pressure is dependent on gravity, it will decrease proportionally with a decrease in gravity. However, cohesion is independent of gravity, and so a change in gravity will lead to this factor having a greater effect on the system. As a result, cohesion in unconsolidated materials may lead to steeper slopes on planets such as Mars that have lower gravity fields than Earth.

Changes in morphology and mass movement behaviors

The subtle relationship shifts between gravity, friction, cohesion, and pore pressure have implications for the behavior of all gravity-driven hillslope processes. One notable example is the maximum height a rock hillslope may achieve under different gravity conditions. Solid rock has significant cohesive strength because its constituent minerals are bonded together, and this strength is independent of gravity. As a result, basalt on Mars is functionally stronger than the same basalt on Earth and can form significantly higher structures there. Mars is home to Olympus Mons, the tallest volcano in the solar

system, which would not have the strength to support its great height in a higher gravity field such as on Earth.

We should note that electrostatic charging on small, airless bodies can significantly modify the behavior of slope materials in very low gravity fields. On these planets, incoming particles from the solar wind may act to charge surface particles on the sunlit side (e.g., Colwell et al., 2005). If the gravity field is relatively low, this charge may be sufficient to cause dust particles to levitate and allow them to become more mobile. Evidence for this behavior may be found on the relatively small asteroid 433 Eros (34 × 11 × 11 km). The surface of this asteroid contains over 200 smooth, flat dust ponds within craters made up of particles << 50 μm in size. Modeling by Hughes et al. (2008) suggests that levitating dust particles will preferentially move toward topographic lows, causing a net movement of small particles downslope to create the observed dust ponding.

More classic types of mass movements may also be expected to behave somewhat differently in a lower gravity field. These processes include slower movement of material via creep as well as sudden failures, such as occurs during rock avalanches and debris flows. Creep encompasses several processes, including the movement of single particles on the slope, movement of an overburden acting as a single mass, and movement of surficial soil deposits. On Earth, creep processes are often associated with changes in soil moisture and seasonal freeze-thaw cycles. As previously discussed, an increase in pore pressure will generally decrease the shear strength of regolith. From Eq. (1.7), we can see

that an increase in soil moisture content (e.g., pore pressure) in a lower gravity field is expected to weaken the slope material more than the same moisture content in a similar terrestrial slope. Thus, rates of creep for similar moisture content may be expected to be somewhat greater under lower gravity conditions. Similarly, the action of frost heave is expected to have a greater effect on downslope transport of slope materials in lower gravity fields than it does on Earth. Observations of lobate morphologies suggestive of solifluction have been made on Mars (e.g. Squyres and Carr, 1986; Mustard et al., 2001; Perron et al., 2003), but as of this writing no direct measurements have been made of rates of movement of these slope materials.

The behaviors of more rapid mass movements are also expected to be altered in different gravity conditions. A lower driving force (gravity) should lead to shorter runout lengths if cohesion remains the same. This has been observed in large landslide deposits on Mars, which have larger ratios of height of drop/length of runout (H/L) than landslides of similar volumes on Earth (McEwen, 1989). The H/L ratio describes the slope angle and is thus related to the coefficient of friction, suggesting that large landslides on Mars have higher coefficients of friction than their terrestrial counterparts. In fact, this result is describing the change in angle of repose that is expected from Eq. (1.4b), which shows that the angle of repose may be increased for cohesive materials in a lower gravity field. The coefficient of friction for a given material does not change with gravity (e.g., Legros, 2002), although changes to the angle of repose will alter the apparent coefficient of friction if cohesionless materials are assumed (e.g., Eq. 1.3).

Interestingly, on both Earth and Mars H/L decreases as landslide volume increases (e.g., McEwen, 1989; Melosh, 1989). In cases of large (> ~ 10^8 m^3) volumes, landslide materials appear to behave in a fluidized manner and have runout lengths that are significantly longer than the total vertical drop. The addition of fluid to slope materials will decrease shear strength and coefficient of friction, and will lead to higher mobility. However, this mechanism may not be viable on drier planets such as the extremely arid Moon, where similar landforms have also been observed. Melosh (1989) suggested that such flows may be supported by the interaction of individual grains with their neighbors, in what is known as acoustic fluidization. In these flows, friction between grains is lessened by a slight local vibration, but significant energy is not lost because there are no hard intergranular collisions. In this way, energy may be transferred as waves of particles interacting together, and ultimately the flow retains more energy as it moves than do lower volume slides that do not behave fluidly.

Acoustic fluidization can account for the apparently long runout distances observed in high volume landslide deposits on Earth and drier planets, without requiring the addition of a friction-reducing liquid. However, few if any terrestrial landslides may be termed ‘dry’ in the same way that a lunar landslide is dry; even in its driest regions, Earth is still a relatively wet place when compared to planets such as the Moon and Mars. Legros (2002) pointed out that similar trends in the terrestrial data used by McEwen (1989) and others with martian landslide data may in fact be demonstrating that martian landslides are not necessarily as bone-dry as was previously supposed. On Mars, many large landslides have volumes that suggest failure planes at significant depths, sometimes to a

few kilometers. This is well within the range of where models predict that subsurface ice may persist in the martian subsurface. Indeed, observations that post-date Legros (2002) have demonstrated that water ice can be found nearly at the surface of Mars, at least at mid to high latitudes (e.g., Holt et al., 2008; Smith et al., 2009a). Without considering the volatile content of the martian subsurface, it is difficult to evaluate the observed mass movement deposits found there. In the next section, we will discuss in more detail how volatile content, both composition and phase, may affect hillslope processes.

The effect of climate

The environment in which a hillslope exists has great influence over the types of processes that may occur there. Climate refers to the long-term variation in parameters such as temperature, atmospheric pressure, humidity, wind, and precipitation. These factors are often quite interdependent, and a change in one can lead to changes in another. The primary driver of climate is the amount of radiation received from the Sun, which directly affects the temperature of the surface at any given time. The transfer of this thermal energy though the atmosphere and surface materials creates wind and ocean currents, which in turn leads to weather that may include precipitation.

Climate determines the long-term distribution of volatiles on the planet, and as a result influences the creation and movement of sediment. On Earth, the hydrologic cycle dominates erosional processes. Water is abundant and can be found as a solid, liquid, and vapor throughout the planet at any given time. The most notable features of Earth when viewed from space are the large, blue water oceans and white water vapor clouds in the

atmosphere. It is impossible to discuss terrestrial hillslope processes without an examination of how water is transported to and through hillslope materials and the consequences of this interaction. Knighton (1998) noted that all of the major hillslope processes—mass movements, surface flow, subsurface flow, and raindrop impact—involve water to some extent, primarily in the liquid phase. Carson and Kirkby (1972) estimated that the total work done by water flow and rainfall impact on Earth is on the order of ~10^6 J m^{-2} y, with the majority of this work being done by streams.

The power of water to transport materials and to erode is tied to gravity, as water cannot flow without this driving force. If we imagine another planet that is just like Earth except that it has a lower gravity field, it would be relatively straightforward to recalibrate our understanding of hillslope hydrology to take this into account. Stream flow, rainfall impact, and mass movements would operate on hillslopes in much the same way, but the driving force would be somewhat lower. However, the terrestrial bodies in our solar system are not as straightforward as our imaginary Earth-like planet. Although water is found on many other planets, it is rarely stable in all three phases. In addition, water may not be the dominant or most abundant volatile material available.

A detailed discussion of all climatic parameters is beyond the scope of this work and, indeed, would be difficult to assess for most planets. Here we shall discuss how changes in two major parameters, insolation and atmosphere, can be expected to affect hillslope processes on extraterrestrial bodies, and how altering the amount and type of volatile materials available on a hillslope may be expected to change slope systems.

Insolation

Insolation is the amount of solar radiation that is received by a planet. Some of this energy is absorbed or reflected by the atmosphere, if there is one, and some reaches the surface. The amount of energy that the Sun provides to a planetary body is dependent on both its distance from the Sun as well as the inclination of its axis of rotation (obliquity), which determines how directly sunlight hits the surface at any given location. The distance of the planet from the Sun varies depending on the eccentricity of its orbit, which is always elliptical. The closest approach occurs at perihelion, while the most distant approach is at aphelion. Both obliquity and eccentricity vary over separate periods, which occasionally line up to produce a maximum insolation value if the axial tilt is toward the Sun when the planet is at perihelion, or a minimum if the axial tilt is away at aphelion. The numerous alignments that produce cycles of varying periodicity are known collectively as the Milankovitch cycles, and the changes in insolation that they produce are a major driver of climate on Earth (e.g., Hays et al., 1976).

Milankovitch-type orbital cycles are not limited to the Earth; all planets experience them to some extent. The orbit of Mars in particular is highly eccentric, and Mars' obliquity cycle is far more drastic than that of Earth (Ward, 1992). The variations in insolation over these cycles can cause significant changes in temperature both in the atmosphere and at the surface; insolation is effective as a climate driver in part because the behavior of volatile materials changes with temperature. When volatile materials are present, hillslope processes are dominated by their behavior.

The mean global average insolation received by a planet is a product of the mean distance and the solar constant. Irradiance decreases by the inverse square of the distance, and so the difference in irradiance between perihelion and aphelion can be described by the inverse square law:

$$\frac{I_p}{I_a} = \left[\frac{r_a}{r_p}\right]^2 \tag{1.8}$$

where I = irradiance at aphelion (a) and perihelion (p); and r = distance from Sun at aphelion (a) and perihelion (p).

On Mars, the maximum irradiance varies by ~ 224 W m^{-2} from aphelion to perihelion, producing ~ 45% difference in insolation (Haberle et al., 1993). Although the average irradiance of the Earth is much larger (~ 1300 W m^{-2}), the Earth's orbital eccentricity is far less, and as a result the irradiance only varies by ~ 6.9% (~ 90 W m^{-2}) from aphelion to perihelion. As a result, orbital eccentricity plays a larger role in determining both seasonal temperature changes and climate on Mars than it does on Earth.

To understand the effect of insolation at the hillslope level, the latitude and aspect of the region of interest must be taken into account. Haberle et al. (1993) described the insolation received by Mars at various times of the year and latitudes; these calculations may be generalized for any given planetary body in the solar system. The maximum amount of sunlight (S_{max}) incident on the atmosphere may be described as

$$S_{max} = \cos z \, S_0 \left[\frac{\bar{r}}{r}\right]^2 \quad (1.9)$$

where z = solar zenith angle; $\bar{r}$ = mean orbital distance; r = current orbital distance; and S_0 = solar irradiance at $\bar{r}$.

The solar zenith angle (z) is related to the latitude of the hillslope and solar declination, which is a measure of how high the Sun may be in the sky at a given time of day and season. As the Sun becomes higher in the sky, the sunlight hits the slope more directly, and the total amount of energy received is increased. Equation (1.9) suggests that if a volatile material is present in slope materials, it may be significantly affected by both diurnal and seasonal changes in insolation, which in turn will affect the availability of liquid for hillslope processes. Figure 1.5 shows a scarp near the martian north pole from which material has apparently just been shed. In this region, there is both water ice in the subsurface and seasonal CO_2 frost at the surface; all the seasonal CO_2 frost sublimates and is removed each spring along with lesser amounts of water ice. This image was captured during the transition from winter to spring as regional temperatures increased. Although it is not clear what triggered this particular mass movement, it is likely that seasonal removal of volatiles played a role in reducing the shear strength of slope materials on the scarp. Note that this image is the only instance of an extraterrestrial mass movement being observed at the moment it occurred.

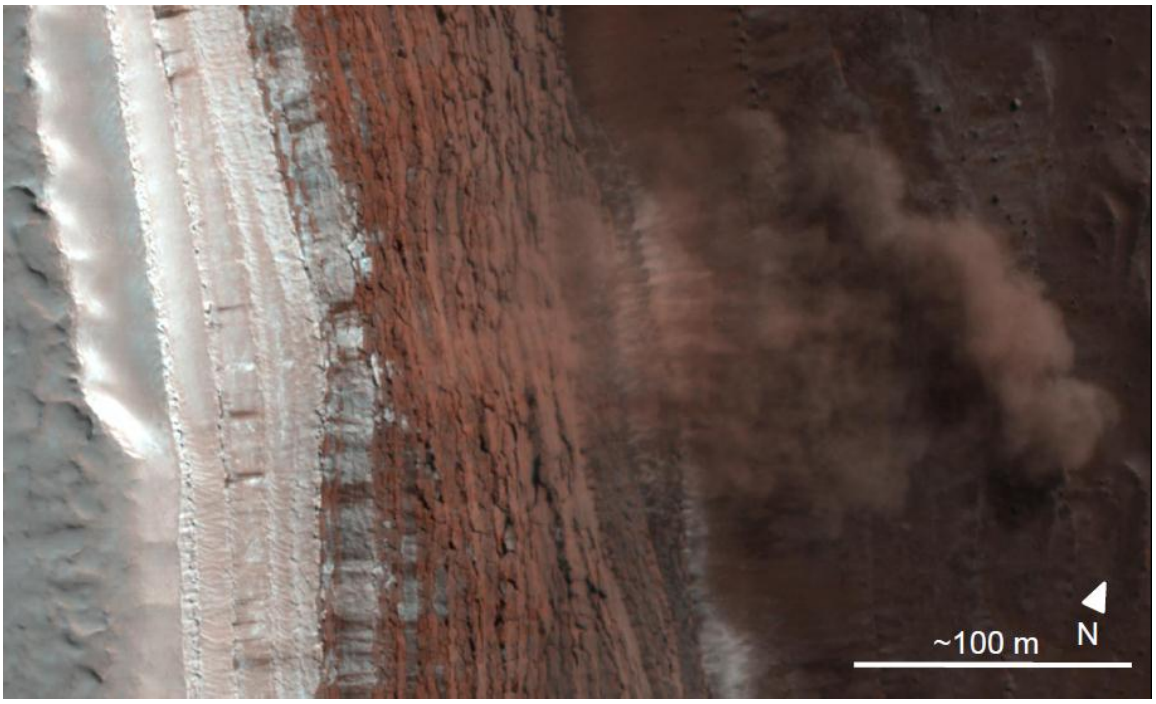

Fig. 1.5. A cloud of material from a recent mass movement event on Mars. By chance, this false color orbital image was captured while several avalanches of material were occurring in the same region, including the one pictured here; these are currently the only extraterrestrial mass movements observed as they occurred. This scarp is located in the northern polar region and is ~700 m high (higher elevation to the left, lower elevation to the right), with slopes as steep as 60°. The bright material visible on the top (left) of the scarp is seasonal CO_2 frost, while the reddish layers below are a mixture of dust and more permanent water ice. The triggering mechanism for these mass movements is unknown, but is likely related to seasonal melting of frost and thermal expansion and contraction of ground ice as temperatures increase during the transition from winter to spring. Image credit: HiRISE PSP_007338_2640 (NASA/JPL/University of Arizona).

Many workers have noted a connection between slope aspect, latitude, and the presence of small-scale gully forms on martian hillslopes (e.g. Malin and Edgett, 2000; Heldmann and Mellon, 2004; Balme et al., 2006; Bridges and Lackner, 2006; Lanza and Gilmore, 2006). This strongly suggests that insolation is affecting a volatile material in these hillslopes, producing fluids that may then do work on the slope material. Although the current surface temperatures and pressures on Mars are generally not conducive to liquid water, many models suggest that if subsurface ice is present in the regolith, it may be melted by insolation and produce transient liquid (e.g. Hecht, 2002). This is because many regions of the martian surface are occasionally at the triple point temperature (0°C)

and pressure (~ 6 mbar) of water. Although CO_2 is more abundant than H_2O, the triple point pressure of CO_2 is relatively high at ~ 5 bar, and so CO_2 is only found in the solid and vapor phases on present-day Mars. As a result, any melt fluid in the near surface is much more likely to be H_2O than CO_2.

The morphological evidence for insolation-triggered ice melt in the form of geologically recent debris flow deposits (e.g., Costard et al., 2002; Mangold et al., 2003; Balme et al., 2006; Lanza et al., 2010a; Levy et al., 2010a) and apparently fluvial gullies (e.g., Christensen, 2003; Balme et al., 2006; Soare et al., 2007) suggests that enough liquid water may be present to produce throughflow and mass movements on Mars. Figure 1.6 compares an image of a terrestrial debris flow deposit with a channeled hillslope on Mars. Note that the martian hillslope contains polygonal fracturing within the slope hollow, a feature which is often indicative of near subsurface ice on Earth. The Phoenix Mars Lander recently touched down on similarly patterned ground in the martian northern hemisphere ~ 60° N. latitude and found water ice only centimeters from the surface (Smith et al., 2009a).

There are far fewer observations of the surfaces of small solar system bodies than there are of Mars; however, insolation also appears to play a major role in surface reprocessing on many comets, asteroids, and moons. Comets are composed primarily of ices, and their highly elliptical orbits can bring them well within the orbit of Earth. At these times, their proximity to the Sun increases received insolation significantly, and hillslopes made of ices may be lowered or simply sublimated away at this time. If hillslope material is

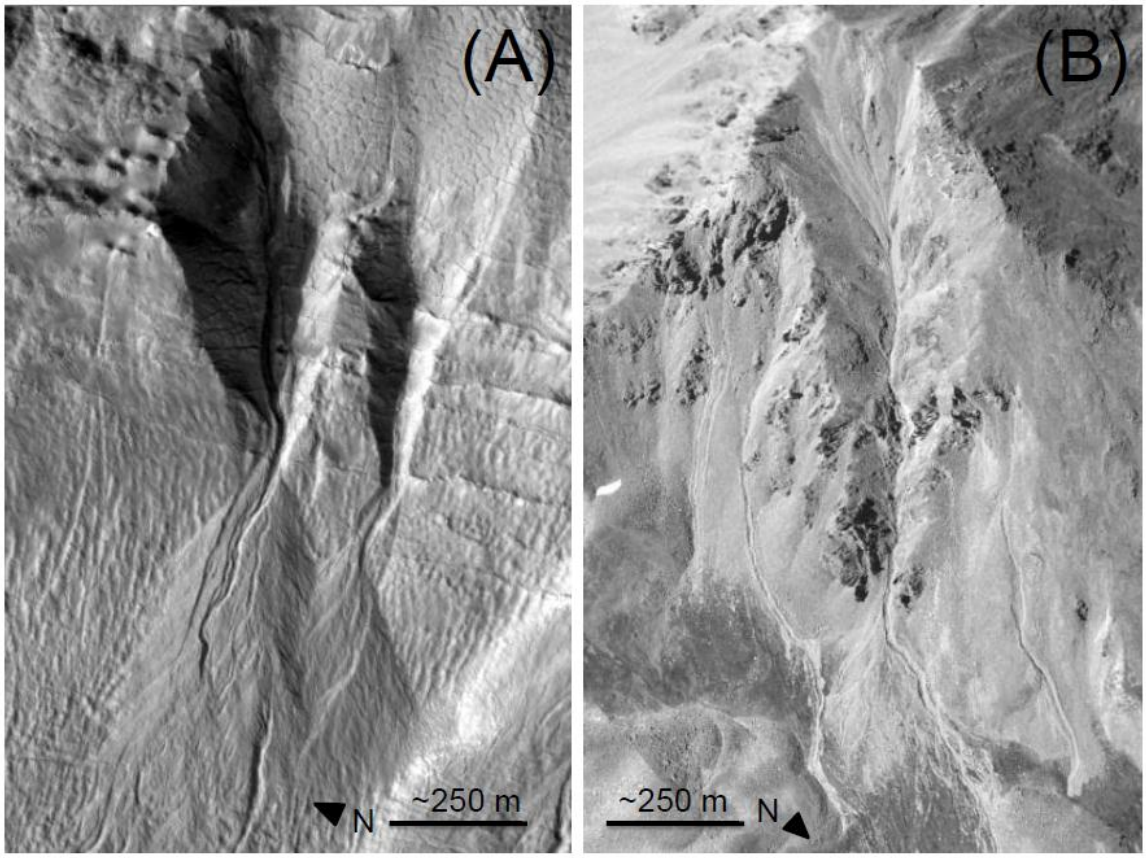

Fig. 1.6. A martian hillslope gully feature (A) and a terrestrial debris flow deposit of the same scale (B) on Torreys Peak, Front Range, CO. Note the polygonal patterned ground within and above the slope hollow in (A) (upper right), suggesting the presence of ground ice. Lobate apron deposits and leveed channels visible in (A) are highly suggestive of debris flow deposits. Image credit: (A) HiRISE PSP_001714_1415 (NASA/JPL/University of Arizona); (B) Google Earth. After Fig.1 in Lanza et al. (2010a).

composed of icy-rock regolith, an increase in insolation may free significant amounts of unconsolidated materials once ice has been removed by melting. This has been observed on Jupiter's moons Callisto and Ganymede and Saturn's moon Iapetus, where slumps of material on hillslopes are associated with ice sublimation (Fig. 1.7; Moore et al., 1999a; Spencer and Denk, 2010).

Atmosphere and precipitation

On Earth, water is most often transported to hillslopes via precipitation, which may take the form of either rain or snow. Precipitation generally occurs as the result of clouds of

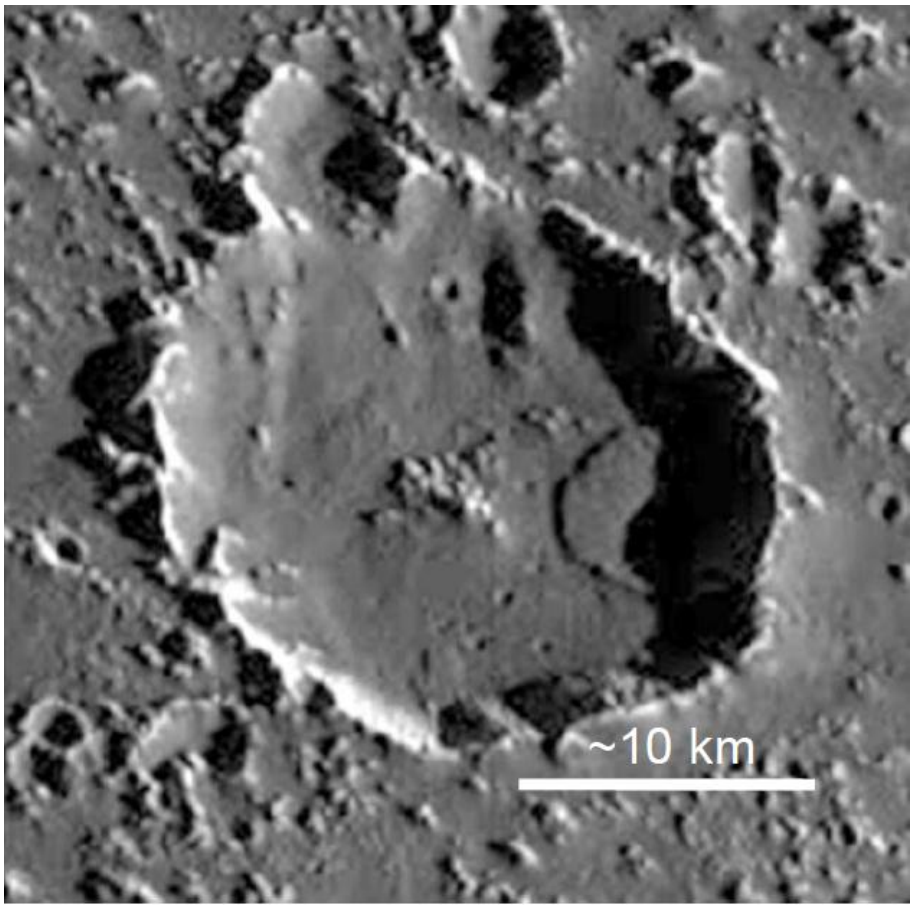

Fig. 1.7. A debris apron inside a crater on Jupiter's moon Callisto, Asgard region (right, partially in shadow). Many such crater wall slumps are observed on this body and are thought to have formed as the result of ice sublimation from unconsolidated surface materials; callistoan surface materials are composed primarily of a mixture of water ice and rocky materials. After Fig. 11 in Moore et al. (1999), Galileo image (NASA/JPL/ASU).

water vapor in the atmosphere becoming saturated; this is defined as reaching the maximum vapor partial pressure, which varies according to temperature and pressure. When saturation is reached, some vapor may begin to recondense as small droplets of liquid or as ice crystals, which then fall to the surface through the influence of gravity. Once on the ground, liquid water (rain) may infiltrate the regolith and percolate down the slope in the subsurface, or it may flow downslope on the surface as overland flow. Snow melt adds to both infiltration and overland flow produced from rainfall.

Precipitation is not possible without an atmosphere. There are few mechanisms available on airless bodies to emplace volatiles in hillslope material other than impactors. As a result, the effects of cohesion and friction are likely to be the most important parameters of hillslope processes on these planets, as previously discussed. For example, although large landslide deposits have been observed on the Moon, the extreme dryness of the regolith and lack of significant atmosphere on that body likely precludes mass movements triggered by a fluid (e.g., Howard, 1973). Even if a significant atmosphere is present, surface conditions do not always allow for precipitation to reach hillslopes. On Venus, precipitation consists primarily of droplets of sulfuric acid, which appears to evaporate before reaching the surface due to extremely high surface temperatures (de Pater and Lissauer, 2004). Although the venusian atmosphere consists primarily of CO_2, there appears to be no mechanism for this volatile to be emplaced in surface materials to do geomorphological work. The lack of fluids and relative lack of wind near the surface cause erosion rates to be quite low on Venus. This in conjunction with the young age of the surface leads to the creation of very little regolith, the depth of which is estimated to be only in the centimeters (Campbell et al., 1997; Saunders, 1999; de Pater and Lissauer, 2004). It is reasonable to expect that hillslope processes on Venus more closely resemble those on the Moon than on the Earth, despite the abundance of available volatile materials.

In addition to precipitation, volatiles may also be transported to hillslope materials though condensation from the atmosphere. On Mars, liquid precipitation is greatly limited because of its relatively thin (~ 6 mbar) CO_2 atmosphere and low average yearly

temperatures (~ 215 K). However, water ice crystals have been observed forming in clouds and falling to the surface (Whiteway et al., 2009), and both CO_2 and H_2O frost has been observed to condense on the surface (Jones et al., 1979). Figure 1.8 shows frost at the Viking 2 landing site in Utopia Planitia, in the northern hemisphere of Mars. Large differences in seasonal insolation cause both water vapor and large amounts of CO_2 (~ 25% of the total atmosphere) to freeze out of the atmosphere in the winter hemisphere (James et al., 1992). During the winter, these atmospheric volatiles may be emplaced in the pore space of slope regolith, where they remain until the next summer. In higher latitudes, water ice may persist through much of the summer. In addition to seasonal volatile deposition, Mars may have also had longer term episodes of ice deposition in the lower latitudes during periods of high obliquity (e.g., Costard et al., 2002; Head et al., 2003; Levy et al., 2010b). Recent results from orbiting ground penetrating radar appear to confirm the presence of large amounts of subsurface ice (Holt et al., 2008).

Condensed volatiles in slope materials have the potential to become a source of liquid, which will have a major influence over the types of hillslope processes that may occur. As previously discussed, the shear strength of slope materials is lowered with an addition of liquid in pore spaces (Eq.1.6). In addition, fluids may also move slope materials through the driving force of gravity. In lower gravity fields, this amount of work is expected to be somewhat lower, although in some cases gravity may not be a particularly important factor. However, without an atmosphere and a volatile cycle of some sort, extraterrestrial hillslope processes are limited to the gravitational effects as previously discussed. Thus far, liquid precipitation that reaches the surface has only been observed

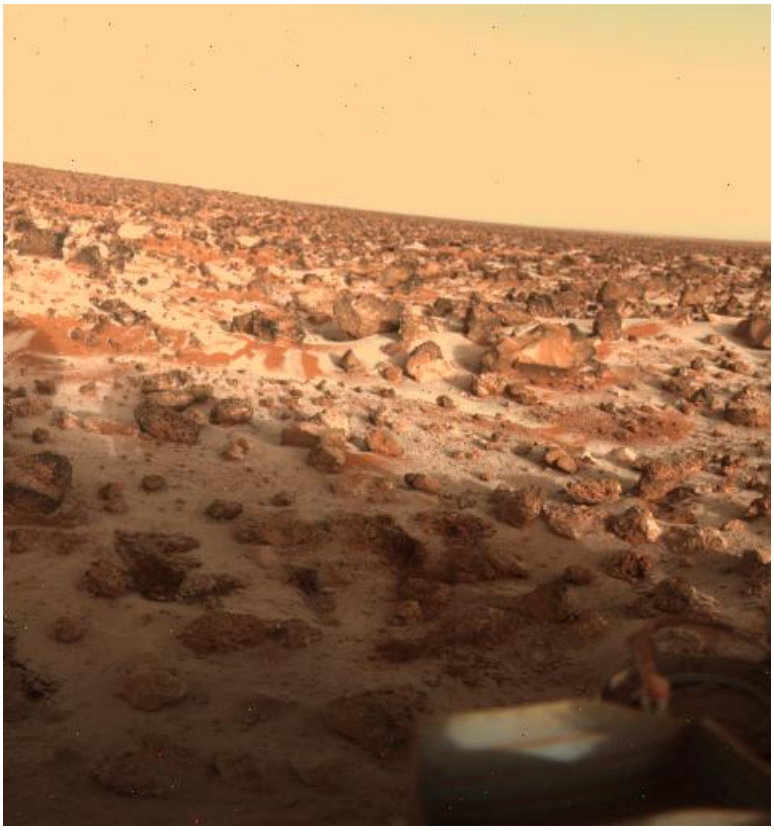

Fig. 1.8. Water ice frost on the martian surface as seen by the Viking 2 lander in 1979. View is to the S-SE from the landing site at Utopia Planitia in the northern hemisphere (~ 44.57° N., 225.74° E.). Image credit: Viking 2 Lander P-21873 (NASA/JPL).

on Earth and Titan, a moon of Saturn (Hueso and Sánches-Lavega, 2006; Graves et al., 2008), although it may have occurred in the past on Mars (Fanale et al., 1992). Titan is relatively distant from the Sun and is much colder than the Earth, and so its volatile cycle is dominated by hydrocarbons, most notably liquid methane (Toon et al., 1988; Tomasko et al., 2005; Hueso and Sánches-Lavega, 2006). As we shall see in the next sections, this compositional difference in liquid precipitation may lead to significant changes in the behavior of these fluids on hillslopes.

Raindrop Impact

For planetary bodies on which liquid precipitation is possible, raindrop impact becomes a potential force for shaping hillslopes. When raindrops collide with a slope surface, they exert both shear and normal forces. The normal component works to compact the slope material, while the shear component works to detach slope material. The raindrop derives its energy from gravity (e.g., falling from some height), and so a raindrop of a particular size under lower gravity conditions might be expected to have a lower energy and less total collisional force. Gabet and Dunne (2003) modeled rain power in terms of kinetic energy (E_k) as a mass of water per unit area colliding with a bare hillslope:

$$E_k = \frac{\rho i t v^2 \cos\theta}{2} \tag{1.10}$$

where ρ = density of fluid; i = rainfall intensity; t = duration of storm; v = raindrop velocity; and θ = slope angle

This relationship shows that changes in gravity and fluid composition should make a significant difference in the total kinetic energy of a raindrop. On Titan, both the gravity field and fluid density are reduced ($\rho_{methane} < \rho_{water}$), and so a raindrop is expected to have less total kinetic energy. Both the rainfall intensity and storm duration also have a large influence over the total energy imparted to the slope, so precipitation from intense storms may have significant erosional power even if individual raindrops have lower total energy.

One should note that the velocity of raindrops is limited not only by gravity but also by the thickness of the atmosphere; once a raindrop reaches its terminal velocity, it cannot accumulate additional gravitational energy with which to impact the surface. The terminal velocity is reached at the point when the weight of the drop is equal to the atmospheric drag forces operating on it (Foote and du Toit, 1969). The relationship can be expressed as

$$mg = \frac{1}{2}\rho_{atm} V^2 C_D \pi r^2 \quad (1.11)$$

where ρ_{atm} = density of the atmosphere; V = terminal velocity; C_D = drag coefficient (determined by raindrop shape); and r = radius of the drop.

What happens when both gravity and atmospheric pressure are reduced? If we take the example of Mars, we can see that although gravity is reduced to 0.33 g, the atmospheric density is reduced to 0.01 ρ_{atm}, making raindrop velocities (and thus kinetic energies) higher on Mars than on Earth. Although liquid rain has not been observed on present day Mars, there is much debate over whether the martian climate may have been significantly warmer and wetter in the past, allowing for the possibility of water rain (e.g., Fanale et al., 1992). On Titan, the gravity field is significantly lower than that on either Earth or Mars (~ 0.14 g), but the atmosphere is significantly more dense (~ 4.3 ρ_{atm}). Lorenz (1995) found that raindrops on Titan are likely to have significantly lower terminal velocities than terrestrial raindrops because of the thick atmosphere and the low surface tension of methane drops, leading to a potential reduction in erosional power.

The relationship in Eq. (1.11) suggests that the total number of raindrops (i.e., rainfall intensity) may make up for the decreased energy of individual raindrops. Knighton (1998) described the rate of detachment (D_r) from raindrop impact as

$$D_r = a\, I^b s^c \tag{1.12}$$

where I = rainfall intensity; s = slope angle; and a, b, c are empirically derived coefficients.

Although gravity does play an indirect role in detachment rate in the form of slope angle (s), the rainfall intensity (I) has a much larger influence overall given the relative values of b (~ 2) and c (~ 0.2-0.3) (Knighton, 1998). Modeling based on observations of Titan's surface suggests that intense rainfall is a common occurrence there (Hueso and Sánches-Lavega, 2006). When evaluating the potential effects of precipitation on extraterrestrial hillslopes, it is likely that the most important parameters are the amount of rain and the time period over which it is delivered, unless the atmosphere is extremely thin and the gravity is high.

Overland Flow

Once raindrops have reached the surface, they may either infiltrate into the regolith, or they may collect and flow downslope along the surface. In both cases, overland flow may be generated depending on the properties of the slope regolith as well as the amount of

water available. There are two main types of surface flows: Hortonian and saturation. In Hortonian overland flow, the infiltration limit of the regolith is reached and excess water flows along the surface as sheetwash. In saturation overland flow, the regolith becomes saturated by the addition of rainwater and cannot absorb additional fluid, and excess water must flow along the surface. In both cases, fluid flow exerts a shear force along the surface that may cause detachment and transport.

Although overland flow on Earth is generally the result of rain, precipitation is not required for such flow to occur. If ice in the regolith melts and saturates slope materials, fluid may be pushed upward and begin to erode the slope surface. Overland flow is a major control on hillslope and, indeed, regional topography. As water flows down hillslopes, it breaks up into smaller, more concentrated flows in rills and gullies, which in turn increase erosion in those areas, creating dissected terrains composed of spurs and gullies. Horton (1945) described the shear strength of infiltration-limited saturation flow (τ_H) as

$$\tau_H = \rho_f g d \sin\theta \tag{1.13}$$

where ρ_f = density of fluid; g = acceleration of gravity; d = depth of flow; and θ = slope angle.

Under a lower gravity field, the shear stress on slope materials from overland flow of water will be proportionally lower than on Earth. In addition, a lower density fluid will

also contribute to a lower total shear strength flow. On both Mars and Titan, the shear strength of overland flow is expected to be decreased as the result of the lower gravity fields on those bodies. In addition, the methane surface fluids on Titan have a significantly lower density than water, further reducing the shear strength of overland flow there.

For detachment to occur, the shear stress must reach some critical value to overcome the shear strength of slope materials. As previously discussed, the cohesion of unconsolidated materials in lower gravity environments is expected to have a greater effect in fine-grained materials. This suggests that channel initiation through overland flow may be somewhat more difficult in very fine grained regolith and may require additional fluid (i.e., increased depth *d*) to occur. However, in materials that already contain some moisture, pore pressure acts to weaken slope materials more under lower gravity conditions. As a result, a reduced depth of overland flow may be needed to detach materials in sufficiently moist materials.

Although no overland flow has been observed on Mars, there are numerous landforms on the surface that suggest that overland flow occurred there in the past, including large- and small-scale channels, streamlined, teardrop-shaped 'islands,' valley networks, and even an apparent delta deposit (Baker et al., 1992; Malin and Edgett, 2003). On martian hillslopes, smaller scale channel features have also been observed. Collectively known as gullies, these features exhibit a range of morphologies that are often suggestive of overland flow (Fig. 1.9). From cross-cutting relationships, martian gullies appear to be

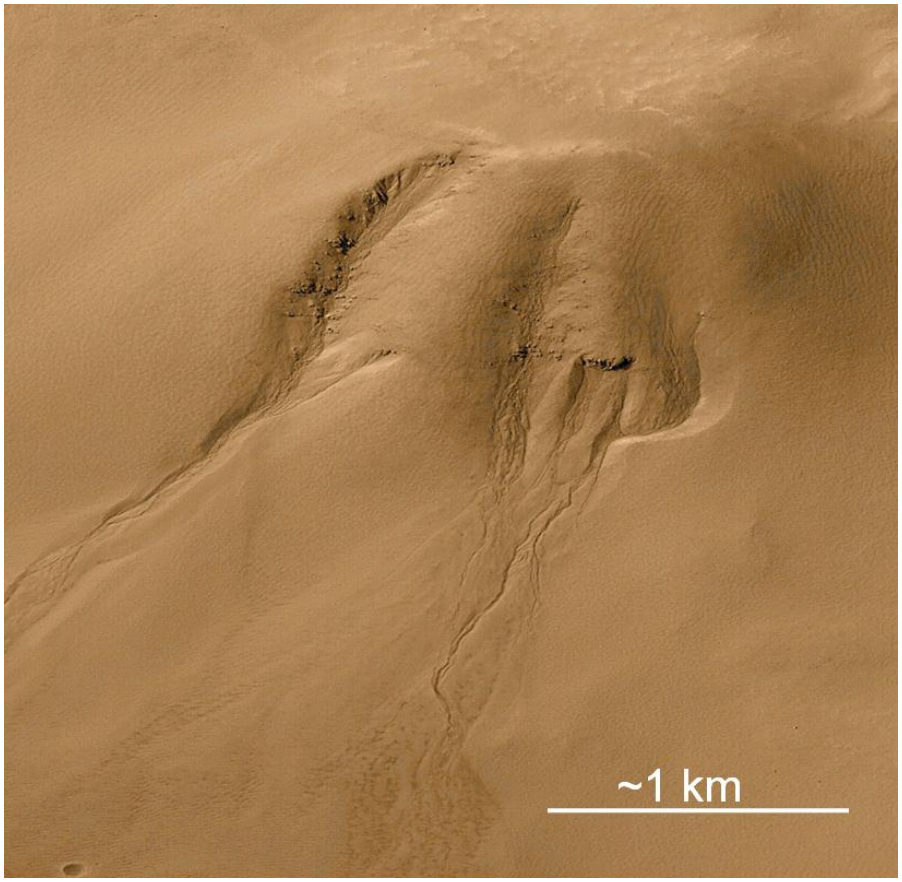

Fig. 1.9. Channeling on a martian crater hillslope in the Noachis Terra region (~ 54.8° S., 342.5° E.). Several types of processes may have operated on this hillslope to form the observed morphologies, including overland flow. Image credit: MOC2-238 (NASA/JPL/MSSS).

younger than many of the other water flow features on Mars, and some have been estimated to have formed within the last ~ 1.25 Ma (Schon et al., 2009). It is difficult to determine the source of the fluid that formed these channels or the exact environment in which they formed; many workers have modeled gully formation via overland flow using different values for parameters such as regolith moisture content, grain size, fluid composition, flow duration, and many more. Nonetheless, we can see from Eq.(1.13) that somewhat more water (greater depth d) is likely to be required to move unsaturated, cohesive, fine-grained material on a martian slope during overland flow conditions.

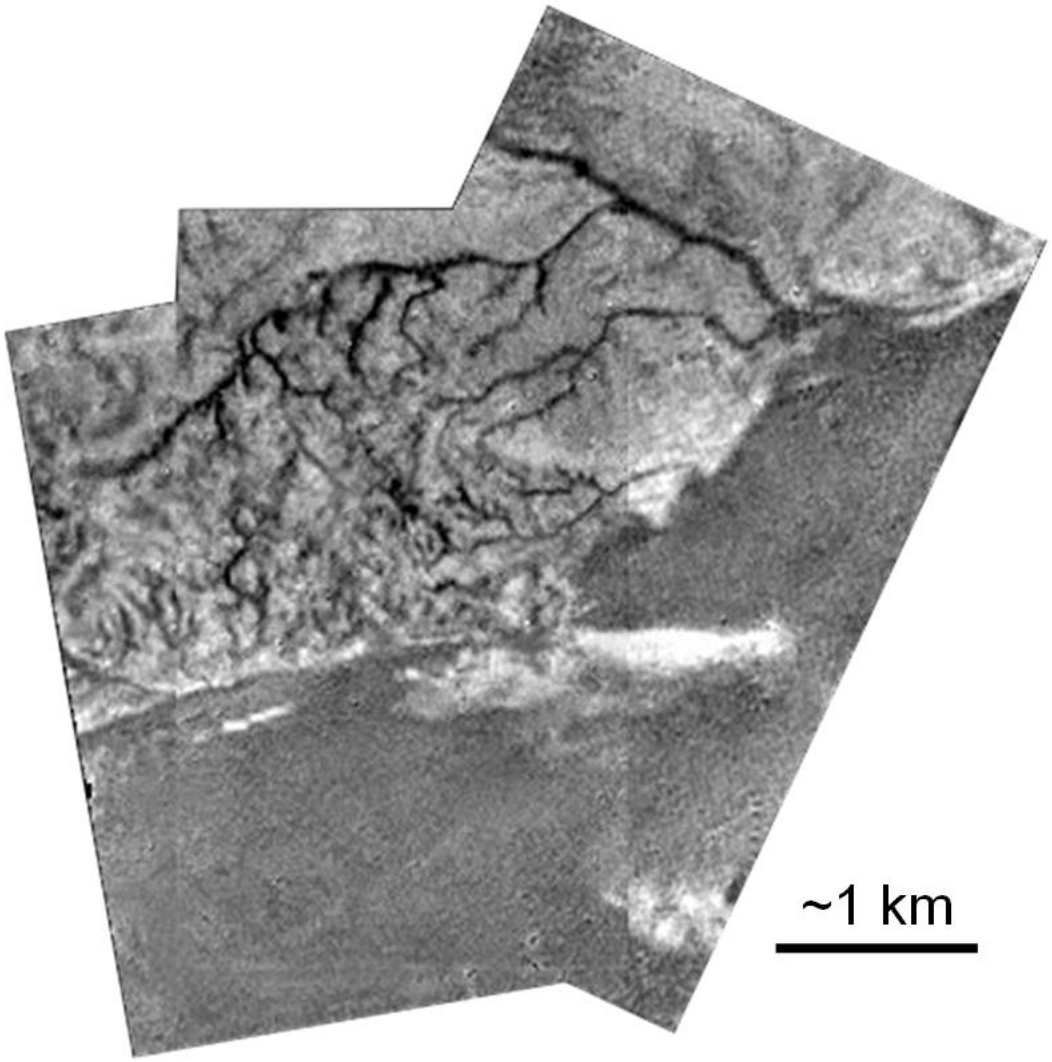

Fig. 1.10. An apparent drainage network for liquid methane on the surface of Titan, a moon of Saturn. The darker albedo region near the bottom of the image may represent an ocean, while the lighter albedo regions to the top of the image may be land composed of water-ice bedrock. The large network appears to originate in high topography near the shoreline and drains toward the right side of the image into the darker albedo region in the upper right. The images in this mosaic were obtained by the Huygens Descent Imager/Spectral Radiometer as it descended through the atmosphere to the surface. Image credit: NASA Planetary Photojournal PIA07236 (ESA/NASA/JPL/University of Arizona).

Recent results from the Huygens probe on Titan suggest that there is significant channeling on the titanian surface in the present day. Figure 1.10 shows an aerial image of what appears to be a drainage network on a hillslope next to a shoreline (Tomasko et al., 2005). The primary bedrock appears to be water ice (Griffith et al., 2003; Zarnecki et al., 2005), although this is likely to be mixed with additional organic materials. Currently,

many characteristics of these surficial materials are unknown, including grain size and cohesiveness. Prior to landing on the surface, the available data sets suggested that mechanical erosion was unlikely to produce significant sediment transport, despite the low average density of icy surface materials (Lorenz, 1995; Lorenz and Lunine, 1996). However, recent images of what appear to be dendritic drainage patterns on the surface (e.g., Fig. 1.9) suggest that there is a mechanism for channel formation. With cohesionless materials and enough rain, overland flow may detach and transport regolith from titanian hillslopes (Burr et al., 2006; Perron et al., 2006). More information about the nature of the unconsolidated material is needed before a full understanding of overland flow on Titan may be reached. Equation (1.13) suggests that it is reasonable to assume that the lower gravity and fluid density would make erosion from overland flow require somewhat more fluid to occur.

Subsurface Flow

Once fluids are present in slope materials, they may move through the subsurface through pore spaces within the regolith. Flow is created by both the gravity acting on the mass of the fluid and tensional forces created by hydraulic pressure. The rate at which fluid moves through regolith (v) is described by Darcy's equation:

$$v = -K\frac{h_1 - h_2}{L} \tag{1.14}$$

where K = hydraulic conductivity; $h_1 - h_2$ = change in hydraulic head; and L = length over which hydraulic gradient is measured.

Here, both gravity and the properties of the fluid are already taken into account when hydraulic conductivity and head are determined. The hydraulic conductivity *K* describes how easily a fluid will move through a particular medium (Heath and Trainer, 1968):

$$K = C d^2 \left(\frac{\rho g}{\eta}\right) \tag{1.15}$$

where *C* = factor describing the geometrical properties of the medium; *d* = factor describing grain size or pore size; ρ = density of the fluid; η = viscosity of the fluid; and *g* = acceleration of gravity.

Although *K* may be estimated for various materials by particle size, it is often empirically measured for a particular system. Equation (1.15) suggests that *K* will generally decrease on planets with lower gravity and will also change depending on the type of fluid. On Titan, both the density and viscosity of methane are lower than liquid water, and the gravity field is also lower. With a fluid density ~ 0.45 ρ_{water}, fluid viscosity ~ 0.12 η_{water}, and gravity ~ 0.14 *g*, the value of *K* will increase for a given material on Titan.

In addition to hydraulic conductivity, Darcy's equation (Eq. 1.14) also includes the change in hydraulic head, which describes the energy gradient that allows fluid to flow. Hydraulic head is dependent on both the elevation and density of the fluid, and can be described as the combination of elevation head and pressure head (Schwartz and Zhang, 2003):

$$h = z + \left(\frac{P}{\rho g}\right) \tag{1.16}$$

where z = elevation of the fluid; P = pressure exerted by the water column; ρ = density of the fluid; and g = acceleration of gravity.

Like hydraulic conductivity, hydraulic head is affected by the fluid density as well as the strength of the gravity field. If either ρ or g is reduced, the hydraulic head at a certain elevation z will also be reduced.

With this understanding of hydraulic conductivity and head, we may return to Darcy's equation (Eq. 1.14) to see that a decrease in gravity will lead to a decreased rate of fluid movement in hillslope materials. In addition, a change in fluid composition will also lead to changes in fluid behavior. Although these are important generalities to keep in mind, it is difficult to evaluate subsurface flow on specific extraterrestrial hillslopes without a better understanding of the characteristics of the specific slope materials. From Eq. (1.15), it is clear that the amount of pore space available, whether from intergrain spaces or fractures, has a large influence over hydraulic conductivity. This is highly dependent on the properties of the slope material, in particular its composition, which may not currently be well understood for most extraterrestrial hillslopes.

Despite these difficulties, there may be surface features that can provide evidence for subsurface flow. Sapping describes the process by which the surface is undermined by

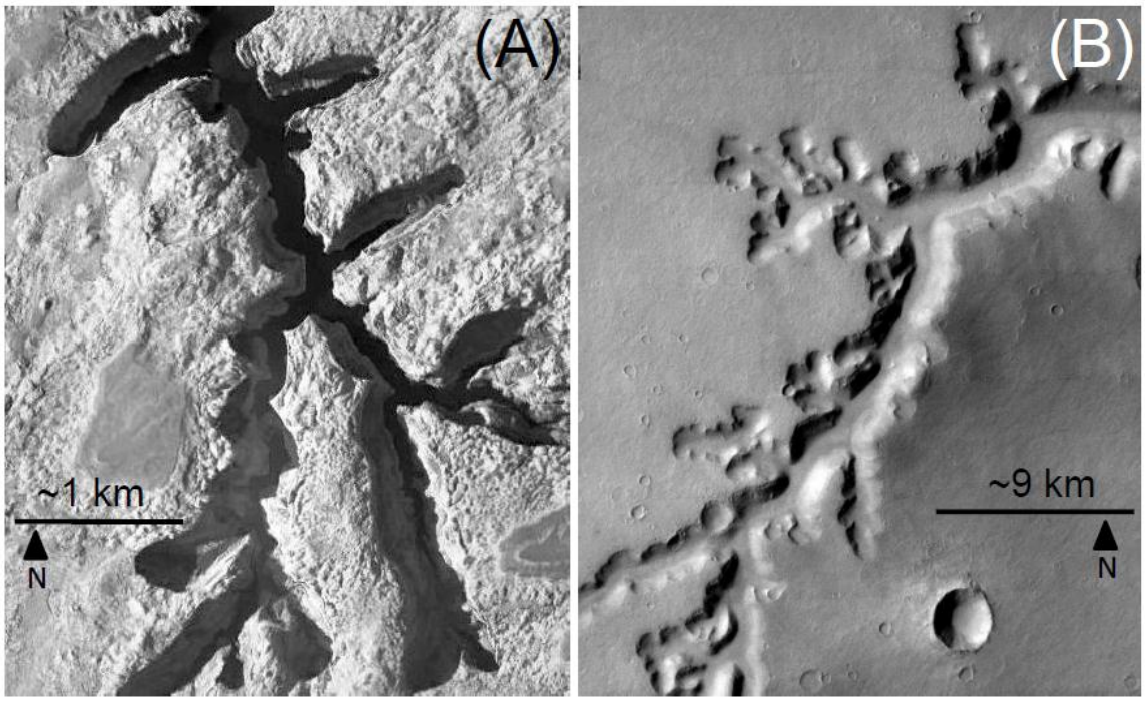

Fig. 1.11. Sapping features found on Earth in Iceberg Canyon, UT, at ~ 37.3° N., 110.7° W. (A) and morphologically similar features on Mars in Nirgal Vallis at ~ 27.1° S., 316.9° E. (B). Note the box headed alcoves present in both (A) and (B). Illumination is from the N-NW in both images. Image credit: (A) Google Earth; (B) THEMIS V01962005 (NASA/JPL/ASU).

the action of subsurface fluid that is often broadly distributed. Features formed by sapping include broad, flat gullies with steep sides and box-headed canyons with sharp edges (e.g., Jones, 1997). Similar features are widely observed on the surface of Mars (e.g., Sharp, 1973, 1980; Laity and Malin, 1985). Figure 1.11 shows an example of sapping features on Earth and a similar landform on Mars.

There is much debate over the origins of these putative sapping features on Mars. Early workers suggested that removal of magma or even ground ice in the past were the likely causes of the so-called fretted terrains on Mars (Sharp, 1973). However, subsequent observations of the martian surface have shown that ground ice may still play an active role in shaping the surface today. It is challenging to model slope hydrology on Mars with little information about the subsurface; nonetheless, it may be possible to come to

some general conclusions about how sapping on Mars may differ from that on Earth. If we combine our understanding of the Coulomb shear strength equation (Eq. 1.6) with Darcy's equation (Eq. 1.14), it is clear that despite lower expected flow rates, adding fluids to martian slope materials will significantly decrease shear strength. This suggests that surface collapse from sapping on hillslopes may be somewhat easier to accomplish on Mars than on Earth, and potentially less water is required as a result. However, much more work on the properties of the martian subsurface is needed to confirm this hypothesis.

Summary

Here, we have explored how hillslope processes may be altered when major environmental parameters are changed from their terrestrial values. As on Earth, extraterrestrial hillslope processes are greatly influenced by gravity and climate, both of which vary significantly throughout the bodies in the solar system. Changes in gravity will lead to changes in slope height, angle, and shear strength, and will lead to different mass movement behaviors and deposits. Changes in climate will affect the amount and distribution of volatiles available for doing geomorphic work and thus also indirectly controls the shear strength of slope materials. Of course, there are an almost infinite number of parameters that can be altered on extraterrestrial slopes, each of which will change the processes—and ultimately landforms—that occur there. Each hillslope must be considered individually, and care must be taken to understand how process leads to form in a particular environment. Analogy with terrestrial forms and processes is useful, as we may study and restudy these freely; and physics operates in much the same way

throughout the solar system. However, it is important to recognize that extraterrestrial environments may produce results that are unique to that body. The example of an asteroid such as Eros is apt in this context; the electrostatic levitation of dust particles certainly has no analogy on Earth. We are also limited by the specific data sets returned from a particular body. Extraterrestrial data sets are dominated by information about Mars and the Moon, while other bodies such as Titan have had few exploration missions sent to them. Nonetheless, much can be learned about hillslopes in these environments from very basic observations. With a solid understanding of the underpinnings of terrestrial hillslope processes, we may allow terrestrial analogy to guide us while remaining open to the possibility of unique or altered hillslope processes on other planets.

Chapter 2

Evidence for debris flow gully formation initiated by shallow subsurface water on Mars

Article citation: Lanza, N.L., Meyer, G.A., Okubo, C.H., Newsom, H.E., and Wiens, R.C. (2010). Evidence for debris flow gully formation initiated by shallow subsurface water on Mars. *Icarus* 205, 103-112.

Abstract

The morphologies of some martian gullies appear similar to terrestrial features associated with debris flow initiation, erosion, and deposition. On Earth, debris flows are often triggered by shallow subsurface throughflow of liquid water in slope-mantling colluvium. This flow causes increased levels of pore pressure and thus decreased shear strength, which can lead to slide failure of slope materials and subsequent debris flow. The threshold for pore pressure-induced failure creates a distinct relationship between the contributing area supplying the subsurface flow and the slope gradient. To provide initial tests of a similar debris flow initiation hypothesis for martian gullies, measurements of the contributing areas and slope gradients were made at the channel heads of martian gullies seen in three HiRISE stereo pairs. These gullies exhibit morphologies suggestive of debris flows such as leveed channels and lobate debris fans, and have well-defined channel heads and limited evidence for multiple flows. Our results show an area–slope relationship for these martian gullies that is consistent with that observed for terrestrial gullies formed by debris flow, supporting the hypothesis that these gullies formed as the result of saturation of near-surface regolith by a liquid. This model favors a source of

liquid that is broadly distributed within the source area and shallow; we suggest that such liquid could be generated by melting of broadly distributed icy materials such as snow or permafrost. This interpretation is strengthened by observations of polygonal and mantled terrain in the study areas, which are both suggestive of near-surface ice.

Introduction

A variety of gully landforms on Mars were first described by Malin and Edgett (2000). Cross-cutting relationships imply that these landforms are relatively young; they overlie features such as dunes that are usually young, transient landforms. Gullies also have sharp relief, which is not expected in older features that have had time to erode or be filled in by either mass wasting or aeolian processes. New bright-toned deposits of unknown material that have low relief and fan-like morphologies have been observed to form on gullied hillslopes over the past 10 years, suggesting that some of these gullies may still be actively forming (Malin et al., 2006). Additionally, recent crater count studies on gullies confirm the youth of these features (Malin et al., 2006). New imagery from the High Resolution Imaging Science Experiment (HiRISE) (McEwen et al., 2007) onboard the Mars Reconnaissance Orbiter (MRO) is providing detailed high resolution images that allow gullies to be examined in greater detail than was possible with previous data sets.

Many workers (e.g. Malin and Edgett, 2000; Edgett et al., 2003; Heldmann and Mellon, 2004) have observed that gullies lie primarily poleward of 30° in both hemispheres. Malin and Edgett (2000) suggested that this latitudinal dependence indicates a

relationship between insolation and gullies, pointing to a thermal control on their formation. Subsequent studies involving larger data sets suggest that gully location also appears to have a poleward limit ~50° latitude in both hemispheres, again supporting the idea that gullies may form preferentially in areas that are thermally suitable (Balme et al, 2006; Bridges and Lackner, 2006). Lanza and Gilmore (2006) examined the amount of insolation received by martian hillslopes in the northern hemisphere both with and without gullies, and found that slopes containing gullies receive a relatively consistent amount of insolation throughout the year as a result of their slope geometries, specifically latitudes and aspects (facing direction). If insolation is used as a proxy for surface temperature, this result implies that slopes containing gullies have a particular thermal environment that favors gully formation.

This relationship between insolation, thermal environment, and gully formation suggests that the release of a fluid may play a role in the gullying process. Numerous studies have attempted to determine the nature of this fluid (e.g. Musslewhite et al., 2001; Costard et al., 2002; Stewart and Nimmo, 2002; Christensen 2003; Heldmann and Mellon, 2004; Soare et al. 2007). From these studies, it appears that the fluid with the most reasonable environmental and abundance parameters is liquid H_2O. Given the temperature-pressure environment on the surface of Mars today, liquid water is not expected to be present on the surface in any significant quantity. Thus, the occurrence of geologically modern gullies apparently formed by processes that include near-surface liquid water on the martian surface presents an interesting problem.

It is important to note that the term ‘gully’ describes a morphologic feature only, and does not imply a specific process. On Earth, the morphometry of a gully and its drainage basin provides information about the mechanism of its formation. A wide variety of martian gully forms have been observed (Malin and Edgett, 2000), suggesting that gullies on Mars, as on Earth, have many different mechanisms of formation. While global studies of martian gully characteristics may aid in a broad understanding of the behavior of water on the planet, it is important to examine the characteristics of individual gully occurrence in order to understand the local processes that result in their formation.

At the local level, terrestrial hillslope gullies form most notably through erosion by surface runoff or by infiltration and saturation-triggered sliding of unconsolidated slope-mantling material that often transforms into debris flow (Montgomery and Dietrich, 1994; Cannon et al., 2001). On Mars, runoff-dominated processes are unlikely to occur today given current environmental conditions. While seasonal condensation of small amounts of volatiles from the atmosphere in the form of frost has been observed (most recently in numerous HiRISE images), low atmospheric pressures and temperature preclude the precipitation of rain in the present day within the latitude ranges in which gullies are found. Although liquid water may theoretically have a residency time of up to a few hours on the surface, this time will be reduced if the source of the water must first be melted from ice or snow (Carr, 1983). Additionally, it is not clear if rapid melting of near-surface ice or snow can produce liquid water in the quantities needed to produce overland flow. The amount of liquid produced by ice or snow melt is limited by the amount of ice or snow initially deposited. Clow (1987) suggests that snow deposition in

non-polar regions of Mars could have been ~1-5 cm per year in more favorable environmental conditions in the past. This amount of snow is relatively small in comparison with the size of typical terrestrial snow packs, which may accumulate several orders of magnitude more H_2O ice in a season. Modeling suggests that the amount of liquid generated from a melting martian snow pack is of the order of ~0.33 mm per day in peak conditions (Christensen, 2003 after Clow, 1987). This result is similar to results of modeling of shallow ice melt, which can produce up to 0.2 mm of liquid water (Kossacki and Markiewicz, 2004). These values are an order of magnitude less than what is produced during either major snow melting events or large rainstorms on Earth, which typically cause significant overland flow. While these models are by no means conclusive, it is reasonable to suggest that overland flow likely occurs far less frequently on Mars than does infiltration of the regolith. Thus, we shall focus our discussion here on the potential for infiltration-triggered sliding and debris flow to produce martian gullies rather than gullying processes triggered by surface runoff.

Debris flow initiated by infiltration-triggered slide involves the failure of a relatively thin layer of unconsolidated material (e.g. slope-mantling colluvium) as a result of saturation with water (Malet et al., 2005). Slide often occurs along a distinct surface of failure at the colluvium-bedrock contact, with a steep headscarp and lateral margins in the slope material. Once failure occurs, the saturated material is transformed into a debris flow as it moves downslope (Hungr et al., 2001). A channel is formed by scouring and entrainment of colluvium as the debris flow progresses downslope (Stock and Dietrich, 2006). Well-defined levees are often present along the channel margins (Hungr et al., 2001). Where

debris ceases to flow, a debris fan or apron is typically formed in the footslope area over successive events. As a result, the debris flow process creates a set of recognizable morphological features that include distinct gully heads, channels, levees, and debris aprons (Johnson and Rodine, 1984; Hungr et al., 2001). These features are similar to the alcove-channel-apron morphology identified in some martian gullies by Malin and Edgett (2000). The morphologic similarity between terrestrial debris flow gullies and some martian gullies has previously been noted by other workers (e.g. Costard et al., 2002; Mangold et al., 2003; Lanza et al., 2008; Conway et al., 2008).

Figure 2.1a shows the relative locations of the alcove (hollow), channel, and debris apron components in a martian gully example. The alcove is the highest of the three components along the slope gradient and is a bowl-shaped depression; the size of this feature can vary greatly between examples. The channel emerges from a distinct initiation point within the alcove, and is characterized by sharply defined, often leveed walls. The channel is usually sinuous and is the primary gully feature. A debris apron lies near the downslope end of the channel. In many cases, the channel is superimposed on the debris apron, as shown in Fig. 2.1a. Figure 2.1b shows an example of a terrestrial debris flow gully and deposit in CO, USA, with the locations of the alcove, channel, and apron labeled. This gully was formed as the result of a debris flow that was triggered by a colluvial slide (soil slip) failure (Godt and Coe, 2003). Numerous smaller debris flow deposits can be seen on either side of the main flow and hollow.

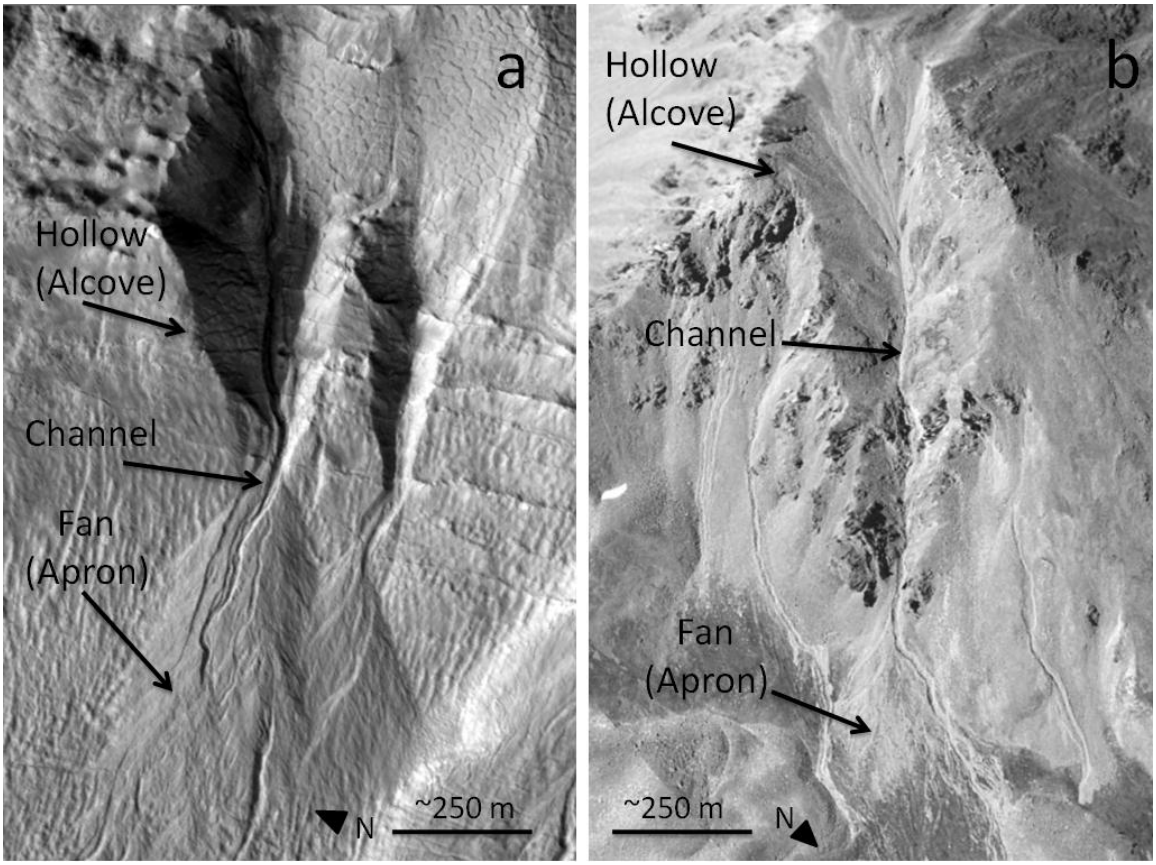

Fig. 2.1. (a) HiRISE image of a debris flow deposit on Mars in a southern hemisphere crater (-38.382°S, 96.804°E; Site 2) with the hollow (alcove), channel, and fan (apron) indicated by arrows. Several channels overlay the debris apron, indicating several episodes of activity. Note the presence of polygonal patterned terrain within the alcove region, which may indicate the presence of near-surface ice. Image credit: HiRISE PSP_001714_1415, NASA/JPL/UA. **(b)** Image of terrestrial debris flow deposits in the Front Range, CO, USA with the hollow, channel, and debris fan (apron) indicated by arrows. Note the smaller debris flow channels and deposits to either side of the marked channel. Image credit: Google Earth.

On Earth, saturation of colluvium typically occurs when rain or snowmelt infiltrates unconsolidated slope materials and moves downslope as shallow subsurface flow over bedrock or another less permeable substrate; this flow is then concentrated in slope hollows by topography. The area within the hollow that acts to concentrate throughflow is called the contributing area. The critical pore pressure needed to trigger slope failure and subsequent debris flow is dependent on the relationship between the size of the contributing area and the slope gradient. Montgomery and Dietrich (1988) found that for

arid climates, a larger contributing area is needed for the same slope gradient. This implies that in arid regions, a larger contributing area is required in order to collect and focus the same amount of water that is needed to initiate a slide failure. The relationship between slope gradient and contributing area creates a topographic signature that has been used successfully to describe the location of terrestrial debris flow channel heads (e.g. Dietrich et al., 1987; Montgomery and Dietrich, 1988, 1989, 1992; Cannon et al., 2001).

The surface environment of Mars differs in many ways from that of Earth, but both planets have steep slope hollows where bedrock is mantled by unconsolidated materials, and any fluid moving through these materials should behave according to the same physical laws on each planet, albeit with different parameters. If martian gullies are formed by debris flow erosion, then debris flow initiation processes on both planets may also share some similarities. In this paper, we review the debris flow initiation and propagation processes to elucidate the origins of this observed correlation between contributing area and topographic slope gradient. We then measure martian gullies in three HiRISE stereo pairs that have debris flow depositional and erosional morphologies (i.e. alcove-channel-apron) for the area-slope relationship in order to test the debris flow formation hypothesis. Of particular importance are the implications that these channel initiation processes have for potential sources of water in the near-surface environment. This study does not attempt to represent all martian gullies, but rather is a preliminary test of the debris flow formation hypothesis for the selected gullies.

Terrestrial debris flow as an analog for martian gullies

Debris flow initiation, behavior, and resultant morphologies

Debris flows often initiate within slope hollows, which are areas on a slope that are topographically concave-out (Reneau and Dietrich, 1987), similar to the martian gully alcove. If unconsolidated slope materials within a hollow become saturated with water, they may fail as a slide of initially rigid material, which is the precursor to debris flow. On Earth, this slide failure is most often the result of heavy rainfall, snowmelt, or both (Malet et al., 2005). Hollows tend to concentrate both surface and shallow subsurface runoff, and so they are more susceptible to saturation failure than other regions on the slope. Unconsolidated material within the hollow is held on the slope through a combination of friction and cohesion known as shear strength. This is described by the Mohr-Coulomb strength model:

$$\tau = C' + (\sigma_n - u)\tan\phi \qquad (2.1)$$

where τ is shear strength, C' is cohesion, σ_n is total normal stress, u is pore pressure, and ϕ is the internal angle of friction. Shear failure occurs when cohesion and frictional strength are overcome. The cohesion, normal stress, and internal angle of friction are unlikely to change over time for a given slope material, while pore pressure may change depending on the amount of water present. As a result, a change in pore pressure is commonly the most significant process reducing the stability of a slope. Once failure occurs, saturated slope material rapidly transforms into flow, which moves into low-order channels and can be strongly erosive. The initial surge of material occurs suddenly, and

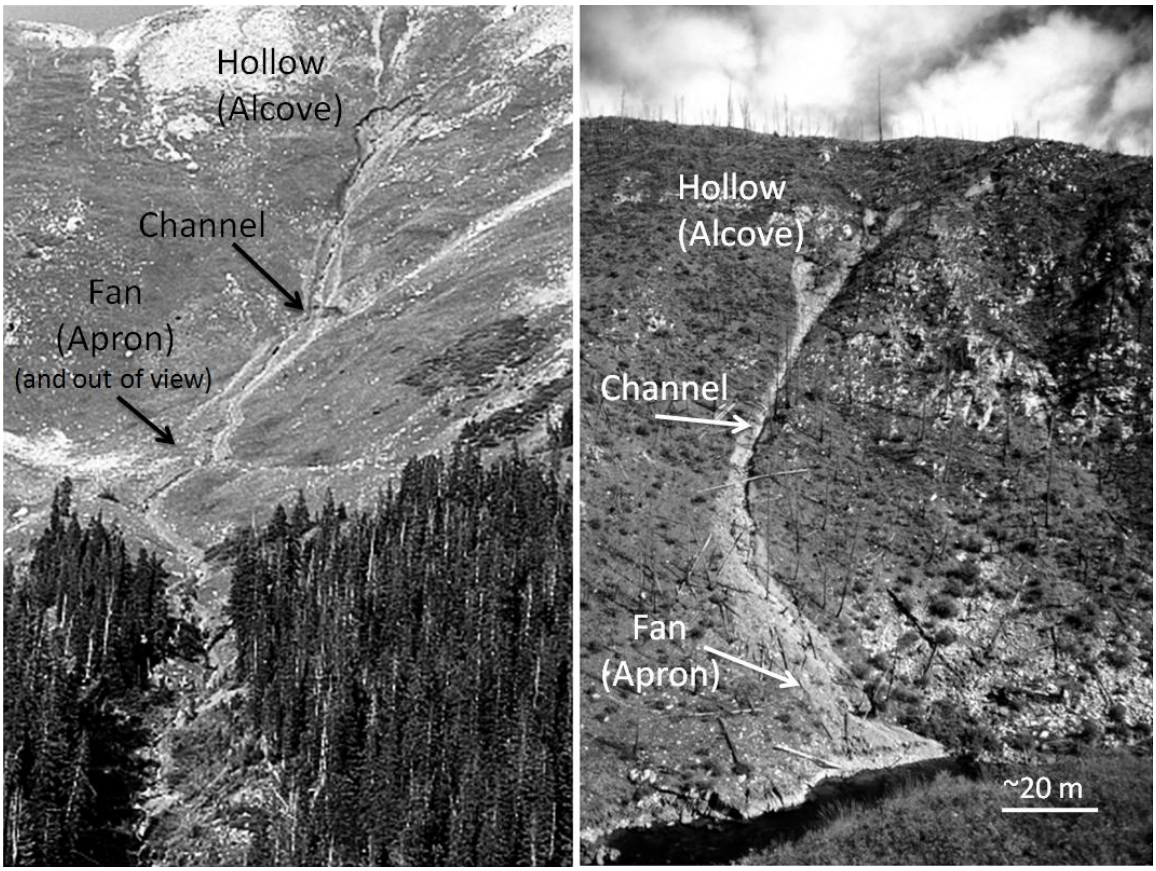

Fig.2.2. (a) Image of a terrestrial hollow containing a debris flow channel in the Front Range, CO, USA. This debris flow was triggered by saturation-induced soil sliding. Note the presence of exposed bedrock in the upper reaches of the hollow and levees marginal to the channel. From Godt and Coe (2007) (Fig.8). **(b)** Image of terrestrial debris flow deposits in Idaho, USA with the hollow (alcove), channel, and fan (apron) indicated by arrows. The apron for the most recent flow is outside the image frame lower on the slope, although a small apron from a previous flow is visible to the left by treeline. Note the presence of exposed bedrock within the hollow.

more than one surge may occur during a single event. Terrestrial debris flows can have peak velocities of 10 m/s, and flow distances are typically in the 0.1-10 km range (Iverson, 1997). Figure 2.2 shows two examples of terrestrial hollows containing landslide-triggered debris flow gullies and deposits as seen from the ground. The hollows in both areas contain soil overlain on bedrock, which can also be seen exposed in some regions of both hollow examples.

Debris flow is characterized by poorly sorted material (Hungr et al., 2001). The solid and liquid fractions of the flow are commonly assumed to act as one fluid material. Pierson and Costa (1987) examined the rheological response of different sediment-water mixtures and concluded that debris flow is a non-Newtonian fluid that exhibits plastic flow behavior. However, Iverson (1997) points out that it is difficult to explain debris flow behavior with a single rheology. He suggests that the interaction between the solid and fluid components leads to the observed behavior and allows the rheology to change as the flow develops. A grain within the flow may interact as part of the solid fraction by bouncing off of other grains, or it may act as part of the liquid fraction if it is suspended only by the viscous forces of the water. This suggests that grains of certain size ranges will behave in different ways within the flow. Experiments in an experimental flume have confirmed that this is the case; the solid fraction of the experimental flow had 1-6% grains finer than sand, while the sediments in the associated effluent fluid contained 94% grains finer than sand (Iverson, 1997). In flows carrying large clasts, an unsaturated front with high intergranular friction often rapidly develops at the head of the flow. Measurements from one of these flume experiments show that the depth, stress, and pressure change significantly within the debris flow over time. These observations emphasize that debris flow cannot be modeled as a single phase, single rheology material.

In terrestrial debris flows initiated by saturation and failure, channel formation is due primarily to scouring and entrainment of colluvium as the debris flow moves past and acquires more slope material (Stock and Dietrich, 2006). The snout or flow front is usually the thickest part of the flow and carries the largest clasts. Iverson (1997) explains

this sorting as developing from kinetic sieving. As the smaller grains translocate through voids, the larger clasts are left closer to the flow surface. Both Iverson (1997) and Hungr (2001) point out that the pore pressure in these large clast regions—the snout and lateral regions—is greatly decreased from the center of the flow. Slower moving materials on the flow margins are deposited along the sides of the channel as levees, often composed of coarser debris from the flow front that have been shouldered aside by the more mobile, saturated debris behind (Fig. 2.2). Pore fluid and finer particles may escape the flow front and form a more rapidly moving flow that precedes the coarse front (Pierson, 1986; Meyer and Wells, 1997). Where debris flows become unconfined and slope gradients start to decrease, a lobate deposit with sleep, discreet margins is typically formed as the coarse front and main body of the flow come to rest. Since debris flows often have several surges per episode, wave forms are sometimes observed in the deposited material.

On Mars, apparent debris flow type deposits are observed in conjunction with some gullies. Figure 2.3 shows a martian gully with extensive lobate deposits. Large boulders within a finer matrix can be seen in a closeup of part of the lobate deposit, as would be expected in debris flow materials, and the top of the deposit has a faint rippling wave-like pattern (Fig.2.3c). Additionally, levees can be seen on the margins of several of the channels (Fig.2.3b). Several distinct lobes of material can be traced, and disconnected sections of channels are also present, suggesting several flow episodes in this area.

Slope gradient plays a significant role in debris flow initiation and propagation. A steep slope gradient promotes slope failure; however, once debris flows are initiated, they do

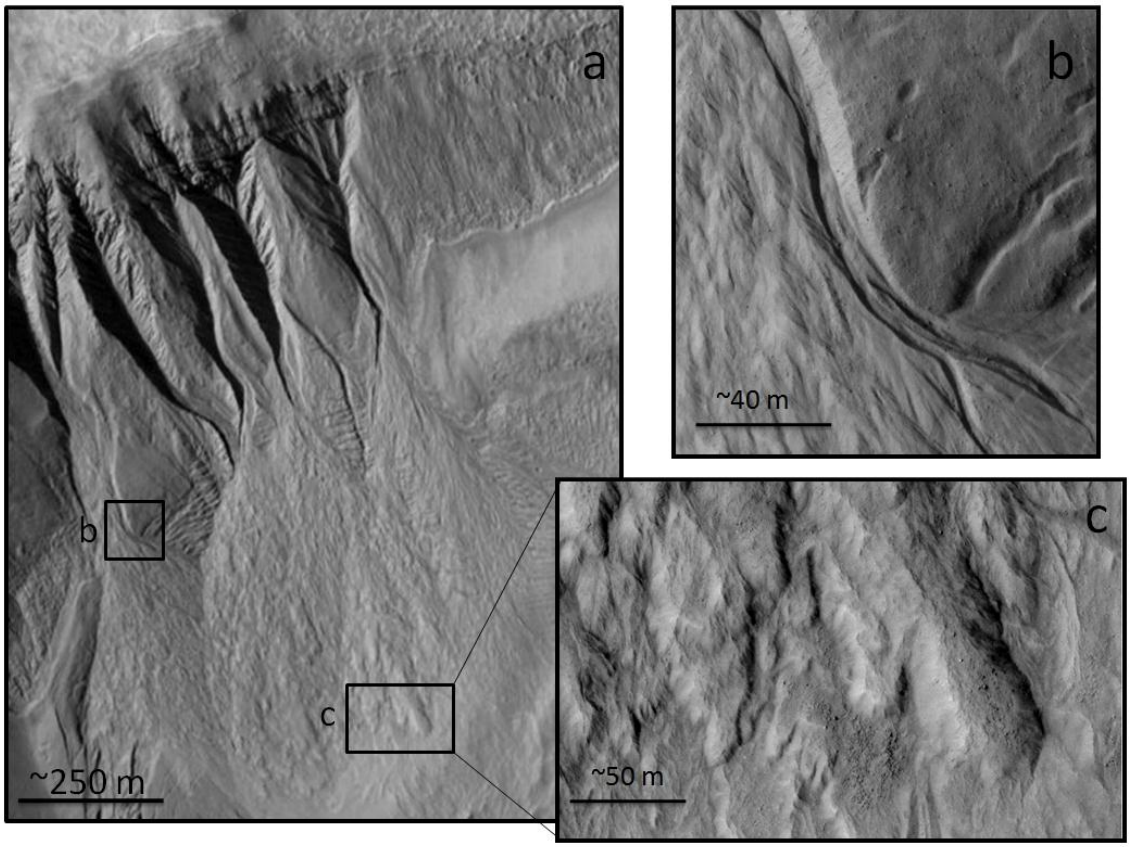

Fig. 2.3. HiRISE image of martian gullies with debris flow morphologies. **(a)** Overview of the hillslope containing gullies. These gullies have large hollow (alcove) areas, leveed channels, and extensive lobate debris deposits in the footslopes. Note the presence of exposed bedrock in the alcove walls. **(b)** Close up of a channel showing sharply leveed walls. **(c)** Close up of part of the lobate debris deposit. Large boulders can be seen within a finer-grained matrix that composes the majority of the deposit material. Wave-like patterns are also observed in the deposit, which are suggestive of several surges of material during each flow event.

not require steep slopes to propagate. Stock and Dietrich (2006) found that terminal debris flow deposits from mountain basins resided on slopes with gradients ranging ~1-6°, indicating that these debris flows were able to flow on the relatively shallow slope gradients just above the depositional area. Additionally, Rodine and Johnson (1976) demonstrate that debris flows carrying large boulders can flow on slopes as low as 5° because of their ability to suspend larger material on the exterior of flows that are composed primarily of finer grains and liquid. As long as the conditions for debris flow initiation are met on the upper slope (e.g. a steep gradient and saturation of

unconsolidated materials), then gentle slopes near the bottom of hillsides can experience debris flow movement. Studies by Heldmann and Mellon (2004) and Lanza and Gilmore (2006) found that martian gullies occur on slopes with average gradients of ~17°, which is well within the range of gradient needed to sustain debris flows.

In summary, the alcove-channel-apron morphologies observed in a subset of martian gullies may be explained by debris flow processes. Debris flows are typically initiated in a preexisting slope hollow. Channel heads are localized by saturation and failure of the slope material within the hollow, and channels are eroded as flow materials move downslope and pick up debris as detailed above. Finally, a debris apron is created when the flow materials lose enough energy and come to rest in the footslope area. Thus, the zones of erosion, transport, and deposition within a debris flow are consistent with the observed alcove, channel, and apron morphologies.

The topographic signature of debris flow

In addition to smaller scale morphological features such as channels, levees, and debris aprons, the location of slope failures and subsequent debris flows as described above may be predictable by morphometric characteristics of the slope hollow. Dietrich et al. (1986) examined both channeled and unchanneled basins located in the same regions to determine whether there were fundamental differences between them. They found that there is a relationship between the contributing area and the slope gradient of channeled (gullied) slopes. The contributing area is defined as the drainage area above the channel head that collects and focuses shallow subsurface throughflow liquid into slope

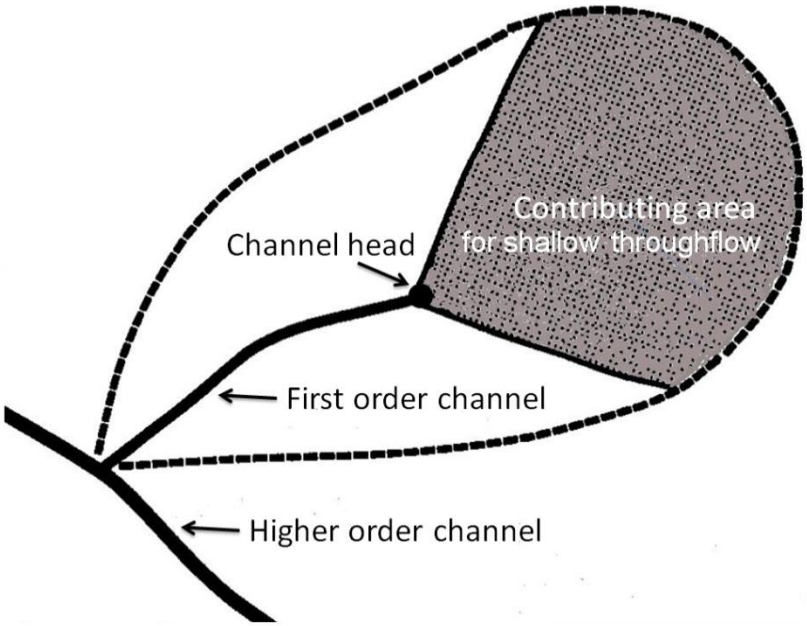

Fig. 2.4. Schematic of the relative positions of contributing area, gully head, and channel. Outlined region indicates the location of the basin containing the channel. Individual contributing areas for this study are defined by local topography at each site. After Montgomery and Dietrich (1989) (Fig. 1).

concavities (Fig. 2.4). This area may be equivalent to the hollow or extend somewhat above it into the crestslope area, or it may be some subset of the hollow area. On Earth, a single saturation-induced failure creates a sharply defined channel head in the alcove where sliding was initiated. Thus, these channel heads are key locations for understanding the triggers of such mass movements. Montgomery and Dietrich (1988) examined the starting locations of channels (e.g. gully heads) in relation to the slopes above the channel and found that slope gradient decreases as the drainage area increases. This indicates that as the slope becomes gentler, greater amounts of throughflow are required to initiate failure because throughflow is concentrated less quickly on shallow slopes. These results are supported by theoretical calculations by Montgomery and Foufoula-Georgiou (1993), which show that smaller source areas are needed to initiate channels on steeper slopes.

The observed area-slope relationship suggests that channels will begin at the first point downslope where there is a large enough source area to support them. Failure occurs at the point on the slope where accumulation of throughflow has caused saturation to a critical depth, and thus a critical pore pressure, to induce failure. This is apparent from Eq. 2.1, in which pore pressure (u) is a key variable controlling slope stability. Landslide failure tends to dominate on steeper slopes, whereas overland flow erosion is generally the dominant channel initiation process on shallower slopes (Montgomery and Dietrich, 1988, 1994). Figure 2.5 shows an empirically derived curve for the area-slope relationship based on measurements of terrestrial gullies and hollows, with the different erosional regimes marked (Montgomery and Dietrich, 1994). In terrestrial landscapes, the

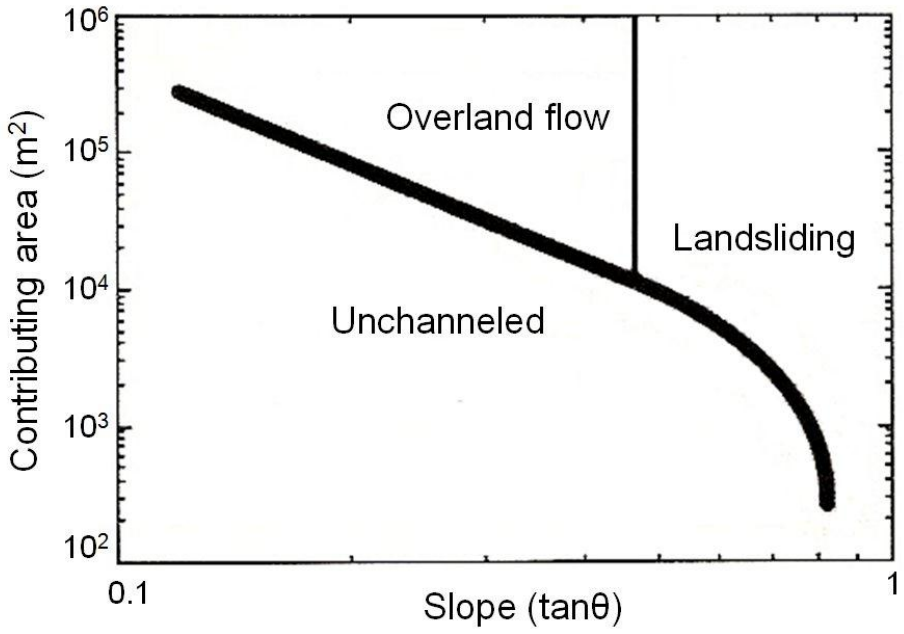

Fig. 2.5. Empirically derived curve for the area-slope relationship in channeled basins based on terrestrial studies. In general, overland flow is the dominant process initiating channels at lower slope gradients, while landsliding dominates gully initiation at steeper slope gradients. On Earth, the boundary between these two processes is commonly set at $\tan\theta > 0.5$ (~25°), but this may vary significantly on both Earth and Mars due to slope material properties. For a given gradient, the contributing area must reach a critical value in order for a channel to initiate; below a threshold area value, no gullies will be initiated. After Montgomery and Dietrich (1994).

slope gradient boundary between landslide failure and overland flow erosion is commonly approximated by $\tan\theta > 0.5$, or ~25° (Montgomery and Dietrich, 1989, 1994), but this boundary can vary significantly depending on the properties of the slope materials. The area-slope relationship shown in Fig. 2.5 cannot be applied directly to the martian environment, as much of the overland flow erosion on Earth is accomplished by perennial steams.

Combining a subsurface flow model and the infinite slope stability model, Montgomery and Dietrich (1994) have developed an expression for the critical drainage area per unit contour length:

$$a_{cr} = \frac{zK \sin\theta \cos\theta}{R}\left[\left(\frac{C'}{\rho_w g z \cos^2\theta \tan\phi}\right) + \left(\frac{\rho_s}{\rho_w}\right)\left(1 - \frac{\tan\theta}{\tan\phi}\right)\right] \quad (2.2)$$

where z is the colluvium thickness, K is the saturated hydraulic conductivity, θ is the ground surface slope, R is the rainfall intensity, C′ is the effective cohesion of the colluvium, ρ_s and ρ_w are the densities of the saturated colluvium and fluid respectively, ϕ is the angle of internal friction in the colluvium, and g is gravity.

The water provided by precipitation on Earth (R) may have an alternative source on Mars in melting snow or ice; the rate of melting—analogous to rainfall intensity—is obviously unknown, but is unlikely to be as great as typical rainfall intensities that generate slope failures on Earth (e.g. Caine, 1980). No studies have quantitatively examined slope materials on gullied martian hillsides, since there have been relatively few lander and

rover missions to the surface of Mars, and none to an area with gullies. However, a relatively thick mantle of regolith can be inferred from qualitative observations of the textural difference on gullied slopes between rugged bedrock outcrops and the smooth surface of a regolith mantle. This type of mantle has been observed in conjunction with many martian gullies (Christensen, 2003; Bridges and Lackner, 2006). Numerous in situ and remote sensing studies have estimated that there is a range of cohesion values in martian regolith ~1-10 kPa (Christensen and Moore, 1992). A study of martian regolith at the Pathfinder landing site found that it had relatively low apparent cohesion averaging ~0.2 kPa (Moore et al., 1999b). These values are significantly lower than soil cohesion values measured in debris flow source areas by Malet et al. (2005), who found that these soils had cohesion values ~16-40 kPa. This difference is likely due to environmental differences on Earth and Mars; on Earth, many soils gain effective cohesion through vegetation roots, as well as small amounts of intergranular moisture. Additionally, measurements of soil cohesion on Mars have been obtained either through large-scale remote sensing or from individual landing sites on flat areas, providing little information about the properties of slope materials specifically. Soil properties on Mars, as on Earth, are likely to vary significantly from location to location.

The relationships in Eqn. 2.2 suggests that the critical contributing area may be smaller if regolith on martian hillslopes has a lower average cohesion than terrestrial hillslope soils, as would be expected given the lack of vegetation on Mars. However, the reduced gravity on Mars (0.38 times that on Earth) will work to counteract this effect. Given our current understanding of martian regolith properties, it is difficult to assess how the area-slope

may be affected by differences between martian and terrestrial soils. Based on Eqn. 2.2, it is reasonable to suggest that soil properties such as cohesion will affect the area-slope signature much less than the angle of the slope itself and the amount of water added to the slope material. In drier regions on Earth where there is less total water provided to a given slope hollow, a larger area is needed to concentrate the necessary amount of water to cause saturation and failure than is needed on the same slope in a wetter climate (Montgomery and Dietrich, 1988). This observation suggests that the critical contributing area required to cause a failure on Mars may be slightly larger than what is required on Earth.

Regardless of the specific regolith properties on martian hillslopes, an observation of a distinct area-slope relationship on Mars would imply that some martian gullies are created by debris flows triggered by throughflow processes, as their morphologies suggest. A topographic signature of this type would indicate that the source of liquid for these gullies is broadly distributed within the contributing area. Thus, through a systematic analysis of slope and area, evidence for the presence of a shallow source of water in gullied areas may be tested on Mars.

Methods and results

Stereo imagery from HiRISE was examined for debris flow erosional and depositional features. In order to examine relatively straightforward area-slope relationships, we selected areas with (1) sharp, well-defined gully heads within first-order basins and (2) limited evidence for multiple flows (e.g. those with small fans below the channel and

well-defined gully heads). Locations with relatively large alcove regions were favored so that contributing areas could be clearly defined. Digital elevation models (DEMs) were created for those locations where such features were identified. All measured features are located on the walls of southern hemisphere craters (Table 2.1). Site 1 is located within the same crater in which Malin et al. (2006) observed recent bright-toned deposits appearing on a gullied crater wall. The features measured in this study are located on a different section of crater wall than those bright-toned deposits.

Three DEMs were analyzed in this study. These were constructed from publicly released stereo HiRISE images (Table 2.1) following the method of Kirk et al. (2008). The HiRISE DEMs are tied to the Precision Experiment Data Records (PEDRs) from the Mars Orbiter Laser Altimeter (MOLA), which helps to preserve regional slope and the slopes of large-scale geomorphic features such as crater walls and the slopes of gullies that were sampled by MOLA. Each HiRISE DEM encompasses roughly 200-250 individual MOLA PEDR data points. The HiRISE images have a pixel scale of 25-28 cm in non-binned channels, and the resulting DEMs contain elevation postings with 1 m spacings. Measurements of area and slope reported here were taken in areas of high correlation between stereo images, and avoided large (>100 m^2) areas of interpolated elevations (due to poor stereo correlation) and other artifacts.

Table 2.1. Observation IDs and locations of the stereo HiRISE images for each study site.

Site	First image	Second image	Latitude	Longitude (E)
1	PSP_004060_1440	PSP_005550_1440	-35.722°	129.428°
2	PSP_001714_1415	PSP_002136_1415	-38.382°	96.804°
3	PSP_003418_1335	PSP_003708_1335	-46.067°	18.819°

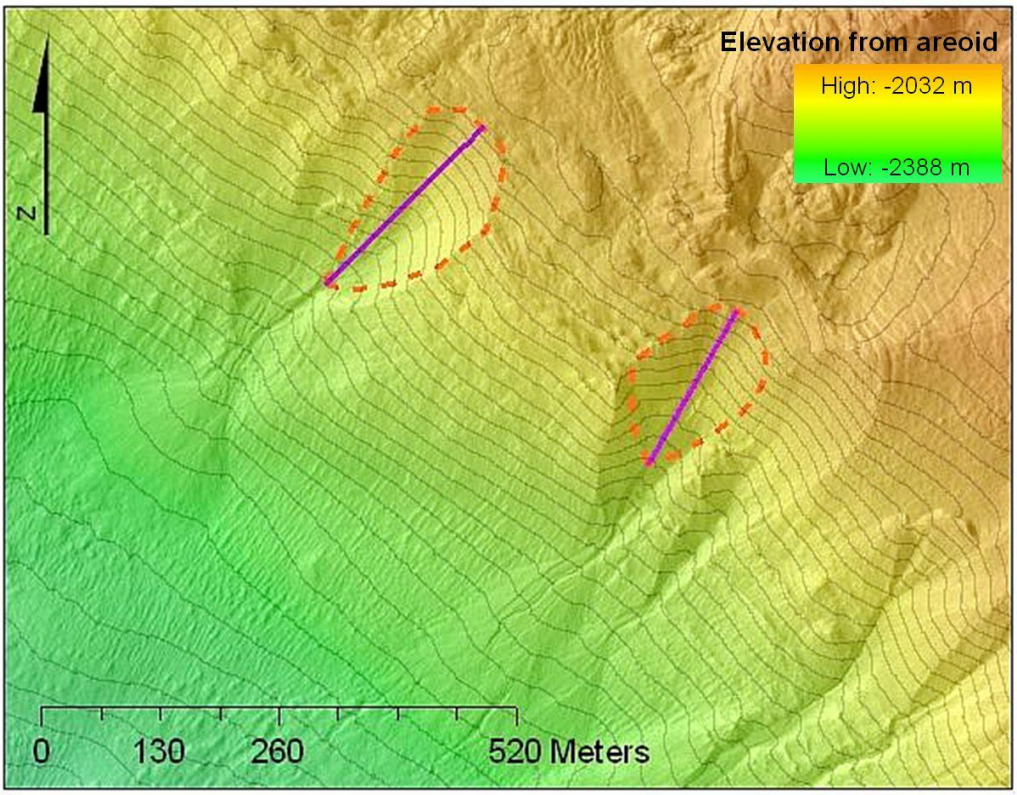

Fig. 2.6. Example measurement locations for slope (purple line) and contributing area (orange dotted line) for two gullies in PSP_1714_1415 (Site 2). Topographic lines are in 10 m intervals.

Orthorectified HiRISE images were overlain on the DEMs in ArcGIS, and measurements of contributing area and slope were made by digitizing regions of interest and extracting values from the DEM. Contributing areas were calculated using the free ArcGIS tool Easy Calculate (5.0). Area was measured using the topography as a guide as the apparent drainage basin in which the gully channel resided, and slope was measured from the top starting point of the channel to the top of the drainage divide (Fig. 2.6) (Dietrich et al., 1986; Montgomery and Dietrich, 1988; Cannon et al., 2001). In some cases the contributing area was equivalent to the gully alcove, while in others it comprised only part of the alcove area. The surrounding regions were carefully evaluated to ensure that the correct area and slope for a particular gully were chosen, and only first-order channels were measured. Thirty-two gullies were measured using stereo image pairs in three

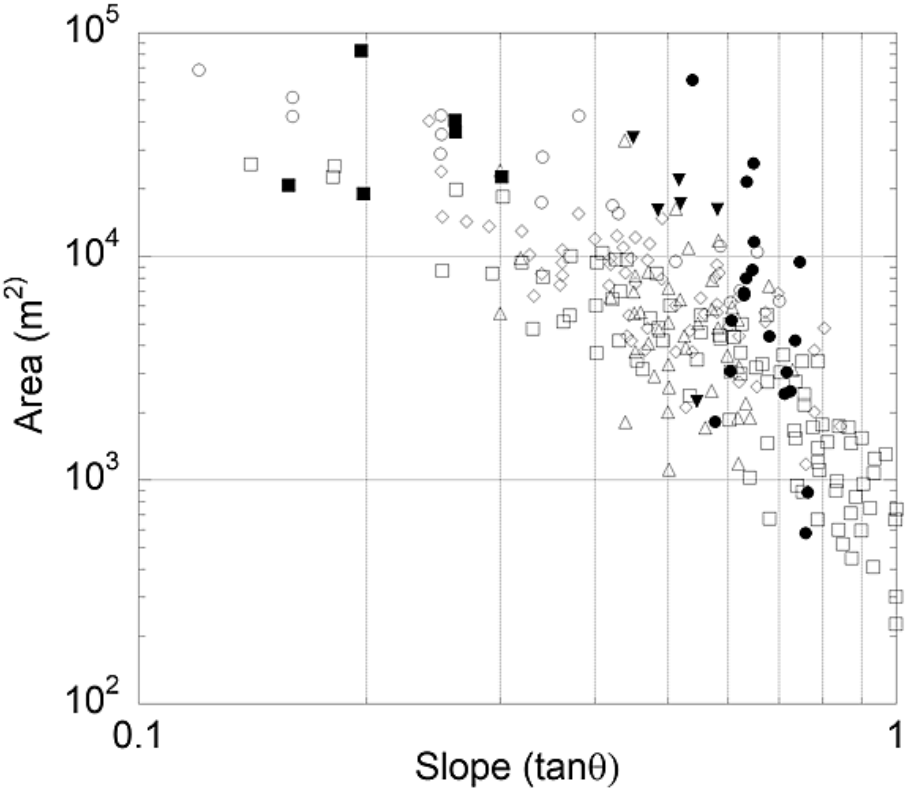

Fig. 2.7. Measured area-slope relationships for martian gullies (filled symbols) and terrestrial gullies (open symbols). Martian gullies were measured in HiRISE images for Site 1 (closed circles), Site 2 (closed triangles), and Site 3 (closed squares) as listed in Table 2.1. Also shown are the results of terrestrial studies of primarily landslide initiated channels in Tennessee Valley, CA (open diamonds) (Montgomery and Dietrich, 1989), Coos Bay, OR (open squares) (Montgomery and Dietrich, 1992), Southern Sierra Nevada, CA (open circles) (Montgomery and Dietrich, 1992), and San Pedro Ridge, CA (open triangles) (Dietrich et al., 1987).

locations (Table 2.1). Figure 2.7 shows the relationship between contributing area and slope for the study set of martian gullies showing debris flow morphology. In order to place these measurements in a terrestrial context, our data were plotted alongside the results for terrestrial studies of the area-slope relationship for channels in Tennessee Valley, CA (Montgomery and Dietrich, 1989), Coos Bay, OR (Montgomery and Dietrich, 1992), Southern Sierra Nevada, CA (Montgomery and Dietrich, 1992), and San Pedro Ridge, CA (Dietrich et al., 1987). The majority of the channels in the terrestrial studies were initiated by colluvial slide failures that transformed into debris flows.

Our initial results show that the martian gullies measured in this study have a broadly similar area-slope relationship to terrestrial debris flows initiated by saturation-triggered failure of slope materials. In both terrestrial and martian data sets, the contributing area decreases as the slope gradient increases. Large variability within the terrestrial data, both within individual study areas and between study areas, is expected given the large number of variables that ultimately determine where a debris flow may initiate on a given slope. Differences in cohesion, permeability, density, and frictional strength of the colluvium affect the critical pore pressure required to cause failure. Additionally, the types and amounts of vegetation on terrestrial slopes will also significantly affect the strength of the slope material, as will the style of precipitation and regional climate. There is limited information available to estimate the properties of the slope materials for the three martian study sites, and some differences between these three areas are expected, as there would be on Earth. Thus, a tight area-slope relationship is not expected nor observed in either the terrestrial or martian data sets shown here. Our results for martian gullies are generally within the range of similar terrestrial studies, despite obvious environmental differences (Montgomery and Dietrich, 1989, 1992; Dietrich et al., 1987). All data sets, both martian and terrestrial, appear to follow the empirically derived curve for debris flow in Fig. 2.5. There is some suggestion that the martian data plot slightly above the terrestrial data in all cases, as was previously predicted from Eqn. 2.2, but this requires additional investigation. As on Earth, martian slope environments are expected to vary from location to location, so differences between the martian and terrestrial environments may be obscured by these variations within the slope environments on each planet.

Implications for gully formation

Our results suggest that at least some martian gullies may have been formed by saturation-induced slide failure and subsequent debris flow. Erosional and depositional features such as leveed channels and lobate debris fans in association with some martian gullies are suggestive of past debris flow. In addition, the observed area-slope relationship in these gullies suggests that topography is acting to focus and concentrate water in the near-surface as it migrates downslope, pointing to a source of water that is broadly distributed and shallow. Although debris flows could be mobilized by a release from a confined aquifer, perched aquifer above an aquiclude, or other concentrated liquid water source such as fracture flow, there is no straightforward mechanism for such sources to produce the observed area-slope relationship. Aquifers are zones of saturation in the subsurface, and thus materials are saturated at or near the point of discharge when aquifers intersect the surface. Several workers have noted the presence of exposed bedrock in conjunction with martian gullies, and they suggest that these outcrops represent continuous, subhorizontal rock layers that block percolation and form perched aquifers that channel liquid water to the crater wall, where it is discharged from a discrete point (e.g. Mellon and Phillips, 2001; Gaidos, 2001; Gilmore and Phillips, 2002). In this scenario, all the water available for saturation of slope materials is already concentrated in a single location. Thus, saturation and failure of colluvium occurs at or near the point at which the discharge occurs. This model assumes a negligible decrease in permeability within the shallow subsurface (e.g. between regolith and bedrock) that would produce throughflow, so that vertical percolation occurs to depths of hundreds of meters.

Therefore, no relationship between hollow size and slope gradient would be expected. Further, the presence of exposed bedrock at or near gully heads may simply reflect the relative instability of unconsolidated materials in these steep areas, rather than an aquifer discharge point. As is common at debris flow initiation points, exposed bedrock can be seen in the terrestrial gully heads shown in Fig. 2.2, which were both formed by rainfall and infiltration-triggered sliding and not by the release of water from an aquifer.

Our observation of an apparent area-slope relationship on the gullied slopes measured in this study points to a source of water in that is more likely to be shallow and broadly distributed within the alcove/hollow region, rather than discharge from a concentrated source such as an aquifer. On Earth, infiltration of precipitation or snowmelt is the typical source of broadly distributed near-surface liquid. However, liquid precipitation has not been observed on the surface of Mars. Additionally, the amount of insolation a slope receives appears to have an effect on whether or not a gully will form on that slope (e.g. Malin and Edgett, 2000; Lanza and Gilmore, 2006; Ollila and Gilmore, 2007), suggesting that temperature controls the availability of the source liquid. A potential source that is shallow, broadly distributed, and temperature controlled is surface or near-surface ice, which, when melted by insolation, could act much as terrestrial throughflow in the near subsurface.

Several types of ice melt have previously been proposed as a source of liquid for martian gullies, including melting of dust-mantled snow (Christensen, 2003), melting of permafrost (Costard et al., 2002; Soare et al., 2007), and melting of shallow ice emplaced

from the atmosphere into the regolith (Mellon and Phillips, 2001; Hecht, 2002). Subsurface ice has been inferred to exist on Mars from surface morphologies (e.g. Head and Marchant, 2003; Head et al., 2003, 2005; Kochel and Trop, 2008), thermal modeling (e.g. Mellon and Jakosky, 1993), and global hydrogen abundances detected by the Gamma Ray Spectrometer (GRS) onboard the Mars Odyssey (Boynton et al., 2002). Frost also accumulates annually in gullied areas in the current climate, as seen in various HiRISE images. Most recently, the Phoenix Mars Lander has detected what appears to be ice covered by a relatively thin mantle of regolith at a high northern latitude (Smith et al., 2009b). Additionally, recent small, fresh impact craters in the northern midlatitudes have excavated a bright-toned material with the spectral characteristics of water, which is highly suggestive of the presence of shallow ice (Byrne et al., 2009). These observations are supported by results from the Shallow Radar (SHARAD) onboard MRO suggesting that there are large deposits of near-surface water ice in the midlatitudes, where gullies are commonly found (Holt et al., 2008). Melting of near-surface ice would provide a source of water that could percolate through the upper regolith, become focused by local topography, and potentially saturate near-surface materials, and could easily trigger slide failures that may transform into debris flow.

The question of whether pure water ice can be melted to produce liquid water in the martian midlatitudes has been discussed and modeled extensively. Modeling by Kossacki and Markiewicz (2004) suggests that a small amount of water may be produced by melting of subsurface ice by insolation in gully locations. While this amount (<0.2 kg/m^3) is unlikely to produce overland flow, it may become focused by topography as it

percolates downslope and cause saturation of regolith. However, this model only takes into account seasonally emplaced H_2O frost; if more persistent ice exists, as observations suggest, the amount of liquid melt may be significantly larger. The stability of near-surface liquid water may be increased by the addition of dissolved salts, which will significantly depress the freezing temperature of water. Precipitates of brines have been observed on Mars by a wealth of mineral studies (e.g. Squyres et al., 2004; Bibring et al., 2006; Osterloo et al., 2008), so it is reasonable to suggest that brines could be operating on the martian surface today.

Gilmore and Phillips (2002) point out that if gullies are globally controlled specifically by a subsurface ice source, either permafrost or emplaced from the atmosphere, rather than by snow, gully heads should emanate from areas that are lower along crater wall slopes (i.e. farther below the crater rim) in regions closer to the equator. This is due to the presumed stability of ground ice as a function of latitude; ice should be less stable in warm equatorial regions than in colder polar regions. In contrast to subsurface ice, snow is not limited to a particular placement along a slope, so snowmelt gullies may emanate from any slope position so long as there is sufficient snow within the hollow to provide the critical amount of water for saturation and slip failure. Measurements of alcove and gully head distances below crater rims indicate a weak relationship between depth and latitude (Heldmann and Mellon, 2004; Lanza and Gilmore, 2006; Heldmann et al., 2007). These results may indicate a subsurface ice source for some martian gullies. However, these studies did not differentiate between gullies with different morphologies as having potentially different formation mechanisms, and so the inclusion of all gully types in

these data sets is likely attenuating the signal of any potential relationship between gully head depth and latitude in a subset of gullies that form from ice melt.

Local morphologies also point to the presence of ground ice in gully-bearing regions, including the areas in this study. Arfstrom and Hartmann (2005) note the presence of glacier-like flow features and moraine-like ridges that appear in conjunction with martian gullies, suggesting the presence of near-surface ice. In addition, polygonal fracturing appears in several alcoves and surrounding regions (Fig. 2.1a). Similar polygonal terrain has been observed in gully locations previously by Bridges and Lackner (2006) and Levy et al. (2008). Levy et al. (2008) note that terrain with polygonal fracturing is associated with permafrost, and they observe terrestrial gullies overlaying polygonal terrain in the Antarctic. They note that many of the polygon fractures appear to predate and control the direction of some gully channels; thus, gullies here may be modified primarily by snowmelt within the polygon fractures rather than permafrost melt. This process involves broadly distributed subsurface flow, and so the observations of polygons in some of our study regions are consistent with a debris flow model of gully formation. Additionally, initial results from the Phoenix Mars Lander indicate that martian polygons do indeed overlie ice (Arvidson et al., 2008; Keller et al., 2009).

Based on the results presented here, it is not possible to differentiate between throughflow generated by melting snow or melting ground ice. Debris flows may be triggered by other processes, including overland flow and aquifer discharge. However, our results suggest that ice and/or snowmelt can better explain the morphologies and

area-slope relationships observed in the martian gullies in this study. This conclusion is supported by multiple independent observations that indicate the presence of ice at or near the surface. Additional detailed studies of gully-bearing regions should help to elucidate the processes in these areas that may control water generation from melting ice. Nonetheless, it is likely that debris flows in general only account for some fraction of the global population of gullies, and there may be other, as of yet unidentified processes that also create gully landforms on Mars.

Conclusions

Measurements of the contributing area and slope gradients above a sample of martian gully heads associated with debris flow morphologies indicate an area-slope relationship similar to that for terrestrial debris flow channel heads. The contributing area acts to generate and focus throughflow in the shallow subsurface, and the slope gradient controls how efficiently this process occurs, as well as the stability of the regolith mantle on the slope. The observed morphologic evidence of debris flow implies the presence of a liquid associated with gullies on Mars, and our findings of an area-slope relationship suggests that the source of this liquid is broadly distributed and shallow. Our study does not attempt to determine the composition of this liquid, but based on previous work and recent results from SHARAD it is likely that this liquid is groundwater. Water ice is predicted to be stable in the martian subsurface, and polygonal terrain on some gullied slopes suggests its presence. This study is a preliminary attempt to better understand the nature of a specific subset of martian gullies and the source of liquid required for their formation. Additional measurements should provide more definitive tests of these

findings. Nonetheless, these results point to an origin for some martian gullies through saturation-induced slide failures and consequent debris flows as a result of a liquid contributed by melting of broadly distributed snow or shallow subsurface ice.

Chapter 3

Calibrating the ChemCam LIBS for carbonate minerals on Mars

Article citation: Lanza, N.L., Wiens, R.C., Clegg, S.M., Ollila, A.M., Humphries, S.D., Newsom, H.E., Barefield, J.E., and the ChemCam Team (2010). Calibrating the ChemCam laser-induced breakdown spectroscopy instrument for carbonate minerals on Mars. *Applied Optics* 49 (13), C211-C217.

Abstract

The ChemCam instrument suite on board the NASA Mars Science Laboratory (MSL) rover includes the first LIBS instrument for extraterrestrial applications. Here we examine carbonate minerals in a simulated martian environment to better understand the LIBS signature of these materials on Mars. Both chemical composition and rock type are determined using multivariate analysis (MVA) techniques. Composition is confirmed using scanning electron microscopy (SEM). Our results show that ChemCam can recognize and differentiate between different types of carbonate materials on Mars.

The ChemCam instrument suite

The first laser-induced breakdown spectroscopy (LIBS) instrument for extraterrestrial applications was selected as part of the ChemCam instrument package onboard the NASA Mars Science Laboratory (MSL) rover 'Curiosity,' scheduled for launch in 2011. ChemCam consists of two instruments: a LIBS instrument and a Remote Micro Imager (RMI). LIBS will provide microbeam (60-200 μm radius) chemical analyses of targeted materials using 5 ns pulses of 1067 nm photons (Wiens et al, 2009). The RMI, with a 20

mRad field of view, is capable of resolving <0.5 mm features at a distance of 5 m, and will provide a telescopic context image of small-scale textures for the LIBS data, similar to a geologist's hand lens (Maurice et al., 2009). The primary objective of the Curiosity rover is to determine past and present habitability on Mars in a variety of environments (Blaney, 2006); this is not a search for life per se, but rather for materials and environments that would support life as it is currently understood on Earth. As such, the detection of H_2O, water-formed minerals, and organic molecules are key aspects to the mission.

The LIBS technique is particularly well suited for an extraterrestrial rover application. ChemCam will be installed on the rover mast ~2 m from the ground and has a standoff distance capability to 7 m (Wiens et al 2009), allowing the rover to remotely obtain information about targets without the need for direct contact with them. In addition, the LIBS technique is sensitive to the majority of elements, and will allow for direct observation of light elements such as H, C, N, O, Li, Be, and B on the martian surface for the first time. Multiple LIBS analysis spots on a single rock will provide information on individual mineral grains as well as providing a bulk rock composition. Additionally, repeated laser pulses on the same spot can be used to remove dust and to create a depth profile of chemical composition within weathering rinds. Analysis times for both the ChemCam LIBS and RMI are relatively short, and total power requirements remain relatively low, allowing ChemCam to efficiently gather large amounts of information about the martian surface.

Detecting carbonate minerals on Mars

Carbonate minerals are based on the $(CO_3)^{2-}$ anion. On Earth, carbonates are widespread and may be emplaced through a variety of geologic processes, most notably as sedimentary deposits but also as secondary weathering products, hydrothermal deposits, and as the result of metamorphism. The carbonate mineral calcite ($CaCO_3$) in particular is very common in sedimentary environments on Earth, both as the main constituent of limestone and as a cement in sandstones. In general, the presence of carbonate indicates the past presence of liquid water.

On Mars, carbonates may form in many of the same environments as they do on Earth provided a source of liquid water is present. Observations of martian soils suggest that hydrothermal activity has occurred on the planet (e.g. Newsom et al., 1999; Yen et al., 2008). Additionally, sediments that have been altered by near-surface groundwater have also been observed on Mars (e.g. Squyres et al., 2004). Geochemical modeling also suggests that large amounts of carbonates may have formed early in the planet's history when water was likely more abundant (Pollack et al., 1987; Fanale et al., 1992). Although conditions on the martian surface appear conducive to carbonate formation, thus far they have only been detected in limited quantities through orbital remote sensing (Ehlmann et al., 2008). Carbonate formation in general requires a relatively neutral pH. While carbonates have been observed in ancient martian meteorites (McKay et al., 1996; Bridges et al., 2001; Rao et al., 2005), observations of sulfate minerals in situ on the martian surface suggest a more acidic environment (Squyres et al., 2004), which is not conducive to carbonate formation. This poses a conundrum that has yet to be resolved,

although differences in local environments or conditions over geologic time scales may be involved (Ehlmann et al., 2008). Complicating the problem is the fact that detecting CO_3 through the ~6 mbar CO_2 atmosphere on Mars poses difficulties for many orbital remote sensing instruments, such as reflectance IR spectrometers currently orbiting the planet (Ehlmann et al., 2008).

Understanding carbonate formation on Mars is important because it not only answers questions about the presence and abundance of water on the planet, but also addresses the type and evolution of aqueous alteration processes that have occurred there. As a result, it is important to be able to recognize carbonate materials in situ should MSL encounter them. The ChemCam LIBS is one of two instruments on MSL that is capable of detecting carbon. Previous work by McMillan et al. (2007) using LIBS has shown that carbonates in natural rock samples can be differentiated from one another under terrestrial conditions. However, LIBS is sensitive to environmental conditions such as atmospheric composition and pressure (Arp et al., 2004; Radziemski et al., 2005), and as a result requires calibration for materials in a specific environment in the laboratory. Here we use LIBS to examine natural carbonate minerals within whole rocks in a simulated martian environment to better understand the LIBS spectra of these materials on Mars. Of particular importance in this initial study is to determine if LIBS can detect carbonate rocks in a CO_2 atmosphere, and whether different types of carbonate materials can be differentiated from one another in this environment.

The sample suite

Four types of carbonate materials were examined: calcite ($CaCO_3$), dolomite ($CaMg(CO_3)_2$), siderite ($FeCO_3$), and rhodochrosite ($MnCO_3$) (Table 3.1). These carbonates are not standards or pure minerals, but rather natural samples from various field locations, some containing multiple minerals within a whole rock. This was done to provide a realistic context for the minerals of interest that mimics the types of geologic samples that may be encountered on Mars by MSL. For example, the three calcite samples probed here contain varying impurities, indicated by different mineral colors. No sample preparation was done; samples were examined as whole rocks or minerals. In addition to the carbonate samples, 12 geological reference materials from Brammer Standard Company, Inc. were also examined as standards in order to determine whether

Table 3.1. Mineral and rock samples and standards used in this study[a]

	Name (no. of samples)	*Composition/ main elements*	*Origin/Main mineral constituents*
Samples	Calcite (3)	$CaCO_3$	UNM mineral collection
	Siderite (2)	$FeCO_3$	UNM (rock); Ivigtut, Greenland
	Rhodochrosite (1)	$MnCO_3$	Sweet Home Mine, Colorado, U.S.A
	Dolomite* (2)	$CaMg(CO_3)_2$	UNM (rock); Selasvann, Norway
Standards	Olivine (2)	Fe, $MgSiO_2$	
	Dolomite* (2)	$CaMg(CO_3)_2$	Dolomite
	Basalt** (3)	Fe, Mg, Si, O, Ca, Na, Al	Olivine, pyroxene, plagioclase
	Andesite** (2)	Fe, Mg, Si, O, Ca, Na, Al, H	Plagioclase, pyroxene, hornblende
	Limestone** (3)	$CaCO_3$	Calcite

[a]Chemical formulas for mineral samples are those of ideal compositions, but impurities and minor solid solution substitutions are possible.
*Both a mineral and a rock
**Rock carbonates could be distinguished from other geologic materials containing similar elements.

carbonates could be distinguished from other geologic materials containing similar elements. These reference materials include igneous materials such as basalt, andesite, and olivine, as well as sedimentary materials including several dolomites and limestones (Table 3.1). It is important to note here that some of these materials are minerals (which have a specific crystal structure) and others are rocks (which are composed of minerals). All standards were prepared as relatively homogenous pressed powder pellets, similar to the calibration targets that will be sent along with ChemCam to Mars on the Curiosity rover (Wiens et al., 2007). These standards are part of a larger group of materials that are being used to calibrate the ChemCam LIBS in the laboratory (Wiens et al., 2010).

Methods

LIBS. A Spectra-Physics Indi Nd:YAG laser operating at 1064 nm, a repetition rate of 10 Hz, and an energy of 17 ± 1 mJ/pulse was used to sample target material. The laser beam was focused on the sample surface, which was positioned at a 7 m standoff distance to simulate data collection on Mars. The samples were placed in a vacuum chamber filled with 7 Torr CO_2 to simulate martian atmospheric pressure and general composition. Some of the plasma emission was collected with a telescope and then directed to a demultiplexer connected to three Ocean Optics HR2500+ spectrometers, spanning the wavelength regions 224.34-326.92 nm (UV), 384.02-472.53 nm (VIS), and 494.62-932.89 nm (VNIR). This range is slightly greater than what ChemCam will use on Mars, and so a reduced range of 245-800 nm was used in this study. The integration time was set to 1 s and five spectra were averaged for each LIBS spectrum, so that each recorded spectrum is the combination of 50 laser shots (Clegg et al., 2009). Each sample was

probed along a profile on five locations on the surface. To account for fluctuations in laser intensity, each spectrum was normalized to the total emission intensity.

MVA. The LIBS data were analyzed using two multivariate analysis (MVA) methods: principal component analysis (PCA) and partial least squares regression (PLS) (Clegg et al., 2009; Sirven et al., 2006). PCA identifies the spectral variations generated from each sample. With the correct training set, PCA can predict the rock type of the sample. Here, the training set consists of Brammer geologic reference materials that include basalt, andesite, olivine, limestone, and dolomite (Table 3.1). In PLS, a model is developed to describe a statistical correlation between each pixel in the LIBS spectrum and the variations in the elemental compositions, using standards with known values to predict the compositions of unknown samples. PLS also identifies correlations between elements and the rest of the sample matrix. Recent work suggests that PLS compensates for most of the chemical matrix effects within a related set of rocks and minerals, assuming an appropriate set of standards is used (Clegg et al., 2009; Harmon et al., 2009). Here, the Brammer standards are used to predict the compositions of the carbonate samples. Both PLS and PCA models were made using the commercially available Unscrambler statistical software following the methods of Clegg et al. (2009). PLS models of composition were built from the standards, and the sample compositions were determined by placing them as unknowns in the model.

SEM. Samples were also examined using a JEOL 5800LV Scanning Electron Microscope (SEM) operating at a low vacuum of 30 Pa, an accelerating voltage of 15-20 kV, and a

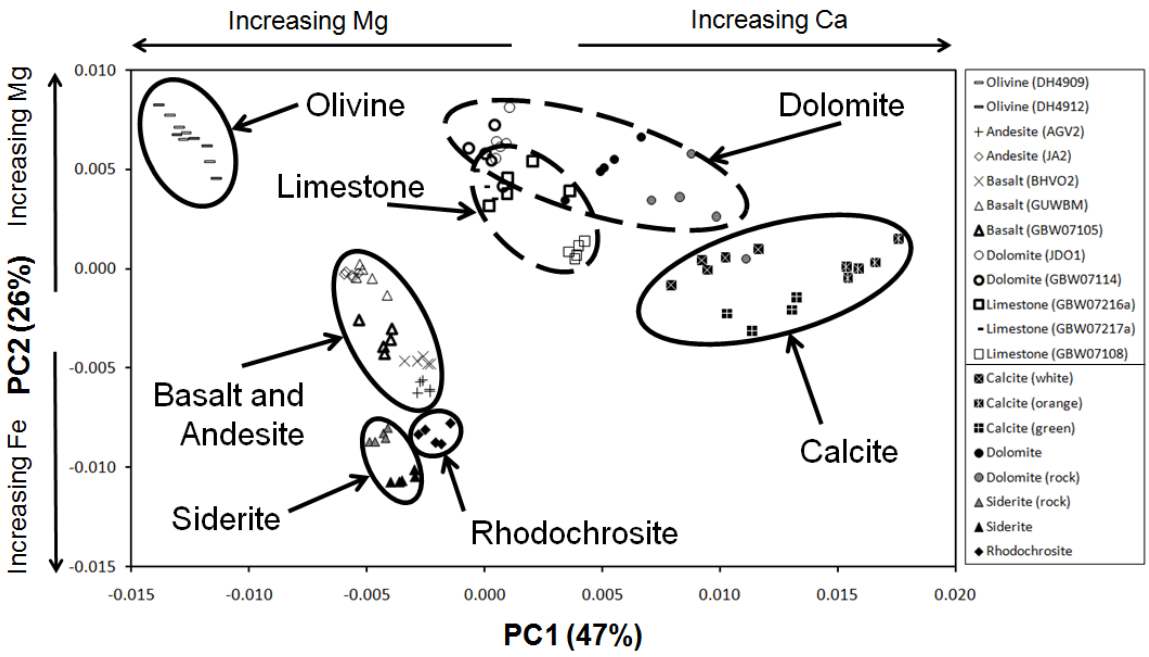

Fig. 3.1. Principal component analysis (PCA) plot of PC1 (47%) versus PC2 (26%) scores for carbonate samples (closed symbols, below line in legend) and geological reference material standards (open symbols). Rock types generally plot together, as seen in labeled circles. For the Ca- and Mg- rich carbonate materials calcite, limestone, and dolomite, there is a range of compositions; since PC1 and PC2 are primarily influenced by Ca, Mg, and Fe, these carbonate materials form groups that overlap somewhat. Note that the limestone standards used are somewhat dolomitic and have significant Mg content.

beam current of 0.66 nA. Samples were placed directly in the chamber with no additional preparation in order to ensure that the samples were in the same condition as during the LIBS experiment. All SEM data were obtained after analysis with LIBS. A quantitative analysis of composition was done at 3-4 locations for each sample with the energy dispersive spectrometer (EDS). These results were then compared with the LIBS PLS results for sample and reference material compositions.

Results

The PCA model correctly clustered materials of similar composition (Fig.3.1). Igneous materials (basalt, andesite, and olivine) are distinct from the sedimentary materials (the carbonate samples and dolomite and limestone standards). The first two principal

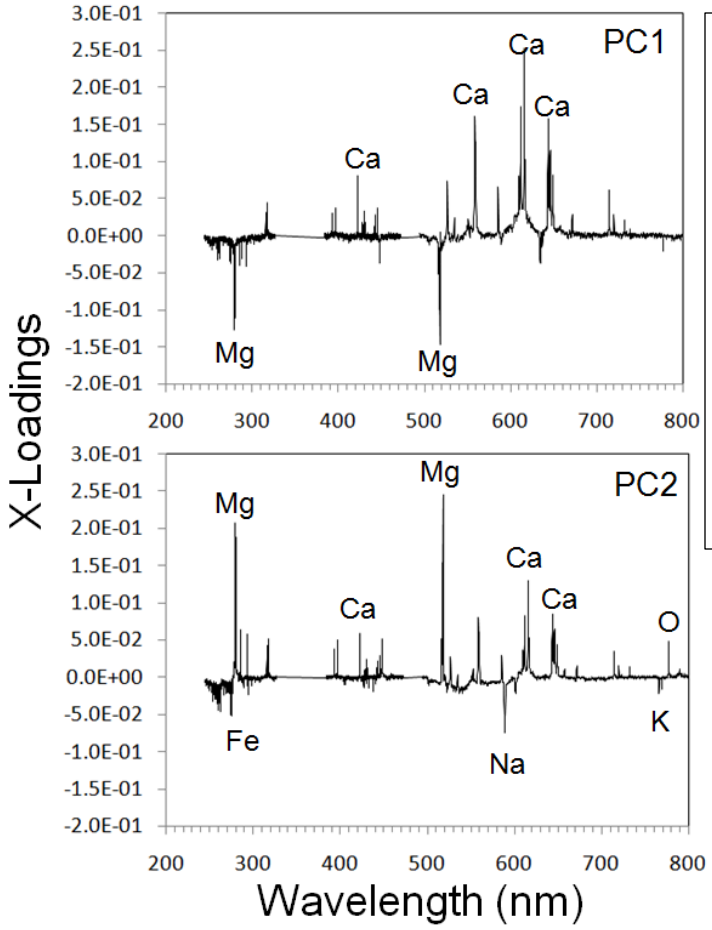

Fig. 3.2. X-loadings for PC1 (47%) and PC2 (26%) by wavelength. The most influential peaks in PC1 belong to Ca (+) and Mg (-); the most influential peaks in PC2 belong to Mg (+) and Fe (-). As a result, materials in the associated PC1 vs. PC2 scores plot (Fig.1) are primarily distributed based on their relative Ca, Mg, and Fe contents. Interestingly, the O peak at 777.4 nm appears to have some influence in PC2 as well, pointing to the fact that as materials gain additional elements (e.g. complex materials such as basalt), the relative O content decreases.

components, PC1 and PC2, account for 47% and 26% of the spectral variability, respectively. As a result, PC1 and PC2 account for only 73% of the total variability, while the remaining 27% is described by PCs greater than 2. This is a fairly typical result when analyzing elementally complex geologic materials (Clegg et al., 2009). The loadings for PC1 and PC2 indicate that the peaks with the greatest influence in PC1 belong to Mg and Ca, and in PC2 to Mg and Fe (Fig.3.2). The LIBS PLS model correctly identified the presence and general amount of the major constituent elements of the calcite and dolomite samples as compared to the SEM EDS results (Table 3.2). Because of the lack of any similar standards for the siderite and rhodochrosite samples, PLS was

Table 3.2. Compositional results for carbonate samples from SEM energy dispersive spectroscopy (EDS) and LIBS partial least squares (PLS) modeling (dolomites and calcites only)[a]

	Calcite											
	Orange				*Green*				*White*			
	LIBS	σ	SEM	σ	LIBS	σ	SEM	σ	LIBS	σ	SEM	σ
Fe			0.07	0.02								
Mg											0.16	0.03
Ca	16.3	1.2	18.4	1.7	13.9	1.6	15.9	0.2	15.1	1.1	16.3	0.3
Mn							0.06	0.01			0.02	0.01
Na												
C	26.5	1.9	19.0	1.1	22.5	2.3	21.0	0.4	21.6	2.2	20.3	0.12
Al												
Si									0.41	0.72		
K	0.72	0.06			0.93	0.04			0.50	0.06		
O	56.5	1.0	62.5	0.7	62.4	1.1	63.0	0.2	62.3	0.7	63.3	0.3

	Dolomite								**Siderite**				**Rhodochrosite**	
	Mineral				*Rock*				*Mineral*		*Rock*		*Mineral*	
	LIBS	σ	SEM	σ	LIBS	σ	SEM	σ	SEM	σ	SEM	σ	SEM	σ
Fe	0.9	0.1	1.74	0.07			0.07	0.01	25.3	1.7	13.7	3.0		
Mg	8.4	0.7	8.78	0.16	3.11	1.07	8.53	0.22	0.23	0.1	1.9	0.3	0.40	0.13
Ca	11.2	0.4	11.2	0.2	12.7	0.3	9.24	1.59			0.25	0.05	0.27	0.25
Mn									1.64	0.07	1.85	0.56	16.3	1.0
Na											0.23	0.38		
C	17.9	1.2	15.7	0.8	21.9	2.2	19.0	1.1	13.2	2.4	16.0	1.7	17.4	1.5
Al											1.18	0.80		
Si											1.51	1.01		
K														
O	61.5	0.4	62.6	0.6	62.3	1.0	63.1	0.8	59.6	4.2	63.2	7.6	65.7	0.9

[a]Both the LIBS and the SEM data reported here are averages of multiple measurements (see text for details), and so standard deviation (σ) for each value is included in an adjacent column. All values are in atomic %.

not used to model their compositions; their compositions from SEM analysis are reported in Table 3.2 to provide context for the PCA results.

Discussion

Our initial results suggest that LIBS can detect carbonates and distinguish between different carbonate minerals and rocks within a martian environment. In our model, the igneous standards of basalt, andesite, and olivine were distinct from the sedimentary carbonate materials, including the Fe- and Mn-rich carbonates siderite and rhodochrosite. In PC1 and PC2, the elements with the greatest influence tend to be the major cations present in the materials. Even though the elements in the carbonate anion (C and O) do not exert a strong influence on either PC1 or PC2, carbonates are still distinguished from other materials because of the absence in these materials of certain major cations. PC2 in particular responds to both Na and K (Fig. 3.2); these elements are not generally found in carbonates, but are often seen in igneous materials such as basalt. The relative abundances of major cations also help to differentiate carbonates from other types of materials. While both basalt and limestone contain Ca, Ca is much more abundant in limestone than in basalt, and thus these materials can be differentiated in part by the relative abundance of the Ca cation. Additionally, information about less influential elements may be obtained by utilizing additional PCs. In particular, Si and Mn are particularly influential in PC3 (8%).

Within the four types of materials represented by the carbonate sample suite, there were clear differences in their LIBS spectra (shown in Fig. 3.3) that allowed the PCA model to

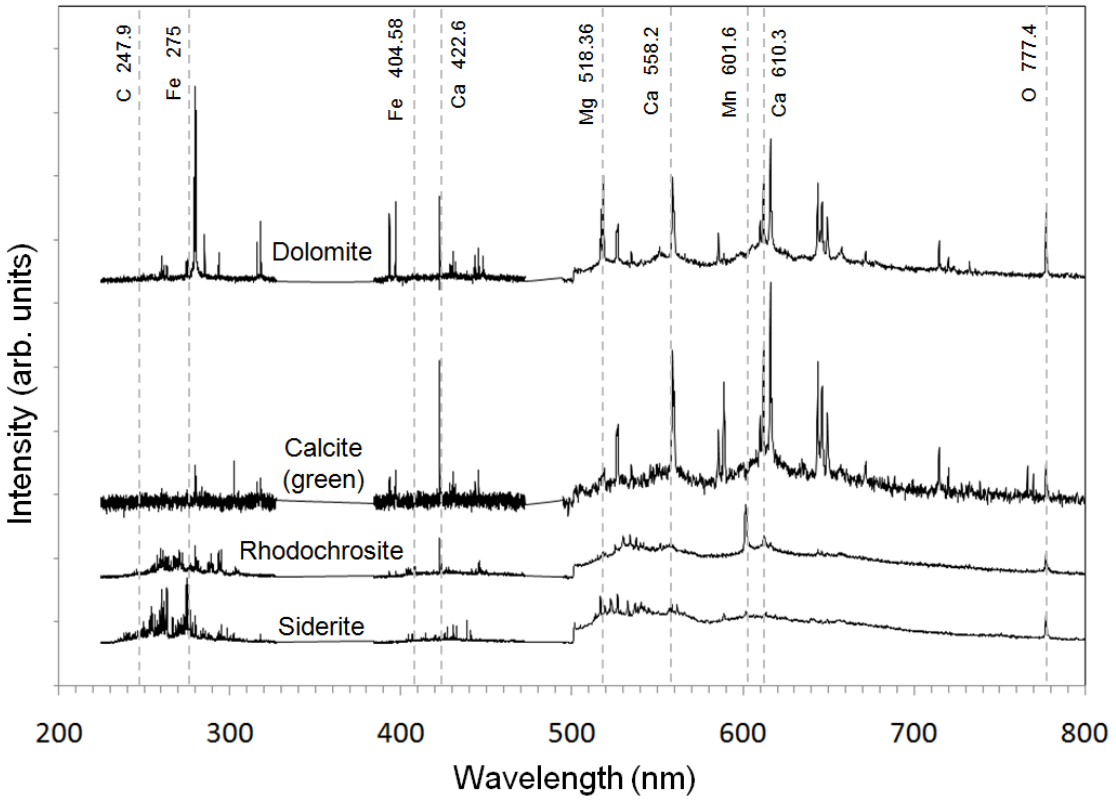

Fig. 3.3. Representative LIBS spectra of the four types of carbonate samples: Dolomite ($CaMg(CO_3)_2$), calcite ($CaCO_3$), rhodochrosite ($MnCO_3$), and siderite ($FeCO_3$).

correctly differentiate between them in general. The dolomites and limestones formed the least distinct clusters in PCA space, and this is very likely due to the fact that dolomite and calcite/limestone are members of a continuum of carbonate compositions (e.g. solid solution) with varying amounts of Mg and Ca. In a crystal matrix, one cation may substitute for another if they have the same charge and their ionic radii are similar. As a result, Ca and Mg are often quite interchangeable within natural minerals and so abundances of these elements will vary. In this PCA model, the elements with the most influence along the PC1 axis are Mg and Ca (Fig. 3.2). In general, the dolomites do plot closer to the Mg end and calcites to the Ca end. It should be noted that the limestone standards GBW07216a and GBW217a are both relatively Mg-rich, while the dolomite rock sample is somewhat Ca-rich. This is because what is called a 'dolomitic limestone'

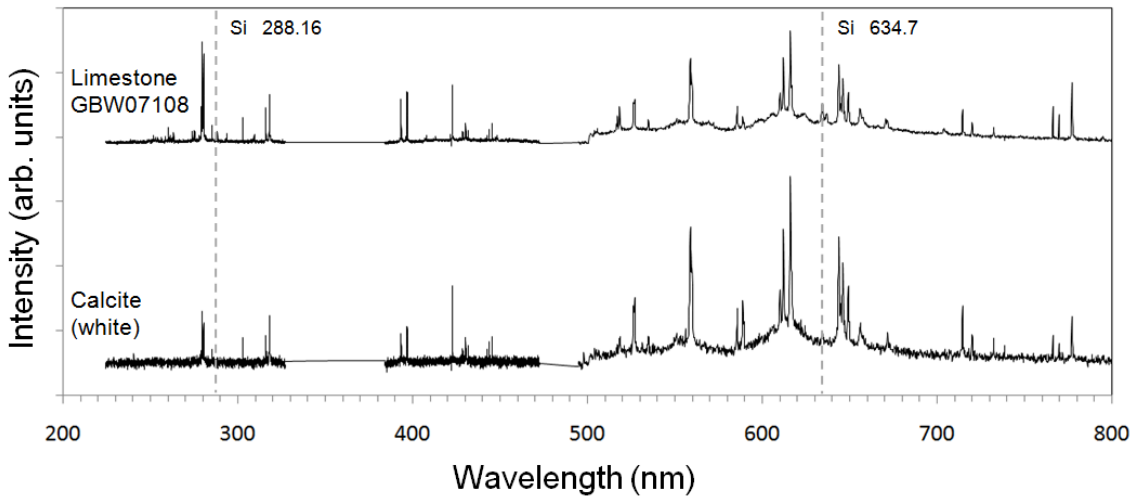

Fig. 3.4. Comparison of the spectra of the limestone standard GBW07108 and the white calcite sample. Limestone is a rock that is primarily composed of the mineral calcite. Note that the spectra are quite similar, with the same major and minor peaks. However, the limestone spectrum contains peaks that the calcite does not, most notably at ~634 and ~288 nm, which correspond to Si. Natural samples such as these often have somewhat variable compositions, and so care must be taken to note how trace element composition affects the spectra, and to obtain appropriate standards accordingly.

by Brammer Standard Company, Inc. could also be identified as a 'Ca-rich dolomite.' Figure 3.4 compares the most Ca-rich limestone standard GBW07108 with the most pure calcite sample (white) in the carbonate suite. The spectra share the same major peaks and most of the minor ones, with a notable exception ~634 nm. Here, there is a peak corresponding to Si visible in the limestone standard that is greatly attenuated or not present in the calcite sample. This is consistent with the reported Si content of the limestone standard by Brammer (~5% by atomic fraction), whereas no Si was detected in the white calcite sample by the SEM. Additionally, the white calcite contains only ~7% of the Mg reported to be present in the limestone. As a result, these two materials appear to be somewhat offset from one another in the PCA plot, with the limestone plotting towards the Mg-rich upper left quadrant (Fig. 3.1). However, they are clearly distinct from other types of materials, and can be identified as part of the Ca-Mg family of carbonates. With additional training materials, it should be possible to improve clustering

in the model given how similar the LIBS spectra are to one another (e.g. Fig. 3.4). Our results show that the four main carbonate samples examined here—calcite, dolomite, siderite, and rhodochrosite—may all be distinguished in PCA both from one another and from the plasma produced by carbon-free silicates in the CO_2 of the martian atmosphere.

The PLS model was able to correctly identify the presence and general abundance of the major elements in the dolomite and calcite samples (Table 3.2). Importantly, PLS determined C values that were within ~2% of the SEM values in all samples except for the orange calcite; in this sample, the model value for C was ~38% higher than the SEM value. This uncertainty could be due to the greater heterogeneity inherent in natural rock compared to the powdered standards. The model also indicated small amounts of non-major elements in the dolomites and calcites. This is likely due to the fact that LIBS is significantly more sensitive to trace amounts of these elements than is SEM EDS. EDS typically has a detection limit ~0.1 wt% in bulk materials, whereas for most elements LIBS has a much lower detection limit ~0.0002-0.1 wt%. When suitable standards are used the PLS analyses appear to compensate for enough of the chemical matrix effects to produce compositions that match SEM results.

The carbonate samples chosen for this study appear to make good training samples to include in future MVA models and laboratory validation experiments should ChemCam detect carbonates on Mars. In particular, adding standards of less common carbonates such as siderite and rhodochrosite will enhance the probability that these materials will be recognized as such if encountered on Mars, and that PLS modeling of these materials'

compositions will be accurate. Future work will involve a more systematic examination of mixtures of carbonate minerals to determine how the major cation and anion affects the LIBS signature, and whether the individual mixture components may be identified and differentiated. Given the importance of detecting carbonates on Mars, it is extremely important that the ChemCam LIBS instrument is calibrated in the laboratory on Earth for these materials so that they may be recognized in situ on Mars.

Chapter 4

Examining natural rock varnish and weathering rinds with laser-induced breakdown spectroscopy for application to ChemCam on Mars

Article citation: Lanza, N.L., Clegg, S.M., Wiens, R.C., McInroy, R.E., Newsom, H.E., and Deans, M.D. (submitted). Examining natural rock varnish and weathering rinds with laser-induced breakdown spectroscopy for application to ChemCam on Mars. *Submitted to Applied Optics on 1 Oct. 2011*.

Abstract

A LIBS instrument will travel to Mars as part of ChemCam on the Mars Science Laboratory rover. Martian rocks have weathered exteriors that obscure their bulk compositions. We examine weathered rocks with LIBS in a martian environment to improve interpretations of ChemCam rock analyses on Mars. Profile data are analyzed using principal component analysis and coatings and rinds are examined using scanning electron microscopy and electron probe microanalysis. Our results show that LIBS is sensitive to minor compositional changes with depth and correctly identifies rock type even if the series of laser pulses does not penetrate to unweathered material.

A LIBS instrument on Mars

A laser-induced breakdown spectroscopy (LIBS) instrument will begin its journey to Mars in late 2011 as part of the ChemCam instrument package onboard the NASA Mars Science Laboratory (MSL) rover *Curiosity*. ChemCam consists of two instruments: a LIBS spectrometer and a Remote Micro Imager (RMI). The LIBS provides microbeam

(80-250 μm radius) chemical analyses of materials of interest, while the RMI provides a telescopic context image for the LIBS sampling location (100 μrad resolution) (Wiens et al., 2011a). The ChemCam laser and telescope are installed on the rover mast ~2 m from the ground and can probe samples at standoff distances 1.5-7 m from the rover. The primary objective of *Curiosity* is to determine the past and present habitability of the martian surface and near-surface (Grotzinger, 2009). Habitability describes environments in which life as it is currently understood may exist; a key criterion for habitability is the presence of liquid water. Thus, the detection of water-formed materials and hydrated minerals will be of particular importance to MSL. The LIBS technique is well suited to these goals because it is sensitive to light elements such as H, O, and C. Because LIBS is sensitive to environmental conditions such as atmospheric composition and pressure (Arp et al., 2004; Radziemski et al., 2005), it requires calibration for materials in a specific environment in the laboratory. Here we use LIBS to examine naturally weathered rock samples in a simulated martian environment to better understand how to analyze and interpret weathered materials encountered by MSL on the surface of Mars.

The formation of rock coatings and weathering rinds

Weathering describes a range of processes that naturally occur on the surfaces of the Earth and other rocky planets that act to physically and chemically break down and alter surface materials. In chemical weathering, these changes are the result of interactions between the rocky surface and the atmosphere, aqueous solutions, and biological processes, amongst others. The chemical composition of a rock may be changed by either adding or removing elements; both are often the result of aqueous alteration, which can

act to both precipitate new materials as well as to leach more soluble elements from the rock. These processes lead to two distinct types of observable chemical weathering features on rock surfaces: coatings and rinds. Although they form in similar environments, coatings and rinds represent two distinct material types that provide complementary chemical information.

Coatings develop when external materials are deposited over an existing rock surface, and are generally chemically unrelated to the host rock. There is a sharp contact between rock and coating, which is often quite thin (on the order of microns). A very common type of rock coating on the Earth is rock varnish, which forms dark, micron-scale coatings dominated by Mn- and Fe-oxides and clay minerals. Because it commonly occurs in arid regions with less plant life, rock varnish is often referred to as 'desert' varnish in terrestrial literature, although it has also been observed in a number of other environments (Dorn, 1998). The exact formation process of rock varnish is still debated, but it appears that the Mn component may be controlled in part by microbial activity (e.g. Northup et al., 2010). The observed enrichments of Mn and Fe are likely derived from external materials with sources such as the atmosphere, wind-blown dust, and regional soils (Allen, 1978; Perry and Adams, 1978; Thiagarajan and Lee, 2004; Engel and Sharp, 1958) rather than the composition of the host rock. The thickness of rock varnish often shows high spatial variability both regionally (Dorn, 1998) and even within a single thin section (Northup et al., 2010).

In contrast to coatings like rock varnish, weathering rinds are the result of element removal from the rock, leading to compositions that are similar to those of the unweathered rocks but depleted in elements that are most mobile. Mobility is dependent on a number of factors, in particular the solubility of the element in a certain fluid. As elements are removed, a gradational weathering front develops from the weathered exterior to the fresher, less altered interior of the rock. Weathering rinds have predicable compositions based on the chemistry of the parent rock and the aqueous alteration environment. By studying the compositional trends in weathering rinds, it is possible to understand the types of fluids to which the rock was exposed. The relative mobility of elements in a rock is dependent on many factors, in particular the amount of available water and its pH and Eh. For most groundwaters with pH ~4-9, the relative mobilities of major rock-forming elements are as follows from most to least mobile:

$$(Ca^{+2}, Mg^{+2}, Na^{+}) > K^{+} > Fe^{+2} > Si^{+4} > Ti^{+4} > Fe^{+3} > Al^{+3}$$

These relative mobilities can vary depending on mineralogy and bond strength (e.g. Chesworth et al., 1981) but are generally related to the ionic potential of the element, which is the ratio of ionic charge to ionic radius.

Coatings and rinds are not mutually exclusive, and may form concurrently or separately in natural settings. Figure 4.1 shows a naturally weathered basalt from this study with both a coating and a rind; the coating appears as a dark pasted-on layer on the rock exterior, while the rind is visible below the coating as a lighter-toned region that grades

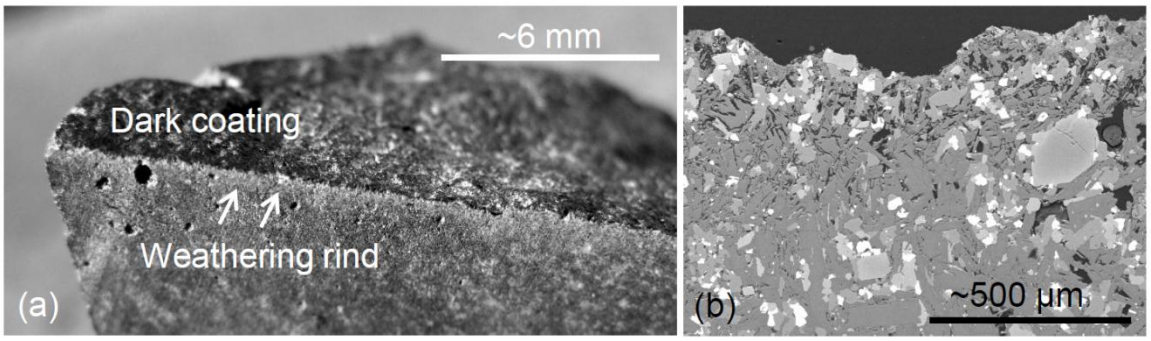

Fig. 4.1. **(a)** A cross section of a naturally weathered basaltic rock sample from this study (N6B). A dark rock varnish coating is visible on the very surface of the rock; directly beneath the coating is a weathering rind that appears as a sub-mm thin region of slightly brighter material. The brighter rind grades into the slightly darker grey interior of the rock. The coating represents material that has been added to the rock surface, while the rind represents a region in which material has been removed. **(b)** A backscattered electron (BSE) image of the same sample in thin section. In this view, the dark varnish is visible at the very top edge of the sample. The weathering rind is visible as a zone with void spaces directly below the coating, indicating regions in which some mineral dissolution has occurred. The rind grades into the fresh rock at the bottom of the image, where fewer void spaces are observed.

into the rock below. Both coatings and rinds can provide significant information about the types of chemical weathering processes that have occurred in a region. On Earth, rock coatings and rinds have been used to determine rock surface ages (McFadden et al., 1989; Birkeland, 2005; Gordon and Dorn, 2005), to study past climate and climate changes (Dorn, 1994), and even to date archeological artifacts (Francis et al., 1993; Clarkson and Dorn, 1995). The rates of coating and rind development vary greatly by weathering environment and rock composition, but can take on the order of thousands of years (Sowers, 2005; Sak et al., 2004).

Interpreting ChemCam LIBS measurements of rock surfaces on Mars

Although coatings and rinds can provide information about weathering processes, the vast majority of geological studies are concerned with the pristine interior, or 'fresh,' compositions of rocks. The composition of the fresh rock provides information about how and when it formed, which is often of more interest than the weathering history of

the rock's surfaces. Field geologists frequently discard the surface portions of their collected natural samples because coatings and rinds obscure the fresh rock compositions. This practice will not be an option on Mars; unlike previous rovers, MSL will not have a tool for abrading rock surfaces to obtain a fresh surface for analysis, though it will carry a brush to remove unconsolidated dust coatings and a drill to retrieve powders from the interiors of rocks (Jandura et al, 2010). Both rock coatings and rinds have been observed in situ on the martian surface (Haskin et al., 2005; McSween et al., 2004; Arvidson et al., 2004), and so these materials are expected to be encountered with MSL. As a result, all analyses from arm and mast instruments will involve the compositions of weathered rock surfaces to some extent (the in situ instruments on MSL use drill and soil powders delivered by the arm). However, because LIBS ablates a small amount of material during a measurement, ChemCam will be able to both analyze and remove thin coatings and weathering rinds that may be present. Martian rock coatings have been observed to be rich in Fe-oxides, similar to terrestrial rock varnish but without the Mn component that appears to be biologically controlled on Earth (e.g. Haskin et al., 2005). Both observations and related geochemical modeling suggest that possible rock coatings on Mars, in addition to Fe-oxides, include amorphous silica (Milliken et al., 2008), sulfates (e.g. Bishop et al., 2002), and potentially evaporites such as halite (Knoll et al., 2008) and chlorides (Osterloo et al., 2008). The goal of this study is to better understand how rock coatings and weathering rinds may be analyzed with LIBS in a martian environment. Of particular importance is observing chemical trends with depth, differentiating between coatings and rinds, and determining whether obtaining a fresh rock composition is possible. While some preliminary work on rock coatings with LIBS has been done

previously (Harmon et al., 2006; Dííaz Pace et al., 2011; Cousin et al., 2011; Wiens et al., 2004), this study represents the first time that weathering rinds are specifically examined and that different rock varnishes are compared.

The sample suite

Four naturally weathered basaltic rock samples were obtained from the Black Point Lava Flow (BPLF), which is located ~50 km north of Flagstaff, Arizona, U.S.A and is part of the San Francisco volcanic field. This basalt flow erupted on the surface ~1.5 Ma ago (Ulrich and Bailey, 1987) and has been exposed to surface weathering processes since that time. Basalt is a volcanic rock that is composed of fine-grained minerals including olivine, pyroxene, and plagioclase; major constituent elements include O, Si, Fe, Al, Mg, Ca, Na, and K. All four samples have dark exterior coatings that appear to be rock varnish and thin (< 1 mm) weathering rinds that are visible by inspection (Fig.4.1). The bulk fresh rock composition of the BPLF is well documented (e.g. Ulrich and Bailey, 1987), although coatings and rinds found on rocks here have not been previously studied. These samples were chosen because they are basalts that have been weathered in a desert environment, similar to basaltic materials on Mars that are also expected to weather in an arid environment. In addition to the basalt samples, eight basaltic reference materials from Brammer Standard Company, Inc. were also examined as standards in order to place sample compositions in the context of similar materials. These standards include MO12, MO13, MO14, GBW 07105, BIR1, JB1b, BHV02, and GUWBM, which are all basalts. All standards were prepared as relatively homogenous pressed powder pellets, similar to those used in in previous studies (e.g. Clegg et al., 2009; Tucker et al., 2010).

These standards are part of a larger group of materials that are being used to calibrate the ChemCam LIBS in the laboratory (Wiens et al., 2011b).

Methods

EPMA

Sample coatings and weathering rinds were imaged using a JEOL 8200 Electron Probe Microanalyzer (EPMA) operating at an accelerating voltage of 15 kV and a beam current of 1.5 nA. BPLF samples were cut into thin section billets at right angles to the rock surfaces so as to present profiles into the rocks. Standard thin sections were prepared and carbon-coated for microanalysis, and compositional images were obtained using backscattered electrons (BSE).

SEM

Sample coating compositions were measured using a JEOL 5800LV Scanning Electron Microscope (SEM). Samples were run twice with two different types of preparation: uncoated rock slabs of the weathered surface and carbon-coated thin sections of rock cross sections. The rock slabs were used in addition to thin sections in order to obtain a good sampling of the surface rock coating. For the uncoated slabs, the SEM was operating at a low vacuum of 30 Pa. In both experiments, the SEM was operating at an accelerating voltage of 15-20 kV and a beam current of ~0.50 nA; calibration was done on Cu. A quantitative analysis of composition was done at 3-4 locations for each sample with the energy dispersive spectrometer (EDS) in order to confirm the presence of elements detected by LIBS.

LIBS

A Spectra-Physics Indi Nd:YAG laser operating at 1064 nm, a repetition rate of 10 Hz, and an energy of 17 ± 1 mJ/pulse was used to sample the surface material of the samples. The laser beam was focused on the sample surface at a 5 m standoff distance to simulate data collection from the rover on Mars. The samples were placed in a vacuum chamber filled with 7 Torr CO_2 to simulate martian atmospheric pressure and general composition. Some of the plasma emission was collected with a telescope and then directed to a demultiplexer connected to three Ocean Optics HR2500+ spectrometers, spanning the wavelength regions 224.34-326.92 nm (UV), 384.02-472.53 nm (VIS), and 494.62-932.89 nm (VNIR). Because this range is slightly greater than what ChemCam will use on Mars, a reduced range of 245-800 nm was used in this study. The integration time was set to 500 ms so that each LIBS spectrum represents the average of five laser shots. Ten such spectra were obtained on a single sampling location such that each subsequent shot samples at a greater depth than the one previous, creating a compositional depth profile. Samples were measured both on the interiors (fresh) and exteriors (weathered). All interior shots were averaged for a total of 50 shots per spot in order to provide a bulk composition for the fresh rock. To account for fluctuations in laser intensity, each spectrum was normalized to the total emission intensity.

PCA

In order to better understand how composition changes from the surface to the interior in the samples, the LIBS data were analyzed using principal component analysis (PCA).

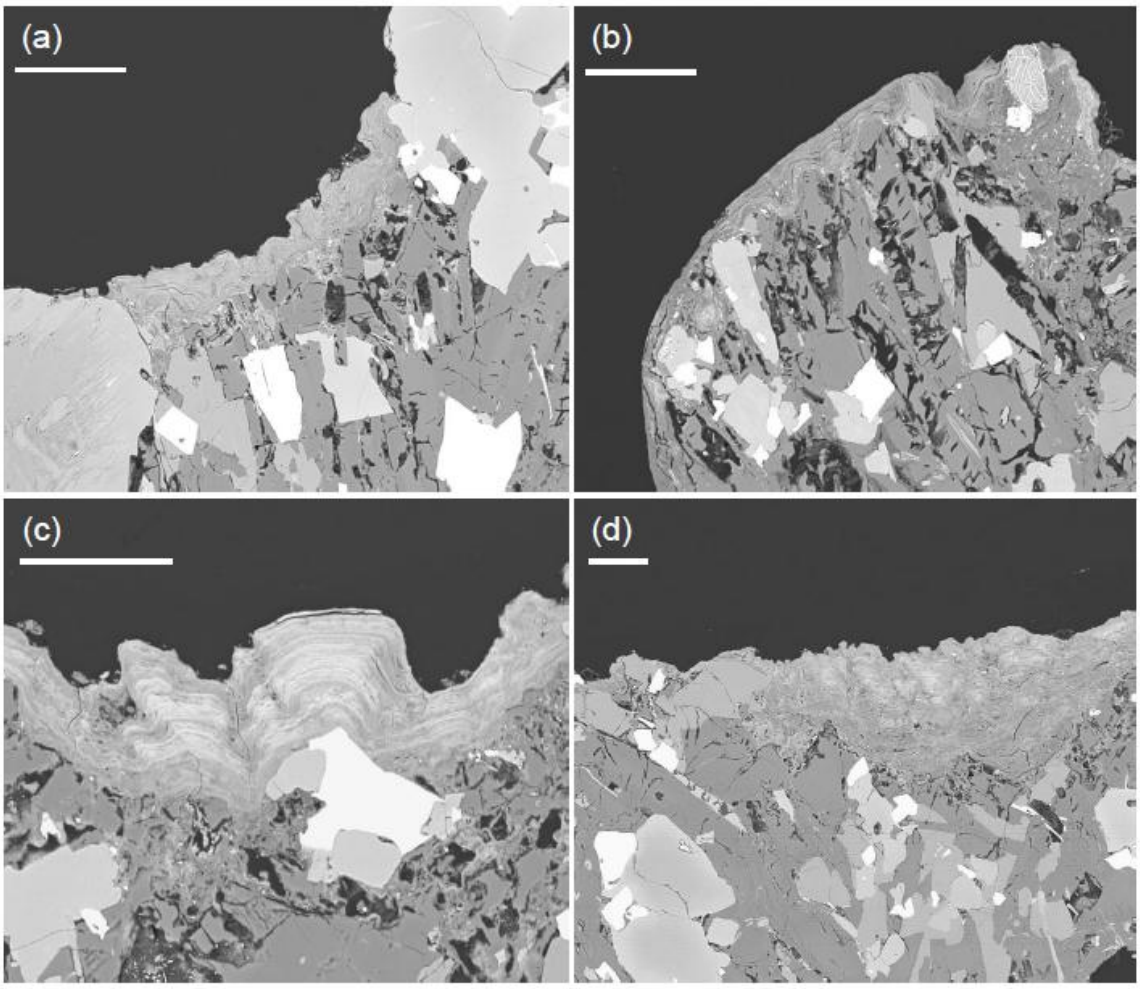

Fig. 4.2. Backscattered electron (BSE) images of the four basalt samples in thin section obtained by electron probe microanalysis (EPMA). Banded coatings are visible on the surfaces of all samples, with significant spatial variations in thickness. Brightness indicates elemental composition, with brighter tones indicating heavier elements. Darker toned void spaces are also visible just below the varnish, indicating the presence of a weathering rind in which mineral grains have begun to dissolve. All scale bars are 50 μm. **(a)** N2B. Varnish does not appear to form on the larger mineral grains at the surface, likely due to their smooth texture. **(b)** N3B. Varnish has filled in topographic irregularities and created a smoother surface texture on this sample. **(c)** N6B. Distinct bands of brighter and darker material in the varnish suggest multiple episodes of deposition during its formation. **(d)** W6B. This sample contains pockets of very thick varnish (center right) that are adjacent to regions with almost no varnish (center left).

PCA identifies the spectral variations found within depth profiles as well as between individual samples. With the correct training set, PCA can predict the rock type of the sample and also show chemical trends along depth profiles. Here, the training set consists of the Brammer basaltic reference materials. PCA models were made using the

commercially available Unscrambler statistical software. PCA is used here in lieu of other techniques capable of determining quantitative composition such as partial least squares (PLS) regression (e.g. Clegg et al., 2009), which would have required a suite of standards that encompassed the compositional range of the samples and most pertinently their coatings.

Results

All samples had observable rock coatings of variable thickness at the 10s of microns scale as well as discernible rinds (Fig. 4.2). In BSE images, rock coatings appeared as bright layers pasted over the rock surface with an average thickness of ~10 μm, but which

Table 1. Compositional results for SEM quantitative EDS measurements on rock varnish found on basalt sample exteriors[a]

	N2B		**N3B**		**N6B**		**W6B**	
	Average	σ	Average	σ	Average	σ	Average	σ
Mn	8.93	4.44	22.55	14.41	9.77	11.87	1.33	1.23
Fe	11.22	1.09	10.27	5.23	12.33	8.39	11.94	9.32
Al	15.02	2.82	5.55	7.85	10.83	4.38	10.33	2.40
Si	15.07	1.92	17.72	2.41	17.40	11.74	24.14	5.30
Mg	2.54	0.61	--	--	2.45	1.57	0.65	1.12
Ca	0.37	0.37	1.70	1.01	1.01	1.03	2.26	3.16
Na	0.99	0.87	--	--	0.92	0.75	--	--
K	2.42	0.58	1.03	1.46	1.23	0.16	1.48	1.11
P	1.64	1.35	1.12	1.58	1.18	0.91	1.67	1.45
Ti	0.40	0.35	1.47	0.53	0.58	0.56	1.16	0.92
Ba	--	--	--	--	1.42	1.76	--	--
S	--	--	--	--	0.14	0.27	--	--
O	41.39	1.18	38.59	2.23	40.73	6.15	45.05	3.44

[a]Data are a combination of measurements on unprepared rock slab surfaces and carbon coated thin sections. Note the extremely high variability in rock coating composition even within a single sample, as indicated by the standard deviation. All values are in element %.

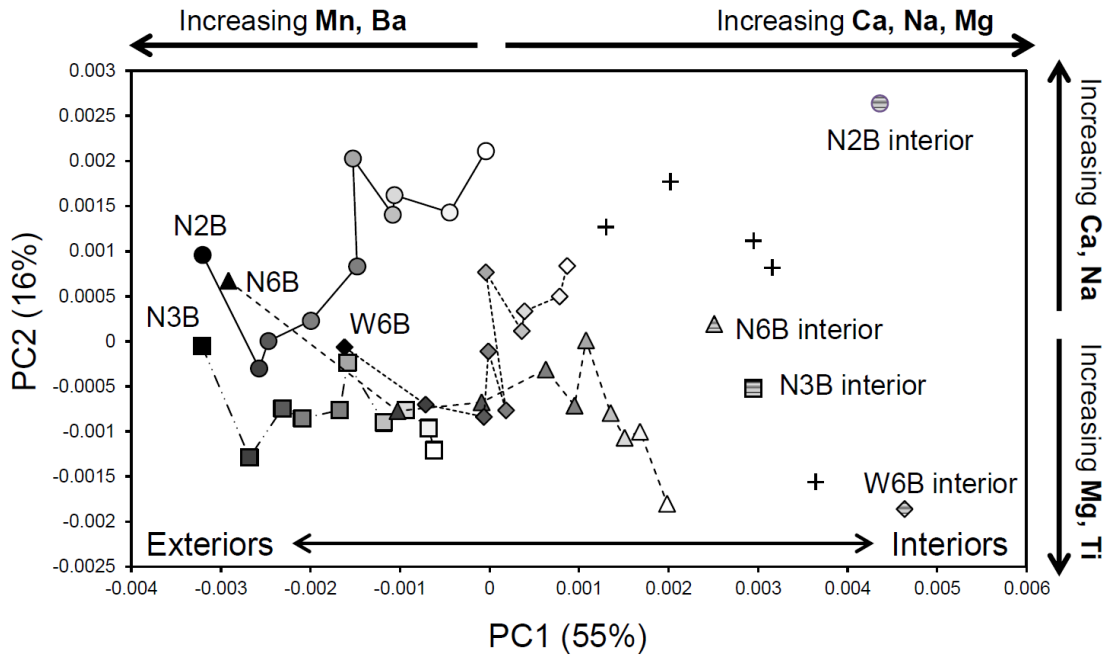

Fig. 4.3. Principal component analysis (PCA) of rock sample depth profiles, interiors, and basaltic geochemical reference material standards (+). Each depth profile is composed of 10 five-shot increments for a total of 50 laser shots. Fill hue gradient of data points indicates shot number, with darker points sampling closer to the surface and lighter points sampling deeper into the sample. The order of depth profile shots is also indicated by a connecting line. All sample exteriors plot first in the Mn and Ba region along PC1 in the negative direction; each subsequent shot group plots closer to the rock interiors in the Ca, Na, Mg region along PC1 in the positive direction. Only sample N6B comes close to its fresh rock composition at the end of the 50-shot depth profile; all other sample depth profiles end at compositions with less apparent Ca, Na, and Mg than their interior compositions. The PC2 axis is controlled in part by Ti in the negative direction, which is likely due to the Fe-Ti-oxide mineral found within the basalt.

varied ~0-100 μm throughout the samples. Regions containing darker-toned void spaces were observed directly below the coating. Quantitative measurements of the samples' surface composition by SEM EDS show the presence of Mn, Fe, Al, Si, Ca, K, P, and Ti in all four samples (Table 1). Sample N6B also contained trace amounts of Ba and S. Not every sample had detections of Mg and Na. The surface compositions show extremely high variability depending on the sampling location, as indicated by the standard deviation values. This is consistent with the EPMA observations of variable coating thickness (Fig. 4.2), as well as previous work on rock varnish by Dorn (1998).

The PCA model shows a systematic change in chemistry with depth for all four samples, with the deepest shots plotting closest to the rocks' fresh compositions (Fig. 4.3). The first two principal components, PC1 and PC2, account for 55% and 16% of the spectral variability, respectively, accounting for 71% of the total variability. This is a typical result for analyses of geological materials, which are elementally complex (Clegg et al., 2009; Lasue et al., 2011). The loadings for PC1 and PC2 indicate that the peaks with the greatest influence in PC1 belong to Ca, Na, and Mg in the positive direction (+) and Mn and Ba in the negative direction (-) and in PC2 to Ca and Na (+) and Mg and Ti (-) (Fig. 4.4). Major peaks for Mn, Ca, Na, and Mg show systematic changes in peak height with depth. Figure 4.5 shows the first 5-shot spectra and the interior spectrum for sample N6B with closeup views of peaks for Mn, Ca, Na, and Mg that include all 10 spectra of the depth profile. Sample interiors plotted in the same general region as the basalt standards, while rock exteriors were distinct from them both.

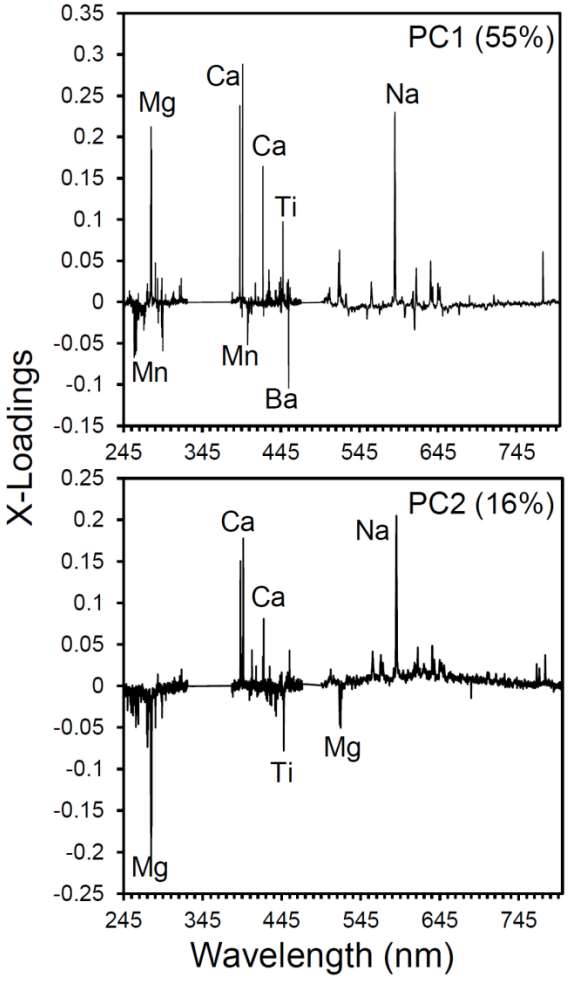

Fig. 4.4. X-loadings for PC1 (55%) and PC2 (16%) by wavelength. The most influential peaks in PC1 belong to Ca, Na, Mg in the positive direction (+) and Mn, Ba in the negative direction (-); the most influential peaks in PC2 belong to Ca, Na (+) and Mg and Ti (-).

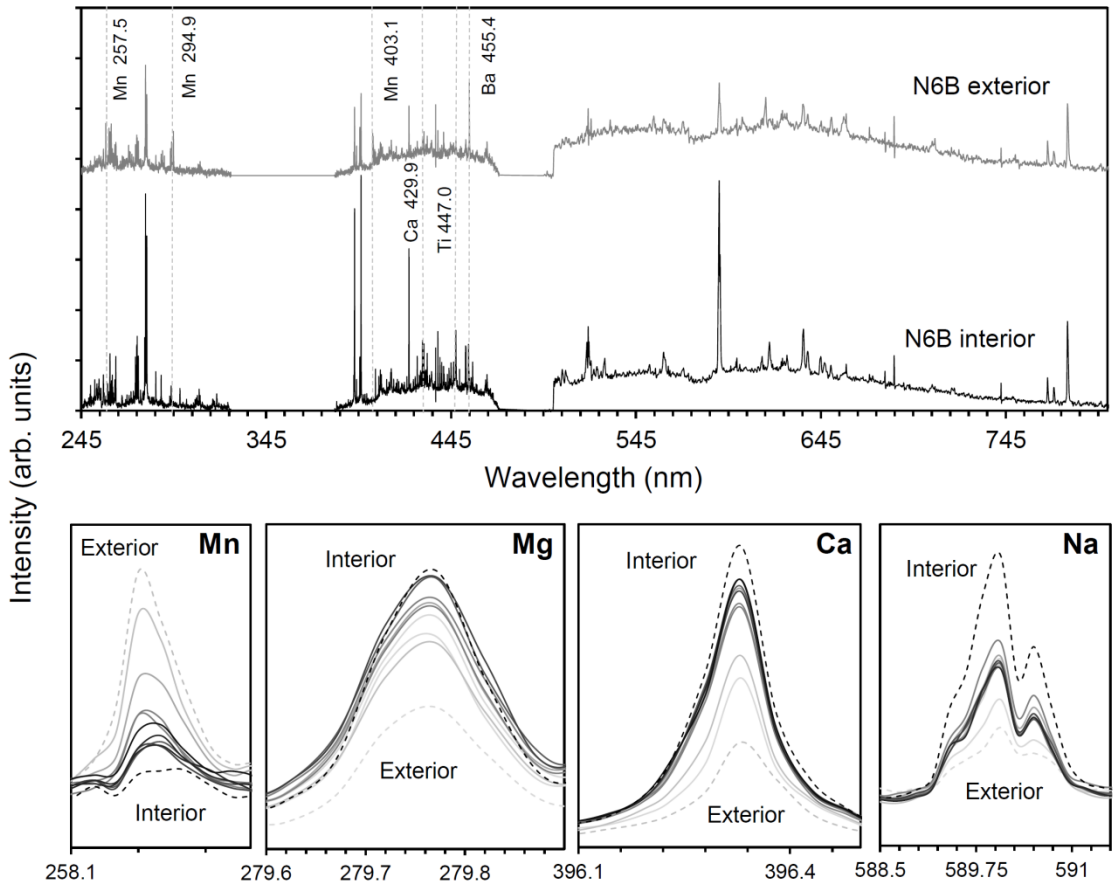

Fig. 4.5. Comparison of the exterior and interior spectra of sample N6B. The first five-shot data point (grey, top) shows peaks for Mn and Ba (labeled) that do not appear in the interior spectrum (black, bottom). Although peaks for Ca, Na, and Mg appear in both the exterior and interior spectra, they are greatly increased in the interior, with additional peaks for Ca appearing there. A peak for Ti (labeled) appears in the interior and not the exterior, likely due to the presence of an Fe-Ti oxide phase within the basalt. This suggests that despite the presence of a Mn-rich varnish, this sample is likely still identifiable as a basalt from the exterior data. Closer views of major peaks for Mn, Ca, Na, and Mg show systematic trends in peak height with depth for these elements (note that intensity is not to scale on close views). The grey dashed line represents the first shots on the exterior while the black dashed line represents the spectrum of the fresh interior; lighter greys indicate earlier shots in the depth profile and darker greys indicate later shots. For Mn, peak height decreases with depth, whereas for Ca, Na, and Mg peak height increases with depth.

Discussion

The PCA model shows an enrichment of Mn in the samples' exteriors as compared to both their fresh rock compositions as well as the basaltic standards, suggesting the presence of a rock varnish. In addition to Mn, the model also indicates surface enrichments in Ba. While not a major constituent of rock varnish, Ba is typically found within the clay component of terrestrial rock varnishes. The SEM EDS results confirm

the presence of both Mn and Ba in the sample surfaces, suggesting that these are good elements to use for differentiating between varnished rock exteriors and interiors. The LIBS data also indicate the presence of an Mn-rich coating; the 257.5 nm Mn peak is highest in the rock exterior, decreases with depth, and is lowest in the interior shots (Fig. 4.5).

The PCA model also suggests depletion in Ca, Na, and Mg in all samples as compared to their interior compositions. This interpretation is strengthened by the systematic increase in peak heights with depth for these elements, pointing to enrichment in Ca, Na, and Mg further from the rock surface. Because these elements tend to be the most soluble in natural weathering environments, their lower abundances in the mid-depth shots is consistent with the presence of a weathering rind. Rinds are also indicated by the observation of darker void spaces below the coatings in BSE images, suggesting that the rocks' constituent minerals have begun to dissolve and lose their more soluble cations in these regions.

Although the entire coating appeared to be removed in all samples, there was no abrupt transition between coatings and rinds in our results. The total depth into the sample made by the LIBS analyses was not directly measured. However, the ChemCam LIBS profiles at ~0.33-0.5 μm per pulse in basalts (Wiens et al., 2011a) and the profiling rate in this laboratory setup may have been slightly higher; this is consistent with removing ~10 μm coatings and additional amounts of weathering rinds. All samples showed compositional changes from the exterior to the interior such that they moved from the Mn and Ba

enriched region toward the Ca, Na, Mg dominated region in PCA space, suggesting a transition from coating to rind. This transition is also inferred from the systematic changes in certain LIBS peak heights with depth; Mn peak height decreases with depth while peak heights for Ca, Na, and Mg increase with depth. The final compositions from the near-surface spectra of samples N6B and W6B plotted close to the field of basalt standards along the PC1 positive axis (+), suggesting that the depth profiles for these samples penetrated through a larger amount of rind than the profiles for samples N3B and N3B. For sample N6B, there was a relatively large change between the first two five-shot data points as compared to other samples (Fig.4.3), which may indicate that most of the coating was analyzed in the first point in the profile. The first data point for W6B starts closer to the mean along the PC1 axis than other samples, which may be an indication of a thinner coating in the sampling location. This is consistent with the BSE data of W6B in which a section of very thick coating is adjacent to a region with little to no coating (Fig.4.2). In general, all sample coatings showed significant variability in thickness over relatively short distances within each sample, and so coatings and rinds were likely often analyzed simultaneously. Additionally, the five-shot averages may have somewhat obscured any sudden compositional changes with depth. However, our results suggest that for this sample suite, such changes may not be discernable even between single shots.

The 50-shot depth profile reached a composition similar to the fresh rock in only one sample, N6B. The final five shots of this sample plot in almost the same location along the PC1 axis (Fig.4.3), suggesting that Ca, Na, and Mg are no longer depleted at this

depth as compared to the fresh rock composition and that the weathering rind has been penetrated. Although the composition at this depth appears to be enriched in Mg and Ti in this model, this is likely due to the laser hitting an Mg-rich mineral grain such as olivine or pyroxene (Mg) or the Fe-Ti-oxide in the sample rather than a difference in bulk composition. For the other three samples, 50-shot depth profiles did not appear to be sufficient to reach a fresh rock composition. Because these samples have fairly thin coatings and rinds, these results suggest that it may be necessary to use more laser shots to do depth profiles on Mars, and that it may not be possible to directly measure fresh rock in some cases. However, it may still be possible to model its composition from a 50-shot depth profile even without a fresh rock composition. Although there are clearly compositional differences between rock exteriors and interiors, rocks with coatings and rinds may still be classified by rock type in LIBS data with PCA. Previous work on basaltic and sedimentary samples found that 50-shot averages of rock interiors and their weathered exteriors did not occupy exactly the same region in PCA space but did always plot by rock type overall (Lanza et al., 2010b). Examining the LIBS spectra here, it appears that the bulk rock composition is manifested to a large degree even in the presence of surface coatings. Figure 4.5 shows the average of the first five shots taken at the surface of N6B along with its interior composition. Although the exterior shows enrichment in Mn and Ba, the major peaks for Ca, Na, and Mg are present in both. From the exterior to the interior, the peaks for Mn and Ba disappear while the peaks for Ca, Na, and Mg increase; no additional major peaks for other elements appear or disappear. As a result, this material would likely be recognizable as a basalt even from surface measurements only. Additional geochemical modeling may allow for a more precise

prediction of fresh rock composition. Such modeling is beyond the scope of this paper but represents an important direction for future studies.

Implications for MSL

Our results demonstrate that the composition of rock varnish coatings and weathering rinds may be differentiated from that of fresh rock by LIBS. In addition, depth profiling revealed compositional changes in the sample suite that are consistent with the development of a coating and a rind. For every sample, 50 LIBS shots were enough to remove rock varnish coatings of variable thickness up to ~100 μm. Our results suggest that even thin weathering fronts on the order of microns at rock surfaces will affect measured compositions, and 50 laser shots may not be enough to reach fresh rock. However, with careful study of the compositional changes found within depth profiles of rocks encountered in situ, the ChemCam LIBS will be able to provide important information about the types of weathering processes that have occurred in that location as well as potentially accessing fresh rock material for chemical analysis.

REFERENCES

Allen, C.C. (1978). Desert varnish of the Sonoran desert: Optical and electron probe microanalysis. *Journal of Geology* 86 (6), 743-752.

Arvidson, R.E. and 30 colleagues (2004). Localization and physical properties experiments conducted by Spirit at Gusev crater. *Science* 305, 821-824.

Arvidson, R., and 21 colleagues (2008). Mars Exploration Program 2007 Phoenix landing site selection and characteristics. *Journal of Geophysical Research* 113 (E00A03), doi:10.1029/2007JE003021.

Arfstrom, J. and Hartmann, W.K. (2005). Martian flow features, moraine-like ridges, and gullies: Terrestrial analogs and interrelationships. *Icarus* 174, 321-335.

Arp, Z.A., Cremers, D.A., Wiens, R.C., Wayne, D.M., Sallé, B., and Maurice, S. (2004). Analysis of water ice and water ice/soil mixtures using Laser-Induced Breakdown Spectroscopy: Application to Mars polar exploration. *Applied Spectroscopy* 58 (8), 897-909.

Baker, V.R. (1993). Extraterrestrial geomorphology: science and philosophy of Earthlike planetary landscapes. *Geomorphology* 7, 9-35.

Baker, V.R., Carr, M.H., Gulick, V.C., Williams, C.R., and Marley, M.S. (1992). Channels and valley networks. In: Kieffer, H.H., Jakosky, B.M., Snyder, C.W., Matthews, M.S. (Eds.), *Mars*. The University of Arizona Press, Tucson, pp. 493-522.

Balme, M., Mangold, N., Baratoux, D., Costard, F., Gosselin, M., Masson, P., Pinet, P., and Neukum, G. (2006). Orientation and distribution of recent gullies in the southern hemisphere of Mars: observations from High Resolution Stereo Camera/Mars Express (HRSC/MEX) and Mars Orbiter Camera/Mars Global Surveyor (MOC/MGS) data. *Journal of Geophysical Research* 111 (E05001), doi:10.1029/2005JE002607.

Banerdt, W.B., Golombek, M.P., and Tanaka, K.L. (1992). Stress and tectonics on Mars. In: Kieffer, H.H., Jakosky, B.M., Snyder, C.W., Matthews, M.S. (Eds.), *Mars*. The University of Arizona Press, Tucson, pp. 249-297.

Batel, W. (1959). Über die Haftfähigkeit trockener feinkörniger Stoffe. *Chemie-Ingenieur Technik* 5, 343-345.

Bibring, J.P., and 51 colleagues (2006). Global mineralogical and aqueous Mars history derived from OMEGA/Mars Express data. *Science* 312 (5772), 400-404.

Birkeland, P.W. and Noller, J.S. (2005). "Rock and mineral weathering," in *Quaternary Geochronology: Methods and Applications*, J.S. Noller, J.M. Sowers, and W.R. Lettis, eds., American Geophysical Union Books Board, pp.293-312.

Bishop, J.L., Murchie, S.L., Pieters, C.M., and Zent, A.P. (2002). A model for formation of dust, soil, and rock coatings on Mars: Physical and chemical processes on the Martian surface. *Journal of Geophysical Research* 107 (E11), doi:10.1029/2001JE001581.

Blaney, D.L. (2006). "The Mars Science Laboratory (MSL) mission," presented at the *Workshop on Martian Sulfates as Recorders of Atmospheric-Fluid-Rock Interactions*, 22-24 October 2006, no. 7034.

Bridges, J.C., Catling, D.C., Saxton, J.M., Swindle, T.D., Lyon, I.C., and Grady, M.M. (2001). Alteration assemblages in martian meteorites: Implications for near-surface processes. *Space Science Reviews* 96, 365-392.

Bridges, N.T. and Lackner, C.N. (2006). Northern hemisphere Martian gullies and mantled terrain: implications for near-surface water migration in Mars' recent past. *Journal of Geophysical Research* 111(E09014), doi:10.1029/2006JE002702.

Boynton, W.V., and 24 colleagues (2002). Distribution of hydrogen in the near surface of Mars: Evidence for subsurface ice deposits. *Science* 297 (5578), 81-85.

Burr, D.M., Emery, J.P., Lorenz, R.D., Collins, G.C., and Carling, P.A. (2006). Sediment transport by liquid surficial flow: application to Titan. *Icarus* 181, 235-242.

Byrne, S. and 18 colleagues (2009). Excavation of subsurface ice on Mars by new impact craters. *Lunar and Planetery Science Conference XL*, Houston, TX, no.1831.

Caine, N. (1980). The rainfall intensity-duration control of shallow landslides and debris flow. *Geografiska Annaler A* (Physical Geography) 62 (1/2), 23-27.

Campbell, B.A., Arvidson, R.E., Shepard, M.K., and Brackett, R.A. (1997). Remote sensing of surface processes. In: Bougher, S.W., Hunten, D.M., Phillips, R.J. (Eds.), *Venus II*. The University of Arizona Press, Tucson, pp. 503-526.

Cannon, S.H., Kirkham, R.M., and Parise, M. (2001). Wildfire-related debris-flow initiation processes, Storm King Mountain, Colorado. *Geomorphology* 39, 171-188.

Carr, M.H. (1983). Stability of streams and lakes on Mars. *Icarus* 56, 476-495.

Carson, M.A. and Kirkby, M.J. (1972). *Hillslope Form and Process*. Cambridge University Press, London.

Carstensen, J.T and Chan, P-C (1976). Relation between particle size and repose angles of powders. *Powder Technology* 15, 129-131.

Chesworth, W., Dejou, J., and Larroque, P. (1981). The weathering of basalt and relative mobilities of the major elements at Belbex, France. *Geochimica et Cosmochimica Acta* 45, 1235-1243.

Christensen, P.R. (2003). Formation of recent martian gullies through melting of extensive water-rich snow deposits. *Nature* 422, 45-48.

Christensen, P.R. and Moore, H.J. (1992). The martian surface layer. In: *Mars*, eds. H.H. Kieffer, B.M. Jakosky, C.W. Snyder, and M.S. Matthews. The Univ. of Arizona Press: Tucson.

Clarkson, P.B. and Dorn, R.I. (1995). New chronometric dates for the puquios of Nasca, Peru. *Latin American Antiquity* 6 (1), 56-69.

Clegg, S.M., Sklute, E., Dyar, M.D., Barefield, J.E., and Wiens, R.C. (2009). Multivariate analysis of remote laser-induced breakdown spectroscopy spectra using partial least squares, principal component analysis, and related techniques. *Spectrochimica Acta B* 64 (1), 79-88.

Clow, G.D. (1987). Generation of liquid water on Mars through the melting of a dusty snowpack. *Icarus* 72, 95-127.

Colwell, J.E., Gulbis, A.A.S., Horányi, M., and Robertson, S. (2005). Dust transport in photoelectron layers and the formation of dust ponds on Eros. *Icarus* 175, 159-169.

Connerney, J.E.P., Acuña, M.H., Wasilewski, P.J., Ness, N.F., Rème, H., Mazelle, C., Vignes, D., Lin, R.P., Mitchell, D.L., and Cloutier, P.A. (1999). Magnetic lineations in the ancient crust of Mars. *Science* 284, 794-798.

Conway, S.J., Balme, M.R., Murray, J.B., Towner, M.C., and Kim, J.R. (2008). Icelandic debris flows and their relationship to martian gullies. *Workshop on Martian Gullies: Theories and Tests*, Houston, TX, no.8024.

Costard, F., Forget, F., Mangold, N., and Peulvast, J.P. (2002). Formation of recent martian debris flows by melting of near-surface ground ice at high obliquity. *Science* 295, 110-113.

Cousin, A., Maurice, S., Berger, G., Forni, O., Gasnault, O., Wiens, R., and the ChemCam team. Depth profiles studies using ChemCam. *Lunar and Planetary Science Conference XLII*, Houston, TX, 7-11 March 2011, no. 1963.

de Pater, I. and Lissauer, J.J. (2004). *Planetary Sciences*. Cambridge University Press, Cambridge, UK.

Dietrich, W.E., Wilson, C.J., and Reneau, S.L. (1986). Hollows, colluvium, and landslides in soil-mantled landscapes. In Hillslope Processes, ed. A.D. Abrahams. *The*

Binghamton Symposia in Geomorphology: International Series no.16. Allen & Unwin, Inc.: Winchester.

Dietrich, W.E., Reneau, S.L., and Wilson, C.J. (1987). Overview: "Zero-order basins" and the problem of drainage density, sediment transport and hillslope morphology. In *Proceedings of the International Erosion and Sedimentation in the Pacific Rim*, eds. Beschta, R.L., Blinn, T., Grant, G.E., Ice, G.G., and Swanson, F.J., International Hydrological Sciences Publication 165, 27-37.

Dííaz Pace, D.M., Gabriele, N.A., Garcimuñño, M., D'Angelo, C.A., Bertuccelli, G., and Bertuccelli, D. (2011). Analysis of minerals and rock by laser-induced breakdown spectroscopy. *Spectroscopy Letters* 44, 399-411.

Dombard, A.J., Barnouin-Jha, O.S., Prockter, L.M., and Thomas, P.J. (2010). Boulders and ponds on the Asteroid 433 Eros. *Icarus* 210, 713-721.

Dorn, R.I. (1994). "Rock varnish as evidence of climatic change," in *Geomorphology of Desert Environments*, A.D. Abrahams and A.J. Parsons, eds., Chapman and Hall, pp. 539-552.

Dorn, R.I. (1998). *Rock Coatings* (Elsevier).

Edgett, K. S., Malin, M.C., Williams, R.M.E., and Davis, S.D. (2003). Polar- and middle-latitude martian gullies: A view from MGS MOC after 2 Mars years in the mapping orbit. *Lunar and Planetary Science Conference XXXIV*, Houston, TX, no.1038.

Ehlmann, B.L., Mustard, J.F., Murchie, S.L., Poulet, F., Bishop, J.L., Brown, A.J., Calvin, W.M., Clark, R.N., Des Marais, D.J., Milliken, R.E., Roach, L.H., Roush, T.L., Swayze, G.A., and Wray, J.J. (2008). Orbital identification of carbonate-bearing rocks on Mars. *Science* 322, 1828-1832.

Engel, C.G. and Sharp, R.P. (1958). Chemical data on desert varnish. *Geolgical Society of America Bulletin* 69, 487-518.

Fanale, F.P., Postawko, S.E., Pollack, J.B., Carr, M.H., and Pepin, R.O. (1992). Mars: epochal climate change and volatile history. In: Kieffer, H.H., Jakosky, B.M., Snyder, C.W., Matthews, M.S. (Eds.), *Mars*. The University of Arizona Press, Tucson, pp. 1135-1179.

Foote, G.B. and du Toit, P.S. (1969). Terminal velocity of raindrops aloft. *Journal of Applied Meteorology* 8, 249-253.

Francis, J.E., Loendorf, L.L., and Dorn, R.I. (1993). AMS radiocarbon and cation-ratio dating of rock art in the Bighorn Basin of Wyoming and Montana. *American Antiquity* 58 (4), 771-737.

Gabet, E.J. and Dunne, T. (2003). Sediment detachment by rain power. *Water Resources Research* 39 (1), doi:10.1029/2001WR000656.

Gaidos, E.J. (2001). Cryovolcanism and the recent flow of liquid water on Mars. *Icarus* 153, 218-223.

Gilmore, M.S. and Phillips, E.L. (2002). Role of aquicludes in formation of Martian gullies. *Geology* 30, 12, 1107-1110.

Godt, J.W., and Coe, J.A. (2003). Map showing alpine debris flows triggered by a July 28, 1999 thunderstorm in the central Front Range of Colorado. *U.S. Geological Survey Open-File Report 03-050*, Washington, D.C. http://pubs.usgs.gov/of/2003/ofr-03-050/ accessed on 17 February 2009.

Godt, J.W. and Coe, J.A. (2007). Alpine debris flows triggered by a 28 July 1999 thunderstorm in the central Front Range, Colorado. *Geomorphology* 84, 80-97.

Graves, S.D.B., McKay, C.P., Griffith, C.A., Ferri, F., and Fulchignoni, M. (2008). Rain and hail can reach the surface of Titan. *Planetary and Space Sciences* 56, 346-357.

Gordon, S.J. and Dorn, R.I. (2005). *In situ* weathering rind erosion. *Geomorphology* 67, 97-113.

Griffith, G.A., Owen, T., Geballe, T.R., Rayner, J., and Rannou, P. (2003). Evidence for the exposure of water ice on Titan's surface. *Science* 300, 628-630.

Grotzinger, J. (2009). Beyond water on Mars. *Nature Geoscience* 2, 1-3.

Haberle, R.M., McKay, C.P., Pollack, J.B., Gwynne, O.E., Atkinson, D.H., Appelbaum, J., Landis, G.A., Zurek, R.W., and Flood, D.J. (1993). Atmospheric effects on the utility of solar power on Mars. In: Lewis, J.S., Matthews, M.S., Guerrieri, M.L. (Eds.), *Resources of Near-Earth Space*. The University of Arizona Press, Tucson, pp. 845-885.

Halajian, J.D. (1964). Gravity effects on soil behavior. In: Salisbury, J.W., Glaser, P.E. (Eds.), *The Lunar Surface Layer: Materials and Characteristics*. Academic Press, New York, pp. 67-91.

Harmon, R.S., DeLucia, F.C., McManus, C.E., McMillan, N.J., Jenkins, T.F., Walsh, M.E., and Miziolek, A. (2006). Laser-induced breakdown spectroscopy—An emerging chemical sensor technology for real-time field-portable, geochemical, mineralogical, and environmental applications. *Applied Geochemistry* 21, 730-747.

Harmon, R.S., Remus, J., McMillan, N.J., McManus, C., Collins, L., Gottfried Jr., J.L., De Lucia, F.C., and Miziolek, A.J. (2009). LIBS analysis of geomaterials:

Geochemical fingerprinting for the rapid analysis and discrimination of materials. *Applied Geochemistry* 24, 1125-1141.

Haskin, L.A., Wang, A., Jolliff, B.L., McSween, H.Y., Clark, B.C., Des Marais, D.J., McLennan, S.M., Tosca, N.J., Hurowitz, J.A., Farmer, J.D., Yen, A., Squyres, S.W., Arvidson, R.E., Klingelhöfer, G., Schröder, C., de Souza Jr., P.A., Ming, D.W., Gellert, R., Zipfel, J., Brückner, J., Bell III, J.F., Herkenhoff, K., Christensen, P.R., Ruff, S., Blaney, D., Gorevan, S., Cabrol, N.A., Crumpler, L.A., Grant, J., and Soderblom, L. (2005). Water alteration of rocks and soils on Mars at the Spirit rover site in Gusev crater. *Nature* 436, 66-69.

Hays, J.D., Imbrie, J., and Shackleton, N.J. (1976). Variations in the Earth's orbit: pacemaker of the ice ages. *Science* 194 (4270), 1121-1132.

Head, J.W. and Marchant, D.R. (2003). Cold-based mountain glaciers on Mars: Western Arsia Mons. *Geology* 31, 7, 641-644.

Head, J.W., Mustard, J.F., Kreslavsky, M.A., Milliken, R.E., and Marchant, D.R. (2003). Recent ice ages on Mars. *Nature* 426, 797-802.

Head, J.W. and 12 colleagues (2005). Tropical to mid-latitude snow and ice accumulation, flow and glaciations on Mars. Nature 434, 346-351.

Heath, R.C. and Trainer, F.W. (1968). *Introduction to Ground-Water Hydrology*. John Wiley and Sons, Inc., New York, 284 pp.

Hecht, M. H. (2002). Metastability of liquid water on Mars. *Icarus* 156, 373-386.

Heldmann, J.L. and Mellon, M.T. (2004). Observations of martian gullies and constraints on potential formation mechanisms. *Icarus* 168, 285-304.

Holt, J.W., Safaeinili, A., Plaut, J.J., Head, J.W., Phillips, R.J., Seu, R., Kempf, S.D., Choudhary, P., Young, D.A., Putzig, N.E., Biccari, D., and Gim, Y. (2008). Radar sounding evidence for buried glacier in the southern mid-latitudes of Mars. *Science* 322, 1235-1238.

Horton, R.E. (1945). Erosional development of streams and their drainage basins; hydrophysical approach to quantitative morphology. *Geological Society of America Bulletin* 56, 275-370.

Howard, K.A. (1973). Avalanche mode of motion: implications from lunar examples. *Science* 180, 1052-1055.

Hueso, R. and Sánches-Lavega, A. (2006). Methane storms on Saturn's moon Titan. *Nature* 442, 428-431.

Hughes, A.L.H., Colwell, J.E., and DeWolfe, A.W. (2008). Electrostatic dust transport on Eros: 3-D simulations of pond formation. *Icarus* 195, 630-648.

Hungr, O., Evans, S.G., Bovis, M.J., and Hutchinson, J.N. (2001). A review of the classification of landslides of the flow type. *Environmental and Engineering Geoscience VII* (3), 221-238.

Iverson, R.M. (1997). The physics of debris flow. *Reviews of Geophysics* 35 (3) 245-296.

James, P.B., Kieffer, H.H., and Paige, D.A. (1992). The seasonal cycle of carbon dioxide on Mars. In: Kieffer, H.H., Jakosky, B.M., Snyder, C.W., Matthews, M.S. (Eds.), *Mars*. The University of Arizona Press, Tucson, pp. 934-968.

Jandura, L., Burke, K., Kennedy, B., Melko, J., Okon, A., and Sunshine, D. (2010). An overview of the Mars Science Laboratory sample acquisition, sample processing, and handling subsystem. *12th International Conference on Engineering, Science, Construction, and Operations in Challenging Environments*, Honolulu, HI, 14-17 March 2010, pp. 941-948.

Johnson, A.M. and Rodine, J.R. (1984). Debris flow. In: *Slope Instability*, eds. Brunsdon, D. and Prior, D.B. Wiley, New York.

Jones, J.A.A. (1997). Subsurface flow and subsurface erosion. In: Stoddart, D.R. (Ed.), *Process and Form in Geomorphology*. Routledge, London, pp. 74-120.

Jones, K.L., Arvidson, R.E., Guinness, E.A., Bragg, S.L., Wall, S.D., Carlston, C.E., and Pidek, D.G. (1979). One Mars year: Viking lander imaging observations. *Science* 204 (4395), 799-806.

Keller, H.U. and 11 colleagues (2009). Physical properties of the icy soil at the Phoenix landing site. *Lunar and Planetary Science Conference XL*, Houston, TX, no.1671.

Kirk, R.L. and 18 colleagues (2008). Ultra-high-resolution topographic mapping of Mars with MRO HiRISE stereo images: Meter-scale slopes of candidate Phoenix landing sites. *Journal of Geophysical Research*, doi:10.1029/2007JE003000.

Knighton, D. (1998). *Fluvial Forms and Processes.* Oxford University Press Inc., New York.

Knoll, A.H. and 16 colleagues (2008). Veneers, rinds, and fracture fills: Relatively late alteration of sedimentary rocks at Meridiani Planum, Mars. *Journal of Geophysical Research* 113 (E06S16), doi:10.1029/2007JE002949.

Kochel, R.C. and Trop, J.M. (2008). Earth analog for high-latitude landforms and recent flows on Mars: Icy debris fan in Wrangell Volcanic Field, Alaska. *Icarus* 196, 63-77.

Kossacki, K.J. and Markiewicz, W.J. (2004). Seasonal melting of surface water ice condensing in martian gullies. *Icarus* 171, 272-283.

Laity, J.E. and Malin, M.C. (1985). Sapping processes and the development of theater-headed valley networks on the Colorado Plateau. *Geological Society of America Bulletin* 96, 203-217.

Lanza, N.L. and Gilmore, M.S. (2006). Depths, orientation, and slopes of martian hillside gullies in the northern hemisphere. Lunar and Planetary Science Conference XXXVII, Houston, TX, no. 2412.

Lanza, N.L., Meyer, G.A., Okubo, O., Newsom, H.E., and Wiens, R.C. (2008). Testing a debris flow source area and initiation hypothesis for simple 'classic' martian gullies. Workshop on Martian Gullies: Theories and Tests, Houston, TX, no.8038.

Lanza, N.L., Meyer, G.A., Okubo, C.H., Newsom, H.E., and Wiens, R.C. (2010a). Evidence for debris flow gully formation initiated by shallow subsurface water on Mars. *Icarus* 205, 103-112.

Lanza, N.L., Deans, M.C., Clegg, S.M, Humphries, S.D., McInroy, R.E., Wiens, R.C., Newsom, H.E., and Ollila, A.M. (2010b). Using LIBS to determine composition of natural rock coatings and weathering rinds for planetary exploration. *LIBS 2010*, Memphis, TN, 13-17 September 2010.

Lasue, J., Wiens, R.C., Stepinski, T.F., Forni, O., Clegg, S.M., Maurice, S., and the ChemCam team. Nonlinear mapping technique for data visualization and clustering assessment of LIBS data: application to ChemCam data. *Analytical and Bioanalytical Chemistry* 400, 3247-3260.

Legros, F. (2002). The mobility of long-runout landslides. *Engineering Geology* 63, 301-331.

Levy, J.S., Head, J.W., and Marchant, D.R. (2008). The role of thermal contraction crack polygons in cold-desert fluvial systems. *Antarctic Science*, doi:10.1017/S0954102008001375.

Levy, J.S., Head, J.W., Dickson, J.L., Fassett, C.I., Morgan, G.A., and Schon, S.C. (2010a). Identification of gully debris flow deposits in Protonilus Mensae, Mars: characterization of a water-bearing, energetic gully-forming process. *Earth and Planetary Science Letters* 294, 368-377.

Levy, J.S., Marchant, D.R., and Head, J.W. (2010b). Thermal contraction crack polygons on Mars: a synthesis from HiRISE, Phoenix, and terrestrial analog studies. *Icarus* 206, 229-252.

Lorenz, R.D. (1995). Raindrops on Titan. *Advances in Space Research* 15 (3), 317-320.

Lorenz, R.D. and Lunine, J.I. (1996). Erosion on Titan: past and present. *Icarus* 122, 79-91.

Malet, J.P., Laigle, D., Remaitre, A., and Maquaire, O. (2005). Triggering conditions and mobility of debris flows associated to complex earthflows. *Geomorphology* 66, 215-235.

Malin, M.C. and Edgett, K.S. (2000). Evidence for recent groundwater seepage and surface runoff on Mars. *Science* 288 (5475), 2330-2335.

Malin, M.C. and Edgett, K.S. (2003). Evidence for persistent flow and aqueous sedimentation on early Mars. *Science* 302 (5652), 1931-1934.

Malin, M.C., Edgett, K.S., Posiolova, L.V., McColley, S.M., and Noe Dobrea, E.Z. (2006). Present-day impact cratering rate and contemporary gully activity on Mars. *Science* 314, 1573-1577.

Mangold, N., Costard, F., and Forget, F. (2003). Debris flows over sand dunes on Mars: evidence for liquid water. *Journal of Geophysical Research* 108 (E4), doi:10.1029/2002JE001958.

Maurice, S., Wiens, R., Parès, L., Bender, S., le Roch, N., Dalmau, J., Berthé, M., Langevin, Y., Herkenhoff, K., Bridges, N., Saccoccio, M., and the ChemCam Team (2009). Characterization of ChemCam (MSL) imaging capability. *Lunar and Planetary Science Conference XL*, Houston, TX, no. 1864.

McEwen, A.S. (1989). Mobility of large rock avalanches: evidence from Valles Marineris, Mars. *Geology* 17, 1111-1114.

McEwen, A.S. and 15 colleagues (2007). Mars Reconnaissance Orbiter's High Resolution Imaging Science Experiment (HiRISE). *Journal of Geophysical Research* 112 (E05S02), doi:10.1029/2005JE002605.

McFadden, L.D., Ritter, J.B., and Wells, S.G. (1989). Use of multiparameter relative-age methods for age estimation and correlation of alluvial fan surfaces on a desert piedmont, eastern Mojave Desert, California. *Quaternary Research* 32 (3), 276-290.

McKay, D.S., Gibson Jr., E.K., Thomas-Keprta, K.L., Vali, H., Romanek, C.S., Clemett, S.J., Chillier, X.D.F., Maechling, C.R., and Zare, R.N. (1996). Search for past life on Mars: Possible relic biogenic activity in martian meteorite ALH84001. *Science* 273 (5277), 924-930.

McMillan, N.J., Harmon, R.S., De Lucia, F.C., and Miziolek, A.M. (2007). Laser-induced breakdown spectroscopy analysis of minerals: Carbonates and silicates. *Spectrochimica Acta B* 62, 1528-1536.

McSween, H.Y., Arvidson, R.E., Bell III, J.F., Blaney, D., Cabrol, N.A., Christensen, P.R., Clark, B.C., Crisp, J.A., Crumpler, L.S., Des Marais, D.J., Farmer, J.D., Gellert, R., Ghosh, A., Gorevan, S., Graff, T., Grant, J., Haskin, L.A., Herkenhoff, K.E., Johnson, J.R., Jolliff, B.L., Kingelhoefer, G., Knudson, A.T., McLennan, S., Milam, K.A., Moersch, J.E., Morris, R.V., Rieder, R., Ruff, S.W., de Souza Jr., P.A., Squyres, S.W., Wänke, H., Wang, A., Wyatt, M.B., and Zipfel, J. (2004). Basaltic rocks analyzed by the Spirit rover in Gusev crater. *Science* 305, 842-845.

Mellon, M.T. and Jakosky, B.M. (1993). Geographic variations in the thermal diffusive stability of ground ice on Mars. Journal of Geophysical Research 98 (E2), 3345-3364.

Mellon, M.T. and Phillips, R.J. (2001). Recent gullies on Mars and the source of liquid water. *Journal of Geophysical Research* 106 (E10), 23,165-23,180.

Melosh, H.J. (1989). The physics of very large landslides. *Acta Mechanica* 64, 89-99.

Meyer, G.A., and Wells, S.G. (1997). Fire-related sedimentation events on alluvial fans, Yellowstone National Park, U.S.A.. *Journal of Sedimentary Research* A67, 776-791.

Milliken, R.E., Swayze, G.A., Arvidson, R.E., Bishop, J.L., Clark, R.N., Ehlmann, B.L., Green, R.O., Grotzinger, J.P., Morris, R.V., Murchie, S.L., Mustard, J.F., and Weitz, C. (2008). Opaline silica in young deposits on Mars. *Geology* 36, 847-850.

Miyamoto, H., Yano, H., Scheeres, D.J., Abe, S., Barnouin-Jha, O., Cheng, A.F., Demura, H., Gaskell, R.W., Hirata, N., Ishiguro, M., Michikami, T., Nakamura, A.M., Nakamura, R., Saito, J., and Sasaki, S. (2007). Regolith migration and sorting on asteroid Itokawa, *Science* 316, 1011-1014.

Montgomery, D.R. and Dietrich, W.E. (1988). Where do channels begin? *Nature* 336, 232-234.

Montgomery, D.R. and Dietrich, W.E. (1989). Source areas, drainage density, and channel initiation. *Water Resources Research* 25 (8), 1907-1918.

Montgomery, D.R. and Dietrich, W.E. (1992). Channel initiation and the problem of landscape scale. *Science* 255 (5046), 826-830.

Montgomery, D.R. and Dietrich, W.E. (1994). Landscape dissection and drainage area-slope thresholds. In: *Process Models and Theoretical Geomorphology*, ed. M.J. Kirkby. John Wiley & Sons, Chichester, UK.

Montgomery, D.R. and Foufoula-Gergiou, E. (1993). Channel network source representation using digital elevation models. *Water Resources Research* 29 (12), 3925-3934.

Moore, J.M., Asphaug, E., Morrison, D., Spencer, J.R., Chapman, C.R., Bierhaus, B., Sullivan, R.J., Chuang, F.C., Klemaszewski, J.E., Greely, R., Bender, K.C., Geissler, P.E., Helfenstein, P., and Pilcher, C.B. (1999a). Mass movement and landform

degradation on the icy Galilean satellites: results of the Galileo nominal mission. *Icarus* 140, 294-312.

Moore, H.J., Bickler, D.B., Crisp, J.A., Eisen, H.J., Gensler, J.A., Haldemann, A.F.C., Matijevic, J.R., Reid, L.K., and Pavlics, F. (1999b). Soil-like deposits observed by Sojourner, the Pathfinder rover. *Journal of Geophysical Research* 104 (E4), 8729-8746.

Musslewhite, D.S., Swindle, T.D., and Lunine, J.I. (2001). Liquid CO_2 breakout and the formation of recent small gullies on Mars. *Geophysical Research Letters* 28 (7), 1283-1285.

Mustard, J.F., Cooper, C.D., and Rifkin, M.K. (2001). Evidence for recent climate change on Mars from the identification of youthful near-surface ground ice. *Nature* 412, 411-414.

Newsom, H.E., Hagerty, J.J., and Goff, R. (1999). Mixed hydrothermal fluids and the origin of the Martian soil. *Journal of Geophysical Research* 104 (E4), 8717-8728.

Northup, D.E., Snider, J.R., Spilde, M.N., Porter, M.L., van de Kamp, J.L., Boston, P.J., Nyberg, A.M.. and Bagar, J.R. (2010). Diversity of rock varnish bacterial communities from Black Canyon, New Mexico. *Journal of Geophysical Research* 115 (G02007), doi:10.1029/2009JG001107 (2010).

Ollila, A.M. and Gilmore, M.S. (2007). Thermophysical properties of gullied and nongullied slopes in Acidalia Planitia, Mars. *Lunar and Planetary Science Conference XXXVIII*, Houston, TX, no.1861.

Osterloo, M.M., Hamilton, V.E., Bandfield, J.L., Glotch, T.D., Baldridge, A.M., Christensen, P.R., Tornabene, L.L., and Anderson, F.S. (2008). Chloride-bearing materials in the southern highlands of Mars. *Science* 319 (5870), 1651-1654.

Perron, J.T., Dietrich, W.E., Howard, A.D., McKean, J.A., and Pettinga, J.R. (2003). Ice-driven creep on Martian debris slopes. *Geophysical Research Letters* 30 (14), doi:10.1029/2003GL017603.

Perron, J.T., Lamb, M.P., Koven, C.D., Fung, I.Y., Yager, E., and Ádámkovics, M. (2006). Valley formation and methane precipitation rates on Titan. *Journal of Geophysical Research* 111 (E11001), doi:10.1029/2005JE002602.

Perry, R.S. and Adams, J.B. (1978). Desert varnish: evidence for cyclic deposition of manganese. *Nature* 276 (5687), 489-491.

Pierson, T.C. (1986). Flow behavior of channelized debris flow, Mount St. Helens, Washington. In: *Hillslope Processes*, ed. A.D. Abrahams. The Binghamton Symposia in Geomorphology: International Series no.16. Allen & Unwin, Inc.: Winchester.

Pierson, T.C. and Costa, J.E. (1987). A rheologic classification of subaerial sediment-water flows. *Geological Society of America, Reviews in Engineering Geology VII*, 1-12.

Pollack, J. B., Kasting, J.F., Richardson, S.M., and Poliakoff, K. (1987).The case for a wet, warm climate on early Mars. *Icarus* 71, 203-224.

Radziemski, L., Cremers, D.A., Benelli, K., Khoo, C., and Harris, R.D. (2005). Use of the vacuum ultraviolet spectral region for laser-induced breakdown spectroscopy-based Martian geology and exploration. *Spectrochimica Acta B* 60, 237-248.

Rao, M.N., Sutton, S.R., McKay, D.S., and Dreibus, G. (2005). Clues to Martian brines based on halogens in salts from nakhlites and MER samples. *Journal of Geophysical Research* 110 (E12S06), doi:10.1029/2005JE002470.

Reneau, S.L. and Dietrich, W.E. (1987). The importance of hollows in debris flow studies; Examples from Marin County, California. *Geological Society of America, Reviews in Engineering Geology VII*, 165-180.

Rodine, J.D. and Johnson, A.M. (1976). The ability of debris, heavily freighted with coarse clastic materials, to flow on gentle slopes. *Sedimentology* 23, 213-234.

Sak, P.B., Fisher, D.M., Gardner, T.W., Murphy, K., and Brantley, S.L. (2004). Rates of weathering rind formation on Costa Rican basalt. *Geochimica et Cosmochimica Acta* 68, 1453-1472.

Saunders, R.S. (1999). Venus. In: Beatty, J.K., Petersen, C.C., Chaikin, A. (Eds.), *The New Solar System*, Sky Publishing Corporation, Cambridge, MA.

Schon, S.C., Head, J.W., and Fassett, C.I. (2009). Unique chronostratigraphic marker in depositional fan stratigraphy on Mars: evidence for ca. 1.25 Ma gully activity and surficial meltwater origin. *Geology* 37 (3), 207-210.

Schwartz, F.W. and Zhang, H. (2003). *Fundamentals of Groundwater*. John Wiley and Sons, Inc., New York.

Sharp, R.P. (1973). Mars: fretted and chaotic terrains. *Journal of Geophysical Research* 78 (20), 4073-4083.

Sharp, R.P. (1980). Geomorphological processes on terrestrial planetary surfaces. *Annual Review of Earth and Planetary Sciences* 8, 231-261.

Sirven, J.B., Bousquet, B., Canioni, L., and Sarger, L. (2006). Laser-induced breakdown spectroscopy of composite samples: Comparison of advanced chemometrics methods. *Analytical Chemistry* 78, 1462-1469.

Sleep, N.H. (1994). Martian plate tectonics. *Journal of Geophysical Research* 99 (E3), 5639-5655.

Smith, P.H. and the Phoenix Science Team (2009a). Water at the Phoenix landing site. *Lunar and Planetary Science Conference XL*, Houston, TX, no.1329.

Smith, P.H., Tamppari, L.K., Arvidson, R.E., Bass, D., Blaney, D., Boynton, W.V., Carswell, A., Catling, D.C., Clark, B.C., Duck, T., DeJong, E., Fisher, D., Goetz, W., Gunnlaugsson, H.P., Hecht, M.H., Hipkin, V., Hoffman, J., Hviid, S.F., Keller, H.U., Kounaves, S.P., Lange, C.F., Lemmon, M.T., Madsen, M.B., Markiewicz, W.J., Marshall, J., McKay, C.P., Mellon, M.T., Ming, D.W., Morris, R.V., Pike, W.T., Renno, N., Staufer, U., Stoker, C., Taylor, P., Whiteway, J.A., and Zent, A.P. (2009b). H_2O at the Phoenix landing site. *Science* 325 (58), 58-61.

Soare, R.J., Kargel, J.S., Osinski, G.R., and Costard, F. (2007). Thermokarst processes and the origin of crater-rim gullies in Utopia and western Elysium Planitia. *Icarus* 191, 95-112.

Sowers, J.M. (2005). Rock varnish chronology. In: *Quaternary Geochronology: Methods and Applications*, J.S. Noller, J.M. Sowers, and W.R. Lettis, eds.. American Geophysical Union Books Board, pp.241-260.

Spencer, J.R and Denk, T. (2010). Formation of Iapetus' extreme albedo dichotomy by exogenically triggered thermal ice migration. *Science* 327, 432-435.

Squyres, S.W. and Carr, M.H. (1986). Geomorphic evidence for the distribution of ground ice on Mars. *Science* 231 (4735), 249-252.

Squyres, S.W., Grotzinger, J.P., Arvidson, R.E., Bell III, J.F., Calvin, W., Christensen, P.R., Clark, B.C., Crisp, J.A., Farrand, W.H., Herkenhoff, K.E., Johnson, J.R., Klingelhöfer, G., Knoll, A.H., McLennan, S. M., McSween Jr., H.Y., Morris, R.V., Rice, J.W., Rieder, R., and Soderblom, L.A. (2004). In situ evidence for an ancient aqueous environment at Meridiani Planum, Mars. *Science* 306, 709-1714.

Stewart, S.T. and Nimmo, F. (2002). Surface runoff features on Mars: Testing the carbon dioxide formation hypothesis. *Journal of Geophysical Research* 107 (E9), 5069, doi:10.1029/2000JE001465.

Stock, J.D. and Dietrich, W.E. (2006). Erosion of steepland valleys by debris flow. *Geological Society of America Bulletin* 118 (9/10), 1125-1148.

Thiagarajan, N. and Lee, C-T.A. (2004). Trace-element evidence for the origin of desert varnish by direct aqueous atmospheric deposition. *Earth and Planetary Science Letters* 224, 131-141.

Tomasko, M.G., Archinal, B., Becker, T., Bézard, B., Bushroe, M., Combes, M., Cook, D., Coustenis, A., de Bergh, C., Dafoe, L.E., Doose, L., Douté, S., Eibl, A., Engle, S., Gliem, F., Grieger, B., Holso, K., Howington-Kraus, E., Karkoschka, E., Keller, H.U., Kirk, R., Kramm, R., Küppers, M., Lanagan, P., Lellouch, E., Lemmon, M., Lunine, J., McFarlane, E., Moores, J., Prout, G.M., Rizk, B., Rosiek, M., Rueffer, P., Schröder, S.E., Schmitt, B., See, C., Smith, P., Soderblom, L., Thomas, N., and West, R. (2005). Rain, winds and haze during the Huygens probe's decent to Titan's surface. *Nature* 438, 765-778.

Toon, O.B., McKay, C.P., Courtin, R., and Ackerman, T.P. (1988). Methane rain on Titan. *Icarus* 75, 255-284.

Tucker, J.M., Dyar, M.D., Schaefer, M.W., Clegg, S.M., and Wiens, R.C. (2010). Optimization of laser-induced breakdown spectroscopy for rapid geochemical analysis. *Chemical Geology* 277, 137-148.

Ulrich, G.E. and Bailey, N.G. (1987). Geologic map of the SP Mountain part of the San Francisco volcanic field, north-central Arizona. *U.S. Geological Survey, Miscellaneous Geologic Investigations Map MF-1956*, scale 1:50000.

Walton, O.R., De Moor, C.P., and Gill, K.S. (2007). Effects of gravity on cohesive behavior of fine powders: implications for processing Lunar regolith. *Granular Matter* 9, 353-363.

Ward, W.R. (1992). Long-term orbital and spin dynamics of Mars. In: Kieffer, H.H., Jakosky, B.M., Snyder, C.W., Matthews, M.S. (Eds.), *Mars*. The University of Arizona Press, Tucson.

Watters, T.R., Robinson, M.S., Beyer, R.A., Banks, M.E., Bell, J.F. III, Pritchard, M.E., Hiesinger, H., van der Bogert, C.H., Thomas, P.C., Turtle, E.P., and Williams, N.R. (2010). Evidence of recent thrust faulting on the Moon revealed by the Lunar Reconnaissance Orbiter Camera. *Science* 329, 936-940.

Whiteway, J.A., Komguem, L., Dickinson, C., Cook, C., Illnicki, M., Seabrook, J., Popovici, V., Duck, T.J., Davy, R., Taylor, P.A., Pathak, J., Fisher, D., Carswell, A.I., Daly, M., Hipkin, V., Zent, A.P., Hecht, M.H., Wood, S.E., Tamppari, L.K., Renno, N., Moores, J.E., Lemmon, M.T., Daerden, F., and Smith, P.H. (2009). Mars water-ice clouds and precipitation. *Science* 325, 68-70.

Wiens, R.C., Kirkland, L.E., McKay, C.P., Cremers, D.A., Thompson, J., Maurice, S., and Pinet, P.C. (2004). Analyses of IR-stealthy and coated surface materials: A comparison of LIBS and reflectance spectra, and their application to Mars surface exploration. *Lunar and Planetary Science Conference XXXV*, Houston, TX, 15-19 March 2004, no. 1695.

Wiens, R.C., Maurice, S., Clegg, S., Vaniman, D., Thompson, J., Dyar, M.D., Sklute, E., Newsom, H., Lanza, N., Sautter, V., Dubessy, J., Boiron, M.C., Fabre, C., Lacour, J.-L., Sallé, B., Mauchien, P., Blaney, D., Langevin, Y., Herkenhoff, K., Bridges, N., Manhes, G., and the ChemCam Team, (2007). Preparation of onboard calibration targets for the ChemCam instruments on the Mars Science Laboratory rover. *Lunar and Planetary Science Conference XXXVIII*, Houston, TX, no. 1180.

Wiens, R.C., Clegg, S., Bender, S., Lanza, N., Barraclough, B., Perez, R., Maurice, S., Dyar, M. D, Newsom, H., and the ChemCam Team (2009). Initial calibration of the ChemCam LIBS instrument for the Mars Science Laboratory. *Lunar and Planetary Science Conference XL*, Houston, TX, no. 1461.

Wiens, R.C., Clegg, S.M., Bender, S., Lanza, N., Barraclough, B., Perez, R., Forni, O., Maurice, S., Dyar, M.D., Newsom, H., and the ChemCam Team (2010). Progress on calibration of the ChemCam LIBS instrument for the Mars Science Laboratory (MSL) rover. *Lunar and Planetary Science Conference XLI*, Houston, TX, no. 2205.

Wiens, R.C., Maurice, S., and the ChemCam Team (2011a). The ChemCam instrument suite on the Mars Science Laboratory rover Curiosity: Remote sensing by laser-induced plasmas. *Geochemical News* 145, 41-47. Available online at http://www.geochemsoc.org/publications/geochemicalnews/gn145jun11/chemcaminstrumentsuite.htm .

Wiens, R.C., Maurice, S., Bender, S., Barraclough, B.L., Cousin, A., Forni, O., Ollila, A., Newsom, H., Vaniman, D., Clegg, S., Lasue, J.A., Blaney, D., DeFlores, L., Morris, R.V., and the ChemCam Team (2011b). Calibration of the MSL/ChemCam/LIBS remote sensing composition instrument. *Lunar and Planetary Science Conference XLII*, Houston, TX, 7-11 March 2011, no. 2370.

Yen, A.S., Morris, R.V., Clark, B.C., Gellert, R., Knudson, A.T., Squyres, S., Mittlefehldt, D.W., Ming, D.W., Arvidson, R., McCoy, T., Schmidt, M., Hurowitz, J., Li, R., and Johnson, J.R. (2008). Hydrothermal processes at Gusev Crater: An evaluation of Paso Robles class soils. *Journal of Geophysical Research* 113 (E06S10), doi:10.1029/2007JE002978.

Zarnecki, J.C., Leese, M.R., Hathi, B., Ball, A.J., Hagermann, A., Towner, M.C., Lorenz, R.D., McDonnell, J.A.M., Green, S.F., Patel, M.R., Ringrose, T.J., Rosenberg, P.D., Atkinson, K.R., Paton, M.D., Banaszkiewicz, M., Clark, B.C., Ferri, F., Fulchignoni, M., Ghafoor, N.A.L., Kargl, G., Svedhem, Delderfield, J., Grande, M., Parker, D.J., Challenor, P.G., and Geake, J.E. (2005). A soft solid surface on Titan as revealed by the Huygens Surface Science Package. *Nature* 438, 792-795.

Zhou, Y.C., Xu, B.H., Yu, A.B., and Zulli, P. (2002). An experimental and numerical study of the angle of repose of coarse spheres. *Powder Technology* 125, 45-54.

Zuber, M.T., Smith, D.E., Cheng, A.F., Garvin, J.B., Aharonson, O., Cole, T.D., Dunn, P.J., Guo, Y., Lemoine, F.G., Neumann, G.A., Rowlands, D.D., and Torrence, M.H. (2000). The shape of 433 Eros from the NEAR–Shoemaker Laser Rangefinder, *Science* 289, 2097-2101.